



**Politecnico  
di Torino**

**Politecnico di Torino**

Master's Degree in Communications Engineering

**Innovative Solutions for Coherent  
Transmission in Optical Access  
Networks**

**Candidate:**

**Peyman Pahlevanzadeh**

**Supervisors:**

**Roberto Gaudino  
Giuseppe Rizzelli**

**December 2024**

# Abstract

The increasing demand for capacity in Passive Optical Networks (PONs) is driving operators and vendors to explore new solutions, including the adoption of unamplified coherent technologies. In this study, we investigate a novel approach to enhance transmitted power in coherent PON systems. Our focus is on the Mach-Zehnder Modulator (MZM) and the process of electrical-to-optical signal conversion, introducing a parameter called the modulation index. We explore how the system can operate closer to the nonlinear region of the MZM's transfer function while maintaining performance. Key performance metrics, including Bit Error Rate (BER) and Optical Distribution Network (ODN) loss, are used to evaluate the system's behavior. Additionally, we examine the effects of filtering and bandwidth limitations, utilizing a technique called pre-emphasis to compensate for these impacts. We have also considered Digital Pre-Emphasis to mitigate the electrical bandwidth limitations at the transmitter (TX). Furthermore, we study two Digital Pre-Distortion (DPD) methods, Polynomial DPD and Neural Network DPD to address the nonlinearities caused by the MZM. Our findings suggest that by reconsidering MZM modulation and accounting for the nonlinear characteristics of the transfer function, it is possible to increase transmitted power in coherent PONs while maintaining the system's performance. Since amplification is not typically used in PONs, these approaches could be a viable solution for next-generation coherent PON systems.

# Abbreviations

This specification uses the following abbreviations.

<b>PON</b>	Passive Optical Network
<b>CPON</b>	Coherent Passive Optical Network
<b>BER</b>	Bit Error Rate
<b>ODN</b>	Optical Distribution Network
<b>ONU</b>	Optical Network Unit
<b>MZM</b>	Mach-Zehnder Modulator
<b>PM-QPSK</b>	Polarization Multiplexed Quadrature Phase Shift Keying
<b>PM-16QAM</b>	Polarization Multiplexed 16 Quadrature Amplitude Modulation
<b>FEC</b>	Forward Error Correction
<b>DAC</b>	Digital-to-Analog Converter
<b>ONU</b>	Optical Network Unit
<b>OLT</b>	Optical Line Terminal
<b>EPON</b>	Ethernet Passive Optical Network
<b>GPON</b>	Gigabit Passive Optical Network
<b>P2P</b>	Point-to-Point
<b>P2MP</b>	Point-to-Multipoint
<b>FTTH</b>	Fiber to the Home
<b>IM-DD</b>	Intensity Modulation Direct Detection
<b>TDM</b>	Time Division Multiplexing
<b>TWDM</b>	Time-and-Wavelength-Division Multiplexing
<b>50G-PON</b>	50-Gigabit-Capable Passive Optical Network
<b>DPE</b>	Digital Pre-Emphasis
<b>DPD</b>	Digital Pre-Distortion

# Acknowledgment

Completing this thesis marks a significant milestone in my academic journey. I would first like to express my heartfelt gratitude to Prof. Gaudino for his trust, and guidance, and for providing me the opportunity to work under his mentorship. His calm manner, kindness, and organizational skills have taught me the valuable lesson that one can be both serious and organized in one's work while maintaining warmth and compassion. I would also like to extend my deep appreciation to Prof. Rizzelli, whose constant support, availability, and encouragement have been extremely helpful. He patiently answered all my questions, no matter how basic, and provided priceless guidance throughout this process.

I would also like to express my gratitude to my parents, who have supported me unconditionally and trusted me without question. Their strong belief in me has always been my greatest motivation, and I do my best to honor that trust in everything I do. I am incredibly thankful to all my friends on the 4th floor of Collegio Einaudi, especially Elena for her infinite kindness, Giulia for her warm heart, and Riccardo and Chiara T for their support. They have become like family to me, always welcoming me with open arms and giving their support. I would like to thank my friend and classmate Alessandra for her constant support throughout my studies. As an international student in Italy, I felt comfortable sharing my experiences and challenges with them, and their kindness made this journey much more meaningful.

*Peyman*



*"Nothing in life is to be feared, it is only to be understood. Now is the time to understand more, so that we may fear less." - Marie Curie*



# List of Figures

2.1	Overview of the optical network architecture illustrating the long-haul (backbone/core nodes), metropolitan (metro nodes), and access (access nodes) segments, enabling connectivity for cloud and edge infrastructures, including data centers[4]. . . . .	5
2.2	A typical architecture for PON systems [5]. . . . .	6
2.3	Architecture of (a) TDM-PON and (b) hybrid WDM(TDM-PON).[8] . . . . .	7
2.4	ITU and IEEE PON standards evolution. . . . .	7
2.5	ODN loss in PON systems from transmitter at Central Office to ONU. . . . .	8
2.6	Hypothetical timeline for Coh-PON development and deployment based on historical PON evolution [11]. . . . .	10
3.1	PM-16QAM Constellation Signal shape . . . . .	15
3.2	Configuration for Generating PM-16QAM Constellation Signal . . . . .	16
3.3	Mach-Zehnder modulator [4] . . . . .	16
3.4	Schematic of Electrical Signal Modulation onto Optical Signal Using a MZM	17
3.5	MZM Transfer Function - Electrical Signal vs. Optical Signal. . . . .	19
4.1	16QAM constellation for different modulation indices. . . . .	26
4.2	One quadrant of the 16QAM constellation displayed for different modulation indices. . . . .	26
4.3	Simplified scheme of a coherent PON . . . . .	28
4.4	RC pulse shaping filter in the time and frequency domain for different values of roll-off factors. . . . .	29
4.5	BER vs. Modulation Index for different Roll-Off Factors in PM-16QAM . . . . .	31
4.6	BER vs. Modulation Index for different Roll-Off Factors in PM-QPSK . . . . .	32
4.7	Transmitted optical power vs modulation index . . . . .	32
5.1	ODN loss in PON systems from transmitter at OLT to ONU. . . . .	35
5.2	BER versus ODN loss [dB] for different modulation indexes and PM-QPSK signal. The dotted line is for target BER = $2 * 10^{-2}$ for finding the maximum ODN loss. The left figure is for roll-off=0.1 and the right figure is for roll-off=0.5 . . . . .	36
5.3	BER versus ODN loss [dB] for different modulation indexes and PM-16QAM signal. The dotted line is for target BER = $10^{-2}$ for finding the maximum ODN loss . . . . .	37
5.4	Contour plot of modulation index versus roll-off factor, showing the maximum ODN loss [dB] for various target BERs using a PM-QPSK signal. . . . .	38

5.5	Contour plot of modulation index versus roll-off factor, showing the maximum ODN loss [dB] for various target BERs using a PM-16QAM signal.	38
6.1	MZM transfer function with nonlinearity terms for ER = 20 dB. The left plot shows the real part, and the right plot shows the imaginary part. . .	41
6.2	The constellation points of the signal for low ER and low modulation index(left); Maximum ODN loss vs Modulation Index vs Extinction Ratio(ER) for Target BER $10^{-2}$ (right). . . . .	41
6.3	Comparison of images with and without bias voltage. . . . .	43
6.4	The constellation points of the signal for low ER and high modulation index(left); Maximum ODN loss vs Modulation Index vs ER for Target BER $10^{-2}$ (right). . . . .	43
6.5	Maximum ODN loss vs Modulation Index vs ER for Target BER $10^{-2}$ . Figure a shows the 16QAM constellation for low ER and low $m_i$ , Figure b shows the 16QAM constellation for low ER and high $m_i$ , Figure c shows the 16QAM constellation for high ER and low $m_i$ and Figure d shows the 16QAM constellation for low ER and high $m_i$ . . . . .	44
7.1	Simulation setup for CPON with SG filtering effect at TX. . . . .	47
7.2	Frequency response of SG filter for different orders . . . . .	48
7.3	Frequency response of SG filter for different 3dB bandwidths . . . . .	49
7.4	Filtering effect on the PSD of the PM-16QAM signal for different 3dB bandwidth of SG filter. . . . .	49
7.5	Filtering effect on the PSD of the PM-16QAM signal for different 3dB bandwidth of SG filter @ $BER = 2 * 10^{-2}$ . . . . .	51
7.6	Filtering effect on the PSD of the PM-16QAM signal for different 3dB bandwidth of SG filter @ $BER = 10^{-2}$ . . . . .	51
7.7	Filtering effect on the PSD of the PM-16QAM signal for different 3dB bandwidth of SG filter @ $BER = 10^{-3}$ . . . . .	51
7.8	Simulation setup of applying DPE for compensating bandwidth limitations of DAC at TX. . . . .	52
7.9	The proposed DPE scheme, based on the work in [19], selects the parameters of $P(f)$ using BER feedback from the RX. . . . .	53
7.10	Transfer Functions of real and desired DAC and Pre-Emphasis Filter . .	54
7.11	Transfer functions of the DAC, Pre-Emphasis Filter, and the desired DAC transfer function. The left plot shows the DAC transfer function with a real third-order Bessel function, and the right plot shows the DAC transfer function with a Super Gaussian (SG) filter. . . . .	55
7.12	Optimization of pre-emphasis filter response through joint tuning of DAC bandwidth and noise adjustment coefficient. Applied to PM-16QAM (28 Gbaud) with real DAC parameters of 16 GHz bandwidth with real DAC 11.2 GHz. . . . .	56
7.13	Maximum ODN loss as a function of roll-off and modulation index with DPE and without DPE for different target BER with $BW = 0.5 * R_s$ . . .	57
7.14	Maximum ODN loss as a function of roll-off and modulation index with DPE and without DPE for different target BER with $BW = 0.35 * R_s$ . .	57

8.1	Simulation setup of applying DPD for compensating bandwidth limitations of DAC at TX. . . . .	63
8.2	16-QAM constellation diagram with and without pre-distortion applied before entering the MZM . . . . .	64
8.3	16-QAM constellation diagram with and without pre-distortion applied after entering the MZM . . . . .	65
8.4	EVM vs Modulation Index for 16-QAM . . . . .	65
8.5	Transmitted Power(the power of the signal at the output of MZM). . . .	66
8.6	BER v.s. modulation index with different degrees of PDPDs and without DPD. . . . .	67
8.7	BER v.s. modulation index with different degrees of PDPDs. . . . .	67
8.8	Maximum ODN vs. roll-off factor and modulation index under bandwidth limitations, with 3 dB bandwidth equal to $0.6 \times$ symbol rate ( $R_s$ ), without DPD. . . . .	68
8.9	Maximum ODN vs. roll-off factor and modulation index under bandwidth limitations, with 3 dB bandwidth equal to $0.6 \times$ symbol rate ( $R_s$ ), with DPD. . . . .	68
8.10	Diagram of a generic neural network architecture . . . . .	69
8.11	Simulation setup with NN-DPD block before DP-IQ-MZM. . . . .	70
8.12	Neural network architecture for pre-distortion, showing input, hidden layers, ReLU activations, and MSE loss calculation. . . . .	71
8.13	Training process for Neural Network pre distortion for DP-16QAM signal using Matlab. . . . .	73
8.14	EVM vs. Modulation Index for Three Scenarios: No DPD, Polynomial DPD, and NN-DPD. . . . .	75
8.15	Predistorted signal output with and without NN-DPD for a signal with a modulation index of 1.8, observed at the receiver side after passing through an AWGN channel, without bandwidth limitations. . . . .	75
8.16	Predistorted signal output with and without NN-DPD for a signal with a modulation index of 1.8, observed at the receiver side after passing through an AWGN channel, with bandwidth limitations $B = 0.5R_s$ . . . . .	76
8.17	BER vs Modulation Index for DP-16QAM signal, comparison of NN-DPD and No DPD without bandwidth limitations . . . . .	76
8.18	Maximum ODN vs. roll-off factor and modulation index under bandwidth limitations, with 3 dB bandwidth equal to $0.6 \times$ symbol rate ( $R_s$ ), with NN-DPD for target BER= $10^{-2}$ (left) and BER= $10^{-3}$ (right) . . . . .	78
8.19	Maximum ODN vs. roll-off factor and modulation index under bandwidth limitations, with 3 dB bandwidth equal to $0.6 \times$ symbol rate ( $R_s$ ), for target BER= $10^{-2}$ with NN-DPD(left) without NN-DPD(right). . . . .	78
8.20	Maximum ODN vs. roll-off factor and modulation index under bandwidth limitations, with 3 dB bandwidth equal to $0.6 \times$ symbol rate ( $R_s$ ), for target BER= $10^{-3}$ with NN-DPD(left) without NN-DPD(right). . . . .	79
8.21	Maximum ODN vs. roll-off factor and modulation index under bandwidth limitations, with 3 dB bandwidth equal to $0.6 \times$ symbol rate ( $R_s$ ), for target BER= $10^{-2}$ with Poly-DPD(left) NN-DPD(right). . . . .	79

8.22	Maximum ODN vs. roll-off factor and modulation index under bandwidth limitations, with 3 dB bandwidth equal to $0.6 \times$ symbol rate ( $R_s$ ), for target BER= $10^{-3}$ with Poly-DPD(left) and NN-DPD(right). . . . .	80
8.23	EVM vs. ER for systems with Polynomial DPD, NN-DPD, and without DPD for $m_{index} = [1, 1.5]$ . . . . .	81
8.24	EVM vs. ER for systems with Polynomial DPD, NN-DPD, and without DPD for $m_{index} = [1.7, 2]$ . . . . .	81

# Contents

<b>Abstract</b>	<b>II</b>
<b>Abbreviations</b>	<b>III</b>
<b>Acknowledgment</b>	<b>IV</b>
<b>List of Figures</b>	<b>VII</b>
<b>1 Introduction</b>	<b>2</b>
1.1 Thesis Structure . . . . .	2
<b>2 Passive Optical Networks (PONs)</b>	<b>4</b>
2.1 What is PON? . . . . .	4
2.1.1 PON architectures . . . . .	5
2.2 Passive Optical Network (PON) Standards . . . . .	5
2.3 PON standards . . . . .	6
2.4 ODN Standards for Different PON Classes . . . . .	6
2.4.1 Parameters for ODN Standards . . . . .	6
2.5 ODN Standards for Different PON Classes . . . . .	8
2.5.1 Motivation for CPON . . . . .	8
2.6 Evolution of Passive Optical Networks (PON) . . . . .	9
2.6.1 50G PON Standardization and Deployment . . . . .	9
2.6.2 Initiation of Coh-PON Studies . . . . .	10
2.6.3 Coh-PON Standardization and Initial Deployment . . . . .	10
2.6.4 Expansion of Coh-PON Applications . . . . .	10
2.6.5 Challenges in CPON . . . . .	11
2.6.6 Recent progress of CPON . . . . .	11
2.7 Conclusion . . . . .	12
<b>3 Fundamentals of Coherent Transmission</b>	<b>13</b>
3.1 Introduction . . . . .	13
3.2 Intensity Modulation with Direct Detection (IMDD) . . . . .	13
3.2.1 Spectral Efficiency in IMDD . . . . .	13
3.3 Coherent Transmission Fundamentals . . . . .	14
3.3.1 I/Q Modulation . . . . .	14
3.3.2 PM-QPSK Modulation . . . . .	14
3.3.3 PM-16QAM Modulation . . . . .	15
3.4 Mach-Zehnder Modulator (MZM) . . . . .	15

3.5	Defenition of Modulation Index . . . . .	18
3.6	Coherent Receiver . . . . .	19
3.6.1	Signal Components . . . . .	19
3.6.2	Basic Photodetection . . . . .	20
3.6.3	Detection by Interference . . . . .	20
3.6.4	Eliminating Unwanted Power Components . . . . .	20
3.6.5	Detecting All Components . . . . .	21
3.7	DSP in Coherent Receivers . . . . .	21
3.8	Conclusion . . . . .	23
<b>4</b>	<b>Impact of Modulation Index and Roll-Off on BER</b>	<b>24</b>
4.1	Problem Statement . . . . .	24
4.2	Balancing Nonlinearity and Transmitted Power . . . . .	25
4.3	Novel Idea: Optimizing the Modulation Index . . . . .	25
4.4	Simulation Setup . . . . .	27
4.4.1	DSP Receiver Overview . . . . .	28
4.4.2	General Parameters . . . . .	28
4.4.3	Step-by-Step Workflow in the Simulation . . . . .	30
4.5	Results . . . . .	31
4.6	Conclusion . . . . .	33
<b>5</b>	<b>Introducing the parameter ODN loss</b>	<b>34</b>
5.1	Optical Distribution Network (ODN) . . . . .	34
5.2	Results . . . . .	35
5.3	Conclusion . . . . .	39
<b>6</b>	<b>Impact of Extinction Ratio on ODN loss</b>	<b>40</b>
6.1	Mathematical model for ER . . . . .	41
6.2	Results . . . . .	42
6.3	Conclusion . . . . .	44
<b>7</b>	<b>Advanced Topics in Coherent Transmission</b>	<b>45</b>
7.1	Filtering Effect . . . . .	45
7.2	Digital Pre-Emphasis (DPE) . . . . .	52
7.2.1	Simulation Setup . . . . .	52
7.3	Results . . . . .	55
7.4	Conclusion . . . . .	58
<b>8</b>	<b>Compensation of Nonlinearities in MZM Using DPD</b>	<b>59</b>
8.1	Introduction . . . . .	59
8.2	The Nonlinear Transfer Function of MZM . . . . .	60
8.3	Polynomial Digital Pre-Distortion (PDPD) . . . . .	60
8.3.1	Polynomial Fitting Using <code>polyfit</code> . . . . .	60
8.3.2	Polynomial Evaluation Using <code>polyval</code> . . . . .	61
8.3.3	Application to Digital Predistortion . . . . .	61
8.3.4	Applying PDPD . . . . .	62
8.4	Simulation Setup . . . . .	62



8.5	Results and Performance Evaluation . . . . .	63
8.5.1	Error Vector Magnitude (EVM) . . . . .	63
8.5.2	Maximum ODN Loss . . . . .	66
8.6	Neural Network for MZM Nonlinearity Compensation . . . . .	68
8.6.1	Neural Network Architecture . . . . .	69
8.6.2	Cost Function . . . . .	70
8.7	Steps for NN-Based Predistortion . . . . .	70
8.7.1	Data Preparation . . . . .	71
8.7.2	Neural Network Architecture . . . . .	71
8.7.3	Training Process . . . . .	72
8.7.4	Applying Predistortion . . . . .	72
8.7.5	Results and Performance Evaluation . . . . .	74
8.8	NN-DPD for Mitigating Nonlinearity Due to Low Extinction Ratio . . .	80
8.9	Complexity Comparison . . . . .	82
8.9.1	Polynomial-DPD . . . . .	82
8.9.2	Neural Network DPD (NN-DPD) . . . . .	82
8.10	Conclusion . . . . .	83
<b>9</b>	<b>Conclusions and open research lines</b>	<b>84</b>
9.1	Conclusion . . . . .	84
9.2	Future Work . . . . .	85

# Chapter 1

## Introduction

A communication system is designed to transmit information from one location to another, whether over a few kilometers or across vast transoceanic distances. This is achieved by encoding information onto an electromagnetic carrier wave, which can range in frequency from a few megahertz to several hundred terahertz. Optical communication systems utilize high-frequency waves ( 200 THz) in the near-infrared region of the electromagnetic spectrum. These systems are commonly referred to as lightwave systems, distinguishing them from microwave systems, which operate at significantly lower frequencies ( 1 GHz).

Fiber-optic communication systems are a type of lightwave system that employ optical fibers to transmit information. Since their widespread deployment in the 1980s, fiber-optic systems have revolutionized telecommunications and played a pivotal role in the development of the “information age” in the 1990s, alongside advancements in microelectronics[1].

This thesis focuses on Coherent Passive Optical Network (PON) systems, a next-generation technology for broadband access. While coherent transmission has traditionally been used for long-haul communication systems, this work investigates the feasibility of using coherent transmission in access networks. Specifically, the research explores techniques at the transmitter side to simplify coherent PON (CPON) systems and make them viable for access networks, which require cost-effective and scalable solutions.

### 1.1 Thesis Structure

This thesis is organized as follows:

- **Chapter 2** provides an overview of Passive Optical Networks (PONs), their standards, and the motivation for transitioning to Coherent PON technology.
- **Chapter 3** focuses on coherent transmission systems in optical networks, with an emphasis on the transmitter and a brief review of coherent receiver. It covers the theoretical background of Quadrature Amplitude Modulation (QAM) and the Mach-Zehnder Modulator (MZM), exploring how information is modulated into the optical signal.
- **Chapter 4** defines the modulation index parameter for the MZM and explores how the roll-off factor influences the determination of optimal modulation index values.

- **Chapter 5** introduces the Optical Distribution Network (ODN) loss concept and examines how optimizing the modulation index and roll-off factor affects achievable ODN loss values. It also discusses whether these values are feasible for Coherent PONs in access networks.
- **Chapter 6** discusses the mathematical modeling of non-ideal MZMs, focusing on the Extinction Ratio (ER). This chapter explores how the nonlinearity of the MZM impacts performance and how ER affects ODN loss.
- **Chapter 7** investigates the filtering effects at the transmitter, bandwidth limitations, and introduces the Digital Pre-Emphasis (DPE) technique. The chapter evaluates how DPE can improve the performance of PONs and compensate for bandwidth limitations at the transmitter.
- **Chapter 8** introduces a concept called Polynomial Digital Pre-Distortion (DPD) and Neural Network DPD, aimed at pre-distorting the input electrical signal to the MZM to mitigate the nonlinearities in its transfer function.
- **Chapter 9** concludes the thesis, summarizing the findings and offering an outlook on potential areas for further research and improvement.

# Chapter 2

## Passive Optical Networks (PONs)

In this chapter, we review the architecture and standards of Passive Optical Networks (PONs). We examine the PON standards established by the International Telecommunication Union Telecommunication Standardization Sector (ITU-T), as discussed in references [2] and [3].

### 2.1 What is PON?

PONs are crucial technology for delivering point-to-multipoint broadband access via passive optical fiber infrastructure. As illustrated in Figure 2.1, the optical network architecture is divided into three key segments: long-haul (backbone/core nodes), metropolitan (metro nodes), and access (access nodes). Passive Optical Networks (PONs) are predominantly utilized within the access network segment to provide high-speed connectivity to end users, such as residential, business, and mobile users. PON technology plays a crucial role in bridging the gap between metropolitan networks and individual user access, ensuring efficient delivery of broadband services in a cost-effective manner.

Introduced in the early 1990s, PONs have been deployed globally to serve residential (Fiber-to-the-Home), business (Fiber-to-the-Office), and mobile (Fiber-to-the-Cell) users. A PON system comprises an Optical Line Terminal (OLT) at the provider's central office and multiple Optical Network Units (ONUs) at customer sites, interconnected by an Optical Distribution Network (ODN). PON systems are categorized mainly into Time-Division Multiplexed (TDM) and Wavelength-Division Multiplexed (WDM) PONs. TDM-PONs share a single wavelength among users, while WDM-PONs assign individual wavelengths to each user, enhancing bandwidth allocation. Over the years, various PON standards, such as ITU-T G.983 for APON/BPON, IEEE 802.3ah for EPON, and ITU-T G.984 for GPON, have been established to ensure interoperability and performance, supporting the increasing demand for higher bandwidth and advanced services like 5G and high-definition video. Standardization continues to evolve, addressing new challenges such as latency, synchronization, and security to meet future network requirements.

Figure 2.2 shows a typical architecture of a PON. The transmission in the PON starts from an OLT situated at the CO. It is connected to an optical splitter with single-mode optical fiber.

A passive optical power splitter divides the incoming optical power into  $N$  separate paths, directing the signal to multiple clients. In an ideal splitter without excess loss, each client receives  $P/N$  of the original power  $P$ . The splitting ratio, determined by the

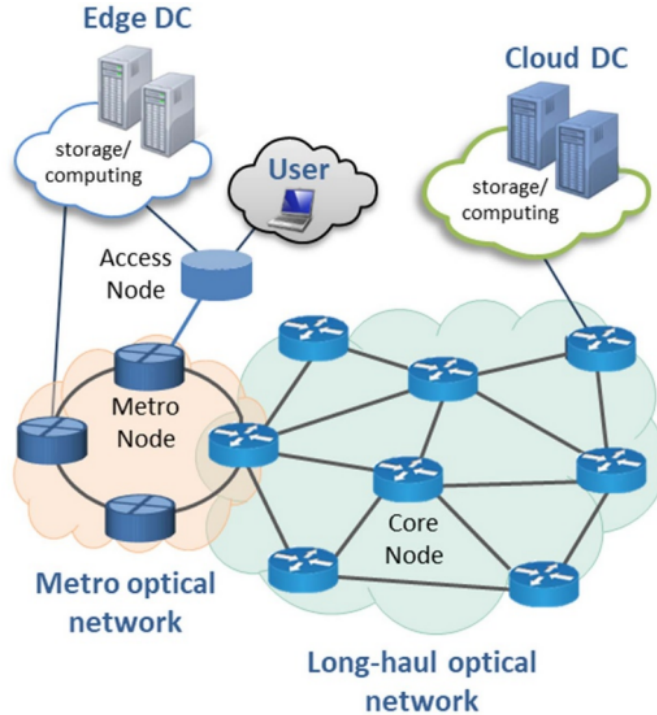


Figure 2.1: Overview of the optical network architecture illustrating the long-haul (backbone/core nodes), metropolitan (metro nodes), and access (access nodes) segments, enabling connectivity for cloud and edge infrastructures, including data centers[4].

specific application, can vary between 2 to 64, but typically values are 8, 16, or 32. After the splitter, individual single-mode fibers are connected to ONUs.

### 2.1.1 PON architectures

Time Division Multiplexing-Passive Optical Network (TDM-PON) and Wavelength Division Multiplexing-Passive Optical Network (WDM-PON) [6] are both passive optical network architectures, as shown in Figure 2.3. In TDM-PON, a passive power splitter broadcasts the same signal from the OLT to multiple Optical Network Terminals (ONTs), with ONTs identifying their data through embedded address labels.

In contrast, WDM-PON utilizes a passive WDM coupler, which routes different wavelength channels to specific ONTs, enhancing privacy and scalability. Each ONT receives only its designated wavelength, and hybrid WDM-TDMA PONs further increase scalability by supporting higher splitting ratios[7].

## 2.2 Passive Optical Network (PON) Standards

Passive Optical Networks (PONs) are fiber-optic telecommunications technology that implements a point-to-multipoint architecture. A PON consists of an Optical Line Terminal (OLT) at the service provider's central office and multiple Optical Network Units (ONUs) near end-users. PON standards define the specifications for these systems, ensuring interoperability and performance across different vendors and implementations.

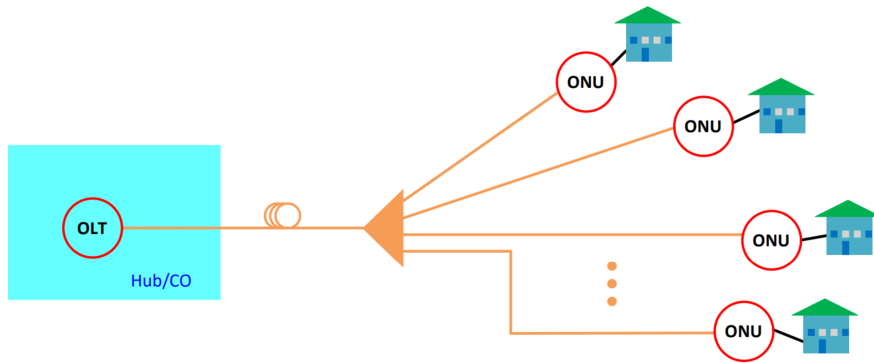


Figure 2.2: A typical architecture for PON systems [5].

## 2.3 PON standards

In Table 2.1, an overview of the key PON standards is provided, highlighting their respective data rates and typical applications. This table outlines the evolution of PON technologies, starting with APON/BPON, which offered up to 622 Mbps downstream and was primarily used for ATM-based services. As the demand for higher bandwidth grew, standards like EPON and GPON were introduced, with EPON reaching up to 10 Gbps and GPON supporting broadband internet, voice, and IPTV. The progression continues with XG-PON, offering 10 Gbps downstream for next-generation broadband, and NG-PON2, which achieves an aggregate data rate of 40 Gbps by combining multiple wavelengths, paving the way for future-proof broadband infrastructure capable of supporting significantly higher bandwidth requirements.

Figure 2.4 [9] illustrates the evolution of PON standardization, starting from G-PON and its IEEE counterpart, Ethernet PON (E-PON), along with potential future developments. The next system after G-PON was 10 Gbps PON, which was standardized in two versions: asymmetric XG-PON (ITU-T G.987 series) and symmetric XGS-PON.

Although the XG-PON standard was published in 2010, widespread deployment only began around 2016. This delay was due to the time required for operators to adopt new technologies into their networks. As a result, a 10-year cycle has emerged, where the deployment of a new system occurs a decade after its predecessor. This trend can also be observed in the wireless access market, where similar timelines apply for technology transitions.

## 2.4 ODN Standards for Different PON Classes

ODNs in PON systems involve passive optical components such as splitters and combiners, which distribute optical signals from the OLT to the ONUs. In Figure 2.5 the schematic for ODN loss is shown. Different classes of PONs have specific requirements for the ODN to ensure signal integrity and system performance.

### 2.4.1 Parameters for ODN Standards

- Loss Budget

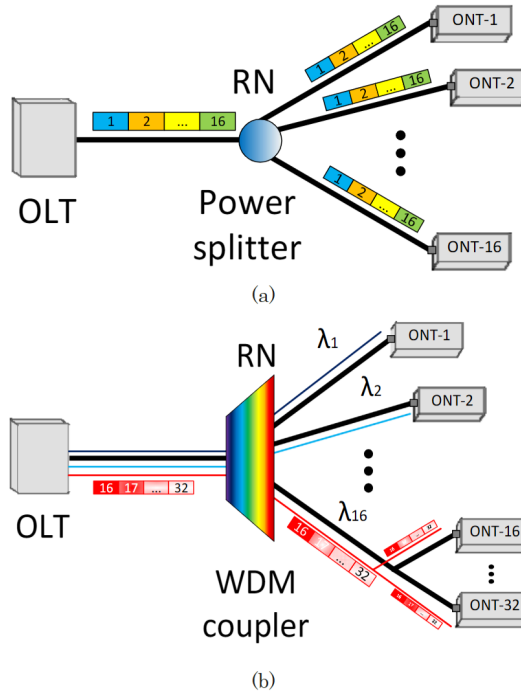


Figure 2.3: Architecture of (a) TDM-PON and (b) hybrid WDM(TDM-PON).[8]

- The total allowable loss from the OLT to the ONU, accounting for fiber, connectors, splices, and splitters.

- **Reach**

- The maximum physical distance between the OLT and the ONU.

- **Split Ratio**

- The number of ONUs that can be supported by a single OLT.

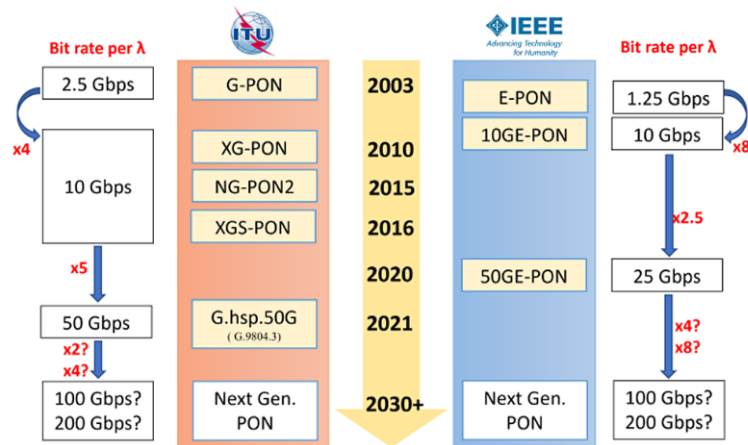


Figure 2.4: ITU and IEEE PON standards evolution.

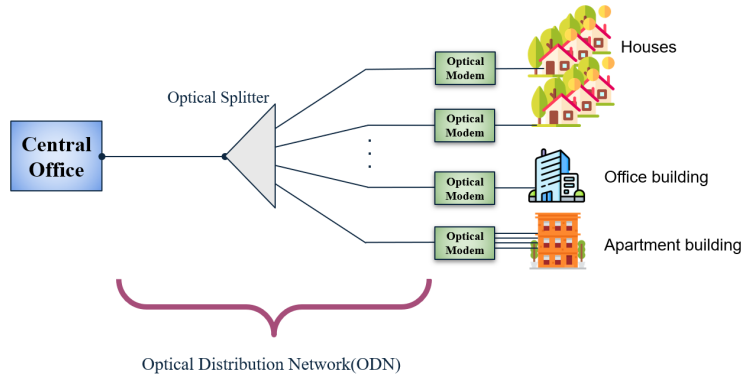


Figure 2.5: ODN loss in PON systems from transmitter at Central Office to ONU.

## 2.5 ODN Standards for Different PON Classes

In Table 2.2, the current loss budgets for various PON standards across different classes are presented. This table highlights the range of ODN standards, showing the different reach and loss budgets required for each PON class. For instance, APON/BPON standards offer up to 20 km reach with a maximum loss budget of 25 dB, while more advanced standards like GPON and NG-PON2 can extend the reach up to 60 km and accommodate loss budgets as high as 35 dB. These variations underscore the evolving requirements of PON technologies to meet the demands of increasing data rates and extended network reach.

## Coherent Passive Optical Networks (CPONs)

PONs are the leading solution for fiber-based access networks, with evolving standards that increase data rates over existing optical distribution networks (ODN). Following ITU-T's standardization of the 50 Gb/s Higher Speed PON (HS-PON) by 2021, research is now focusing on the next generation: Very High Speed PON (VHSP). VHSP is expected to follow a similar progression in bitrate as previous generations, likely reaching 200 Gb/s [10]. All PON technologies have traditionally used IM/DD because of their simple and cheap implementations. However, the chromatic dispersion (CD), which increases with the baud rate, can be a significant challenge for IM/DD at 200 Gb/s. Due to the limitations of IM/DD, coherent PON is gaining interest as a potential solution for VHSP. However, full coherent links have significantly higher complexity and cost, particularly on the optical network unit (ONU) side.

### 2.5.1 Motivation for CPON

The primary motivation for developing CPON lies in addressing the growing demand for higher data rates and better network performance. Traditional IM-DD-based PONs are nearing their limits, especially as data rates per wavelength exceed 25 Gbps. Coherent optics, which have already transformed long-haul and metro networks, present a viable solution for access networks by offering improved optical power distribution, enhanced power budgets, and the ability to support higher split ratios over longer distances.



PON Standard	Standard	Data Rates	Applications
<b>APON/BPON (ATM/Broadband PON)</b>	ITU-T G.983	Up to 622 Mbps downstream, 155 Mbps upstream	Early applications, primarily ATM-based services
<b>EPON (Ethernet PON)</b>	IEEE 802.3ah (EPON), IEEE 802.3av (10G-EPON)	1.25 Gbps (EPON), 10 Gbps (10G-EPON)	Ethernet-based services, widely used in Asia
<b>GPON (Gigabit PON)</b>	ITU-T G.984	2.488 Gbps downstream, 1.244 Gbps upstream	Broadband internet, voice, and IPTV
<b>XG-PON (10 Gigabit-capable PON)</b>	ITU-T G.987	10 Gbps downstream, 2.5 Gbps upstream	Next-generation broadband services
<b>NG-PON2 (Next-Generation PON 2)</b>	ITU-T G.989	40 Gbps aggregate (combining multiple wavelengths)	Future-proofing broadband infrastructure, supporting higher bandwidth requirements

Table 2.1: PON Standards Overview

Moreover, CPONs enable a more efficient use of spectral resources, potentially supporting data rates of 100 Gbps and higher per wavelength. This capability makes CPON attractive for operators aiming to expand their network coverage and capacity without incurring the high costs associated with deploying new fiber infrastructure.

## 2.6 Evolution of Passive Optical Networks (PON)

Passive Optical Networks (PON) have evolved significantly over the past few decades, with each generation bringing substantial advancements in data rate capabilities, standardization, and deployment scope. The recent development of Coherent Passive Optical Networks (Coh-PON) represents the next leap in this evolution, integrating coherent optical technology into TDM-PON systems. Figure 2.6 illustrates a hypothetical timeline for Coh-PON based on past PON standardization and deployment history. Here, we review the evolution of PON based on the study conducted in [11]

### 2.6.1 50G PON Standardization and Deployment

In 2021, the 50G PON standard was finalized, marking the latest generation in high-speed PON technology. Following the standardization phase, deployment of 50G PON began in 2023, allowing network operators to implement and expand this technology in real-world applications. Historically, each PON generation takes several years to move

PON Standard	Class	Reach	Loss Budget
APON/BPON	Class A	Up to 10 km	20 dB
	Class B	Up to 20 km	25 dB
EPON	Standard EPON	Up to 20 km	29 dB
	10G-EPON	Up to 20 km	29 dB
GPON	Class B+	Up to 20 km	28 dB
	Class C	Up to 60 km	35 dB
XG-PON	Class N1	Up to 20 km	29 dB
	Class N2	Up to 40 km	31 dB
NG-PON2	Class N1	Up to 20 km	29 dB
	Class N2	Up to 40 km	31 dB

Table 2.2: ODN Standards for Different PON Classes

50G PON Standard	50G PON Deployment	Coh-PON Study Starts in ITU	Coh-PON Standard	Coh-PON Systems Available	Coh-PON for 6G xHaul	Coh-PON in FTTH
2021	2023+	2024	2026+	2028+	2029+	2030+




Figure 2.6: Hypothetical timeline for Coh-PON development and deployment based on historical PON evolution [11].

from standardization to widespread deployment, typically around eight years.

## 2.6.2 Initiation of Coh-PON Studies

Building on the advancements in 50G PON, researchers in academia began studies for the next generation of PON, known as Coh-PON, in 2024. These studies aim to explore the feasibility and technical requirements for incorporating coherent optical transmission techniques into TDM-PON systems, potentially offering enhanced performance for high-capacity and long-reach applications.

## 2.6.3 Coh-PON Standardization and Initial Deployment

According to the timeline, standardization of Coh-PON is anticipated around 2026, approximately two years after the study phase. This timeline follows the typical cycle seen in previous PON generations, where a new standard is developed approximately every five to ten years. By 2028, Coh-PON systems are expected to be commercially available, with initial deployments likely targeting lower-volume applications, such as business services.

## 2.6.4 Expansion of Coh-PON Applications

The deployment of Coh-PON will gradually expand to medium- and high-volume applications. Around 2029, Coh-PON technology could support 6G xHaul networks, which

involve high-capacity transport networks for the upcoming 6G mobile networks. By 2030, Coh-PON is projected to be viable for Fiber-to-the-Home (FTTH) applications, bringing high-speed, reliable fiber connectivity to residential customers.

### 2.6.5 Challenges in CPON

Coherent Passive Optical Networks (CPON) present a promising solution for meeting the increasing demand for higher data rates in access networks. However, several challenges must be addressed to make CPONs viable for widespread adoption, especially considering the unique constraints of access network environments.

One of the primary challenges in CPON implementation is the cost and complexity associated with coherent systems. Traditionally used in long-haul networks, coherent systems rely on Erbium-Doped Fiber Amplifiers (EDFAs) to compensate for signal attenuation over long distances. However, in access networks, which typically follow a point-to-multipoint (P2MP) architecture, the use of EDFAs is not feasible due to their high cost and complexity. This necessitates the exploration of alternative solutions that can enhance the transmitted power at the transmitter side without significantly increasing system nonlinearities or costs.

Moreover, CPON systems face challenges in both upstream and downstream transmission. In the downstream direction, simplifying the optical network unit (ONU) to reduce costs can increase the bandwidth requirements of the components, complicating the receiver design. In the upstream direction, achieving high transmission power is crucial, yet without the use of EDFAs, this becomes difficult. As such, innovative approaches, such as the use of roll-off pulse shaping filters and pre-emphasis techniques, are being explored to optimize system performance while managing power levels and minimizing nonlinearity. These challenges highlight the need for careful design and optimization of CPON systems to balance performance, cost, and complexity, ensuring they meet the demands of future access networks.

### 2.6.6 Recent progress of CPON

Recent advancements in CPON have been driven by the need to address the increasing demand for higher data rates while maintaining cost-efficiency in access networks. The transition towards coherent technology in PONs, especially for very-high-speed PON (VHSP) applications, is being actively explored by researchers and industry players. One of the major contributions in this field is the work on simplified coherent optical network units (ONUs) for time-division multiplexed PON (TDM-PON) [12]. This approach uses a single polarization heterodyne receiver and an electro-absorption modulated laser (EML)-based transmitter. Recent experiments demonstrated successful bidirectional transmission over distances of 20 km and 40 km with power budgets exceeding 29 dB, showcasing the viability of coherent technology for VHSP.

Moreover, digital signal processing (DSP) has become a key enabler for coherent optical systems in PONs, allowing advanced modulation formats and increased spectral efficiency. This study [13] explored the role of DSP in various receiver architectures, including Kramers-Kronig (KK) and coherent receivers. They highlighted the importance of DSP for addressing challenges like burst-mode operation and forward error correction (FEC) in PON systems. Additionally, the integration of simplified analog coherent re-

ceivers was discussed as a potential pathway for reducing system costs while maintaining high performance.

CableLabs [5] has also made significant progress in coherent PON development by releasing the CPON architecture specification, which outlines the framework for 100 Gbps single-wavelength coherent PON. This specification highlights the need for coexistence with legacy PON technologies and point-to-point coherent transmissions, focusing on optimizing the link budget and achieving a balance between split ratio and reach. The specification describes scenarios such as a 512:1 split ratio at 20 km and an 80 km reach for rural deployments, with a target link budget of 35 dB. These advancements underscore the potential of CPON to revolutionize access networks by enabling high-capacity, cost-effective, and scalable solutions.

## 2.7 Conclusion

In conclusion, this chapter has provided an essential overview of the evolution of communication systems, specifically within the realm of optical and fiber-optic technologies. The chapter highlighted the foundational principles of optical communication, the development of Passive Optical Networks (PONs), and the role of fiber-optic systems in shaping the information age. As demands for higher data rates and efficient broadband access continue to grow, the transition from traditional Intensity Modulation/Direct Detection (IM/DD) systems to Coherent Passive Optical Networks (CPON) offers a promising pathway for next-generation access networks.

The need for coherent technology in access networks is driven by the limitations of current IM/DD-based PONs, particularly as data rates and split ratios increase. CPONs hold the potential to meet these demands by leveraging coherent detection techniques that enhance spectral efficiency and optical power budgets, thus extending the feasible reach and performance of the network. Despite the benefits, several challenges remain, including the high cost and complexity of coherent systems, which are traditionally reserved for long-haul applications, and the need for innovative solutions to simplify and optimize the CPON architecture for access network requirements.

# Chapter 3

## Fundamentals of Coherent Transmission

### 3.1 Introduction

In the evolving field of optical communications, coherent transmission has become a fundamental technology essential for modern high-capacity networks. As the demand for faster and more reliable data transmission grows, coherent transmission techniques offer significant advantages in terms of spectral efficiency, sensitivity, and robustness against impairments [14]. These qualities make them indispensable for long-haul and high-capacity optical communication systems.

### 3.2 Intensity Modulation with Direct Detection (IMDD)

Before delving into coherent transmission, it is important to understand Intensity Modulation with Direct Detection (IMDD), a traditional method used in optical communication. In IMDD systems, the primary parameter modulated is the optical power. Here's a closer look at its characteristics and limitations:

#### 3.2.1 Spectral Efficiency in IMDD

- **Modulation:** IMDD systems modulate the optical power, typically using binary modulation schemes like on-off keying (OOK), where the presence or absence of light represents binary 1 or 0, respectively.
- **Bit Rate and Symbol Rate:** In IMDD systems using binary modulation, 1 bit is transmitted per symbol. Therefore, the bit rate ( $R_b$ ) is equal to the symbol rate ( $R_s$ ), i.e.,  $R_b = R_s$ .
- **Occupied Spectrum:** Assuming the minimum possible occupied spectrum, the bandwidth ( $B$ ) is equal to the symbol rate,  $B = R_s = R_b$ .

This implies that the spectral efficiency of IMDD systems is severely limited. Even though higher-order modulation schemes like Pulse Amplitude Modulation (PAM-4 or PAM-8) can theoretically increase the spectral efficiency to 2 or 3 bits/s/Hz, these schemes suffer from poor noise tolerance and limited transmission distance, making them impractical for long-haul, high-capacity systems.

## 3.3 Coherent Transmission Fundamentals

Coherent transmission offers a solution to the limitations of IMDD by leveraging the full potential of the optical field. Light, being an electromagnetic wave, has an electric field that can be described analytically as:

$$E(t) = A(t) \cdot e^{j\phi(t)} \cdot e^{j2\pi f_0 t}$$

Where:

- $A(t)$  represents the amplitude of the electric field.
- $\phi(t)$  is the phase of the electric field.
- $f_0$  is the carrier frequency.
- $e^{j2\pi f_0 t}$  represents the carrier wave.

In coherent transmission, both the amplitude  $A(t)$  and phase  $\phi(t)$  can be modulated to encode information, significantly enhancing the data-carrying capacity and spectral efficiency of the system. Here's how it works:

### 3.3.1 I/Q Modulation

I/Q modulation is a cornerstone of coherent transmission, involving the modulation of in-phase (I) and quadrature (Q) components. Mathematically, this can be described as:

$$\begin{aligned} \text{In-phase (I) Component : } & I(t) = A_I \cos(\omega t + \phi_I) \\ \text{Quadrature (Q) Component : } & Q(t) = A_Q \sin(\omega t + \phi_Q) \end{aligned}$$

The combined signal  $S(t)$  is then:

$$S(t) = I(t) + jQ(t) = A_I \cos(\omega t + \phi_I) + jA_Q \sin(\omega t + \phi_Q)$$

### 3.3.2 PM-QPSK Modulation

PM-QPSK is an advanced modulation format used in coherent transmission. It involves encoding data onto the phase of the optical carrier, with two orthogonal polarization states:

- **Phase Modulation:** In QPSK, each symbol represents two bits, resulting in four possible phase states:  $0, \pi/2, \pi, 3\pi/2$ .
- **Polarization Multiplexing:** The modulated signal is split into two orthogonal polarization states, X and Y. Each polarization carries a QPSK signal, doubling the data rate.

The transmitted PM-QPSK signal can be expressed as:

$$S(t) = S_X(t) + S_Y(t)$$

Where:

$$S_X(t) = A_X e^{j(\omega t + \theta_X)} \quad \text{and} \quad S_Y(t) = A_Y e^{j(\omega t + \theta_Y)}$$

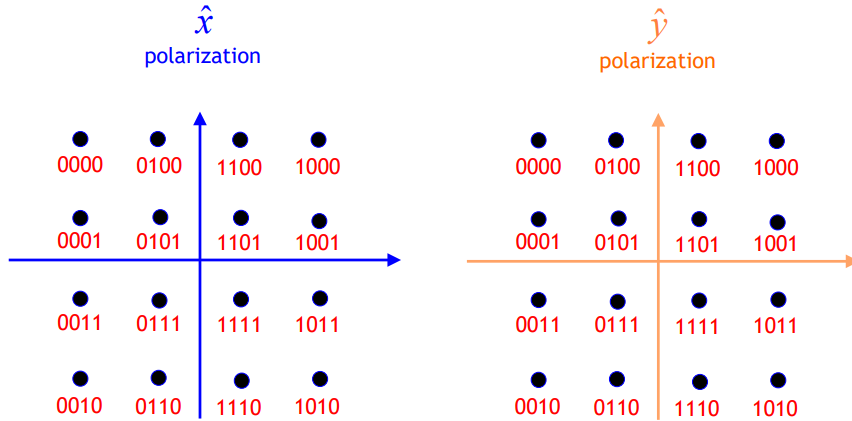


Figure 3.1: PM-16QAM Constellation Signal shape

### 3.3.3 PM-16QAM Modulation

PM-16QAM offers even higher spectral efficiency by utilizing both amplitude and phase:

- **Amplitude and Phase Modulation:** In 16QAM, each symbol represents four bits, with 16 possible states defined by different amplitude and phase combinations.
- **Polarization Multiplexing:** Similar to PM-QPSK, the signal is split into two orthogonal polarization states, each carrying a 16QAM signal.

The transmitted PM-16QAM signal is:

$$E(t) = E_X(t) + E_Y(t)$$

Where each polarization component is:

$$E_X(t) = A_X e^{j(\omega t + \theta_X)} \quad \text{and} \quad E_Y(t) = A_Y e^{j(\omega t + \theta_Y)}$$

In PM-16QAM, the amplitudes  $A_X$  and  $A_Y$  and phases  $\theta_X$  and  $\theta_Y$  correspond to the 16QAM constellation points, allowing for a higher bit rate per symbol. In Figure 3.1, the shape of the constellation of PM-16QAM is shown in both x and y polarizations.

This diagram 3.2 illustrates the setup for generating a PM-16QAM signal using MZMs. The setup includes two laser sources, each driving a pair of MZMs for both in-phase (I) and quadrature (Q) components in x and y polarizations. The output from each pair is combined with a  $\pi/2$  phase shift and then combined via a polarization beam splitter (PBS) to form the PM-16QAM signal. The electric field components are represented as  $E_{Rx}(t)$ ,  $jE_{Ix}(t)$ ,  $E_{Ry}(t)$ , and  $jE_{Iy}(t)$  in the x and y polarizations, respectively.

## 3.4 Mach-Zehnder Modulator (MZM)

A Mach-Zehnder Modulator (MZM) is an optical device used in fiber-optic communication systems to modulate the amplitude and/or phase of an input light signal. It operates based on the principle of interference, splitting the input light into two arms, applying a voltage-induced phase shift in each arm, and then recombining the light. The resulting

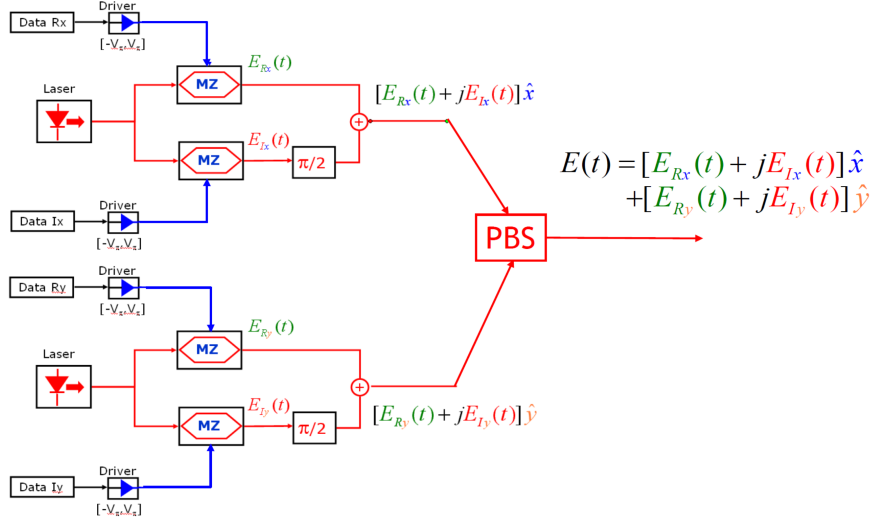


Figure 3.2: Configuration for Generating PM-16QAM Constellation Signal

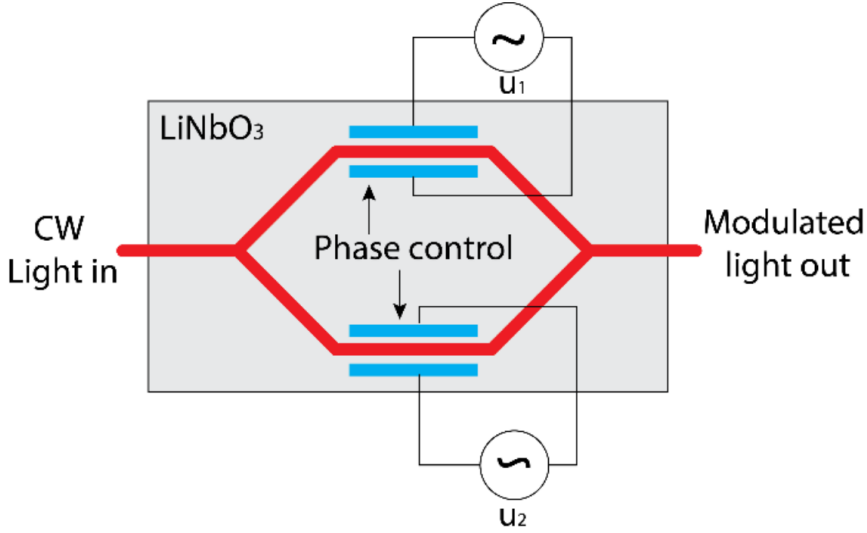


Figure 3.3: Mach-Zehnder modulator [4]

interference pattern at the output depends on the relative phase shifts introduced in the two arms. As shown in Figure 3.3, the MZM can operate in two distinct modes: push-push and push-pull. In push-push mode, where  $u_1(t) = u_2(t)$ , an identical phase shift is induced in both arms, resulting in pure phase modulation. Conversely, in push-pull mode, where  $u_1(t) = -u_2(t)$ , one arm experiences a phase shift opposite to that of the other, leading to chirp-free amplitude modulation[15].

## Key Parameters

- $E_{in}(t)$ : Input electric field.
- $E_{out}(t)$ : Output electric field.
- $v_p$ : Voltage applied to the first arm of the MZM.



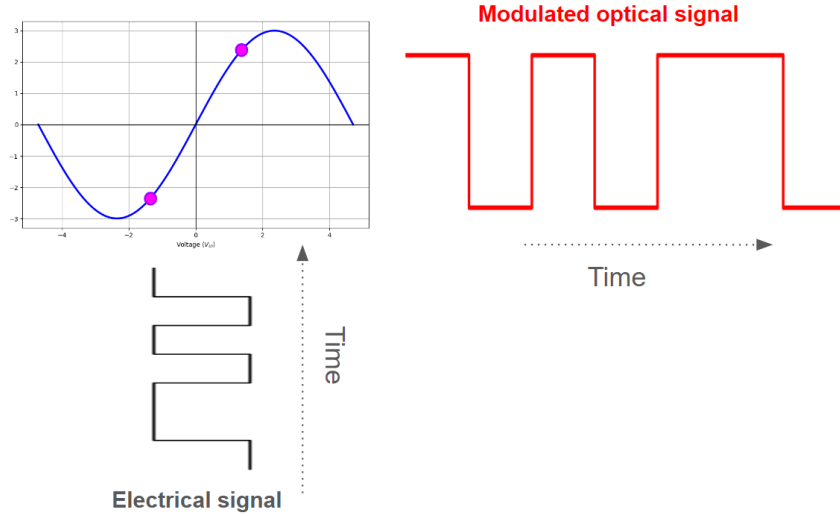


Figure 3.4: Schematic of Electrical Signal Modulation onto Optical Signal Using a MZM

- $v_q$ : Voltage applied to the second arm of the MZM.
- $v_\pi$ : Half-wave voltage of the MZM. This is the voltage required to induce a phase shift of  $\pi$  radians.
- $ER$ : Extinction ratio. This parameter indicates the efficiency of the modulator in suppressing the light in the off state.

## Transfer Function

The transfer function of a Mach-Zehnder Modulator (MZM) defines the relationship between the output optical field and the input electrical signal, accounting for factors such as the voltages applied to the modulator's arms and the extinction ratio. In Figure 3.4, we illustrate how the peak and trough values of a two-level electrical signal are mapped onto the optical signal output. The maximum amplitude of the resulting optical signal is influenced by the modulation scheme applied to the electrical input, which determines how the electrical signal translates into the optical field.

### General Case

$$E_{\text{out}}(t) = E_{\text{in}}(t) \frac{1}{2} \left\{ \sin\left(\frac{\pi v_p}{2v_\pi}\right) - \frac{j}{\sqrt{ER}} \cos\left(\frac{\pi v_p}{2v_\pi}\right) + j \left[ \sin\left(\frac{\pi v_q}{2v_\pi}\right) - \frac{j}{\sqrt{ER}} \cos\left(\frac{\pi v_q}{2v_\pi}\right) \right] \right\}$$

### Ideal Case ( $ER = \infty$ )

In the ideal case where the extinction ratio is infinite, the modulator perfectly suppresses the off-state light. The transfer function simplifies to:

$$E_{\text{out}}(t) = E_{\text{in}}(t) \frac{1}{2} \left\{ \sin\left(\frac{\pi v_p}{2v_\pi}\right) + j \sin\left(\frac{\pi v_q}{2v_\pi}\right) \right\}$$

## Detailed Explanation

1. **Input Electric Field ( $E_{\text{in}}(t)$ ):** This is the electric field of the light entering the MZM. It can be represented as a sinusoidal wave with a certain amplitude and frequency.
2. **Sinusoidal and Cosine Terms:**
  - $\sin\left(\frac{\pi v_p}{2v_\pi}\right)$  and  $\sin\left(\frac{\pi v_q}{2v_\pi}\right)$ : These terms represent the modulation effect of the applied voltages ( $v_p$  and  $v_q$ ) on the light's phase. The sine function indicates how the phase shift depends on the applied voltage relative to the half-wave voltage ( $v_\pi$ ).
  - $\cos\left(\frac{\pi v_p}{2v_\pi}\right)$  and  $\cos\left(\frac{\pi v_q}{2v_\pi}\right)$ : These terms also relate to the phase modulation but are scaled by the extinction ratio. They represent the residual light that is not fully suppressed due to a finite extinction ratio.
3. **Extinction Ratio (ER):**
  - The term  $\frac{1}{\sqrt{ER}}$  indicates the efficiency of the modulator. Higher ER values mean better suppression of the off-state light. In the ideal case where  $ER \rightarrow \infty$ , this term goes to zero, simplifying the expression.
4. **Imaginary Unit ( $j$ ):**
  - The presence of  $j$  (the imaginary unit) indicates a phase shift of 90 degrees, corresponding to a quarter-wavelength shift. This is characteristic of the output field in an MZM.

## 3.5 Definition of Modulation Index

The modulation index is a critical parameter in optical communication systems, particularly when dealing with coherent receivers and advanced modulation formats such as PM-QPSK (Polarization-Multiplexed Quadrature Phase Shift Keying) and PM-16QAM (Polarization-Multiplexed 16-Quadrature Amplitude Modulation). The modulation index is defined as follows [16]:

$$m_{\text{index}} = \frac{v_{\text{pp}}}{v_\pi}$$

### Parameters of MZM:

The parameters of MZM  $v_{\text{pp}}$  and  $v_\pi$  are shown based on the 4-level signal in Figure 3.5.

1. **Peak-to-Peak Voltage ( $v_{\text{pp}}$ ):**
  - This is the difference between the maximum and minimum voltages applied to the modulator. It represents the full range of the voltage swing that drives the modulator.
2. **Half-Wave Voltage ( $v_\pi$ ):**

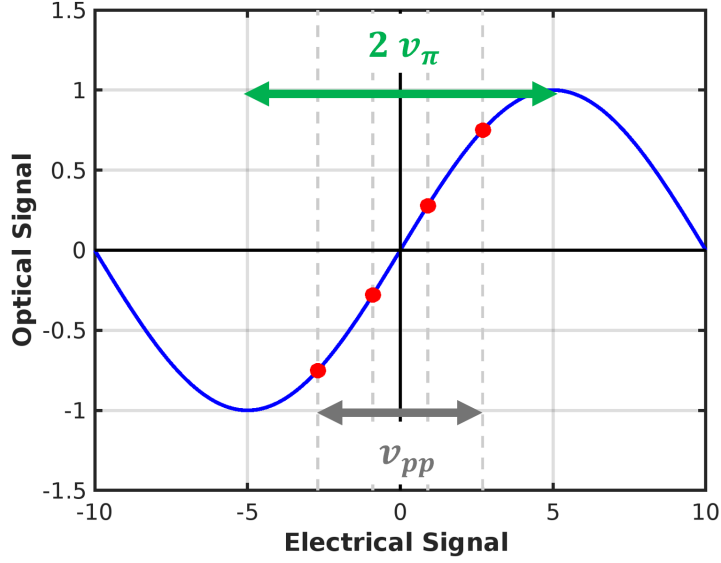


Figure 3.5: MZM Transfer Function - Electrical Signal vs. Optical Signal.

- The half-wave voltage is the voltage required to induce a phase shift of  $\pi$  radians in the modulator. This is a key characteristic of the modulator, indicating its sensitivity to the applied voltage.

### 3. Modulation Index ( $m_{\text{index}}$ ):

- The modulation index is a dimensionless parameter that quantifies the effectiveness of the modulation. It is the ratio of the peak-to-peak voltage to the half-wave voltage.
- A higher modulation index indicates a stronger modulation effect, meaning the modulator is driven more strongly relative to its half-wave voltage.

## 3.6 Coherent Receiver

The coherent receiver is a component in optical communication systems, designed to detect all four transmitted signal components. These components include the real and imaginary parts of the electric field in both x- and y-polarizations. In this section, we explain how the coherent receiver operates.

### 3.6.1 Signal Components

A typical optical signal can be represented as:

$$E_{Tx}(t) = [E_{Rx}(t) + jE_{Ix}(t)] \hat{x} + [E_{Ry}(t) + jE_{Iy}(t)] \hat{y} \quad (3.1)$$

where  $E_{Rx}(t)$  and  $E_{Ix}(t)$  are the real and imaginary components of the signal in the x-polarization, and  $E_{Ry}(t)$  and  $E_{Iy}(t)$  are the real and imaginary components in the y-polarization.

### 3.6.2 Basic Photodetection

In a basic photodiode, the optical signal is converted into an electrical current proportional to the square of the electric field magnitude:

$$i(t) \propto E(t) \cdot E(t)^* \quad (3.2)$$

Substituting for  $E_{Tx}(t)$ :

$$\begin{aligned} E(t) \cdot E(t)^* &= \{[E_{Rx}(t) + jE_{Ix}(t)] \hat{x} + [E_{Ry}(t) + jE_{Iy}(t)] \hat{y}\} \\ &\quad \cdot \{[E_{Rx}(t) - jE_{Ix}(t)] \hat{x} + [E_{Ry}(t) - jE_{Iy}(t)] \hat{y}\} \\ &= |E_{Rx}(t)|^2 + |E_{Ix}(t)|^2 + |E_{Ry}(t)|^2 + |E_{Iy}(t)|^2 \propto P(t) \end{aligned} \quad (3.3)$$

In this case, all phase and polarization information is lost because the photodiode only detects the total power  $P(t)$ .

### 3.6.3 Detection by Interference

To recover the phase and polarization information, a local oscillator (LO) signal is introduced at the receiver. The resulting photocurrent is proportional to the interference between the received signal  $\vec{E}_{ph}(t)$  and the LO  $\vec{E}_{LO}$ :

$$i(t) \propto \left| \vec{E}_{ph}(t) + \vec{E}_{LO} \right|^2 = \left[ \vec{E}_{ph}(t) + \vec{E}_{LO} \right] \cdot \left[ \vec{E}_{ph}(t) + \vec{E}_{LO} \right]^* \quad (3.4)$$

To detect a specific component, we align the LO with that component. For example, to detect the real part of the x-polarization, we use:

$$\vec{E}_{LO}(t) = E_{LOx} \hat{x} \quad (3.5)$$

The resulting photocurrent becomes:

$$\begin{aligned} i(t) &\propto \left| \vec{E}_{ph}(t) + E_{LOx} \hat{x} \right|^2 = \left[ \vec{E}_{ph}(t) + E_{LOx} \hat{x} \right] \cdot \left[ \vec{E}_{ph}(t) + E_{LOx} \hat{x} \right]^* \\ &= |E_{Rx}(t)|^2 + |E_{Ix}(t)|^2 + |E_{Ry}(t)|^2 + |E_{Iy}(t)|^2 + |E_{LOx}|^2 \\ &\quad + 2E_{LOx}E_{Rx}(t) \\ &= P_{ph}(t) + P_{LOx} + 2E_{LOx}E_{Rx}(t) \end{aligned}$$

In this equation, the term  $2E_{LOx}E_{Rx}(t)$  represents the desired real part of the x-polarization, while the terms  $P_{ph}(t)$  and  $P_{LOx}$  are unwanted power components.

### 3.6.4 Eliminating Unwanted Power Components

To eliminate the unwanted power components, balanced detection is used. The idea is to launch opposite-sign LO signals and subtract the resulting photocurrents. For an LO with opposite sign:

$$\begin{aligned} \bar{i}(t) &\propto \left| \vec{E}_{ph}(t) - E_{LOx} \hat{x} \right|^2 \\ &= P_{ph}(t) + P_{LOx} - 2E_{LOx}E_{Rx}(t) \end{aligned}$$

By subtracting the two photocurrents:

$$i(t) - \bar{i}(t) \propto 4E_{LOx}E_{Rx}(t) \quad (3.6)$$

This eliminates the unwanted squared terms and amplifies the signal component of interest. This setup is known as a balanced detector.

### 3.6.5 Detecting All Components

To detect all four components (real and imaginary parts of both x- and y-polarizations), four balanced detectors are used, each aligned with one of the components. A special optical device called a 90-degree hybrid is used to split the LO into multiple copies, with each copy phase-shifted by 90 degrees. This allows for the extraction of all four components.

## 3.7 DSP in Coherent Receivers

After the photodiodes detect the optical signal, the receiver processes the electrical signals using Digital Signal Processing (DSP) [17] to correct impairments, recover the transmitted data, and compensate for system imperfections. The DSP chain involves several key steps, which are detailed below.

### Amplification and Analog-to-Digital Conversion (ADC)

Once the signals are detected by the photodiodes, they are first amplified by *Trans-impedance Amplifiers (TIAs)* to strengthen the weak electrical signals resulting from photodetection. The amplified signals are then digitized using *Analog-to-Digital Converters (ADCs)* to enable further processing in the digital domain. The four signals—representing the real and imaginary components of both x- and y-polarizations—are now prepared for digital processing.

### IQ Imbalance Compensation

The first DSP operation is *IQ imbalance compensation*, which corrects any amplitude, phase, or timing mismatches between the in-phase (I) and quadrature (Q) components. These mismatches can occur due to imperfections in the IQ modulator or receiver components. The IQ imbalance can lead to significant performance degradation, especially in advanced modulation formats, if left uncompensated. Compensation algorithms restore the proper alignment between the I and Q components, ensuring orthogonality. Techniques such as *Gram-Schmidt orthogonalization* or *Lowdin orthogonalization* may be used to achieve this.

### Digital Equalization

The next step in the DSP chain is *digital equalization*, which compensates for the linear impairments introduced by the optical fiber channel, such as *Chromatic Dispersion (CD)* and *Polarization Mode Dispersion (PMD)*. These impairments can cause pulse spreading

and intersymbol interference (ISI), especially over long distances. Equalization is divided into two stages:

- **Static Equalization:** This compensates for constant, predictable distortions such as CD.
- **Dynamic Equalization:** Adaptive filters are used to track and compensate for time-varying phenomena like PMD, which can change over time due to temperature fluctuations or fiber movement.

Adaptive equalization adjusts in real-time to the changing channel conditions using algorithms like the *Least-Mean-Square (LMS)* method.

## Timing Recovery

Precise synchronization between the transmitter and receiver is critical in optical communications. The DSP performs *timing recovery* to correct any timing errors, which may result from clock drift or jitter. Incorrect timing can lead to misalignment of data samples, causing significant errors in data recovery. DSP algorithms estimate and correct the symbol timing to ensure proper alignment with the transmitted symbols.

## Frequency and Phase Recovery

The next step is *frequency and phase recovery*, which compensates for the frequency mismatch between the transmitting laser and the local oscillator (LO) at the receiver. Additionally, phase recovery compensates for *phase noise* introduced by both the transmitter and receiver lasers. These steps are essential for ensuring accurate coherent detection. Common techniques used for this purpose include *Phase-Locked Loops (PLLs)* and *Maximum Likelihood Phase Estimation (MLPE)*.

## Symbol Estimation and Decoding

After compensating for the various impairments, the DSP estimates the transmitted symbols and performs *Forward Error Correction (FEC)*, is applied to detect and correct any errors that occurred during transmission. This step is crucial in improving the *Bit Error Rate (BER)* performance of the system, especially in the presence of noise and channel impairments.

## Nonlinear Impairment Compensation

In long-haul optical systems, the transmitted signal is affected by *nonlinear effects* such as *Self-Phase Modulation (SPM)* and *Cross-Phase Modulation (XPM)*. These nonlinearities can degrade the signal quality over extended distances. Advanced DSP algorithms are employed to compensate for these nonlinear impairments, further improving the received signal quality.

## 3.8 Conclusion

In this chapter, we reviewed the core components of coherent transceivers, focusing on the transmitter and receiver. At the transmitter, the Mach-Zehnder Modulator (MZM) modulates the optical signal, enabling advanced modulation formats like QAM to improve spectral efficiency. At the receiver, coherent detection, with the help of a local oscillator (LO), allows for the recovery of the signal's amplitude and phase, ensuring full extraction of polarization information.

Digital Signal Processing (DSP) is essential in compensating for transmission impairments such as chromatic dispersion (CD), polarization mode dispersion (PMD), and laser phase noise. It also corrects hardware imperfections like IQ imbalance and timing errors, enabling accurate data recovery.

While DSP-based coherent transceivers have revolutionized long-haul networks, extending this technology to shorter-reach systems faces challenges due to power consumption and cost constraints. However, with ongoing advancements, DSP is anticipated to play a crucial role in future optical networks, particularly in Coherent PON technology, where designing low-cost, low-complexity DSP receivers will be essential for widespread adoption.

# Chapter 4

## Impact of Modulation Index and Roll-Off on BER

In this chapter, we examine the impact of the modulation index, a parameter previously discussed for modulating electrical signals onto optical signals using a Mach-Zehnder Modulator (MZM). Additionally, we perform simulations for pulse shaping with a raised-cosine (RC) filter using different roll-off factors. The main goal of this chapter is to see how the parameters mentioned can effect on the BER and find the optimum values of the modulation index and roll-off which leads to the best performance in transmission for different modulation formats.

### 4.1 Problem Statement

In optical communication systems, **Mach-Zehnder Modulators (MZM)** is used for converting electrical signals into optical signals. However, the challenge arises from the **nonlinear transfer function** of the MZM which we have seen in the previous chapter, it follows a sinusoidal response. The transfer function is typically represented as:

$$E_{\text{out}} \propto \sin\left(\frac{\pi v_p}{2V_\pi}\right)$$

This sinusoidal transfer function creates **linear** and **nonlinear regions**. The **linear region** of the MZM's response is near the center of the transfer curve, where the input-output relationship is approximately linear. In contrast, the **nonlinear region** is encountered when the MZM is driven with higher modulation levels, which results in increased transmitted power but also introduces signal distortion.

The challenge is to **balance the trade-off** between **higher transmitted power** and **nonlinear distortion**. Increasing the modulation index boosts the transmitted optical power, but it also causes more distortion due to the nonlinearity. The focus of this work is to determine the **optimum modulation index**  $m_{\text{index}} = \frac{V_{\text{pp}}}{V_\pi}$  that maximizes transmitted power while keeping distortion under acceptable limits.



## 4.2 Balancing Nonlinearity and Transmitted Power

### Low Modulation Index

When the modulation index is low, the MZM operates primarily within the **linear region** of its transfer function. This results in lower nonlinearity and thus less signal distortion. However, **transmitted power** is also lower, as the modulation index is not fully utilizing the MZM's capability.

### High Modulation Index

As the modulation index increases, the MZM is driven into its **nonlinear region**. This results in higher transmitted power, which is advantageous for longer-distance transmissions and higher signal strength at the receiver. The downside is that the signal suffers from **distortion**, including **harmonic distortion** and **intermodulation**, which can degrade signal integrity and lead to higher BER. The optimization is based on determining the point where increasing the modulation index leads to diminishing returns in terms of signal quality. This point, defined as  $m_{\text{opt}}$ , is the modulation index where the system achieves the **maximum transmitted power** with **minimal nonlinearity**.

Thus, the problem lies in finding an **optimum modulation index** that provides sufficient power without introducing excessive distortion. This trade-off between power and nonlinearity is the focus of our work.

In Figure 4.1, we illustrate the 16QAM constellation of the signal after passing through the MZM for various modulation indices. As the modulation index increases, the signal encounters the nonlinear region of the MZM's transfer function, causing unequal spacing between neighboring constellation points and resulting in a distorted constellation shape.

In Figure 4.2, we show one quadrant of the 16QAM constellation for three different modulation indices, alongside the MZM transfer function for reference.

## 4.3 Novel Idea: Optimizing the Modulation Index

Our approach introduces a novel method for finding the **optimal modulation index** that balances **nonlinearity** and **transmitted power**. By treating both the **modulation index** and the **roll-off factor** of the pulse shaping filter as variable parameters in our simulations, we achieve this optimization.

### Main parameters of transmission

- **Modulation Index** ( $m_{\text{index}}$ ): We vary the modulation index to observe how it impacts both transmitted power and signal distortion.
- **Roll-Off Factor**: The **roll-off factor** of the pulse shaping filter is another variable that influences the **bandwidth efficiency** and **inter-symbol interference (ISI)**. By adjusting the roll-off factor, we can control the signal bandwidth, which helps mitigate the nonlinear effects of the MZM.

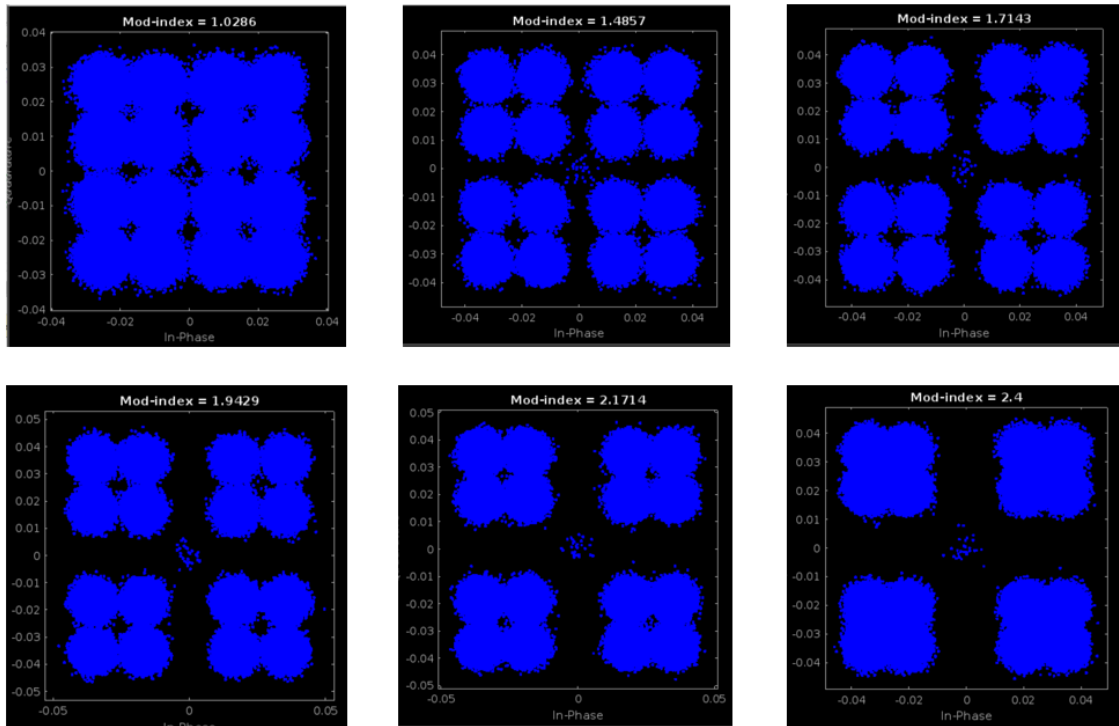


Figure 4.1: 16QAM constellation for different modulation indices.



Figure 4.2: One quadrant of the 16QAM constellation displayed for different modulation indices.

- **Objective:** The goal is to find the **optimal modulation index** ( $m_{\text{opt}}$ ) that maximizes the **transmitted optical power** while maintaining an acceptable level of distortion.

## Impact of Roll-Off Factor

- The **roll-off factor** controls the bandwidth of the transmitted signal and the degree of **inter-symbol interference (ISI)**. A **lower roll-off** can help reduce ISI, but it may also introduce bandwidth inefficiencies.
- By **optimizing both the modulation index** and the **roll-off factor**, we can achieve better signal quality while maintaining higher transmitted power, even when operating near the nonlinear region of the MZM.

## 4.4 Simulation Setup

The simulation setup 4.3 includes components for a simplified coherent transmission system with a fixed value of AWG noise power and common ODN loss values. At the transmitter, we generate a PM-QPSK or PM-16QAM sequence and apply a Raised Cosine (RC) FIR pulse-shaping filter. RC filter delay is fixed to 60 (samples). The signal is then modulated using an IQ-MZM, with the laser power fixed at 12 dBm.

The channel includes impairments such as attenuation and AWG noise. At the receiver, we have an ADC and a coherent DSP receiver. The main component of the coherent DSP receiver is its equalizer. Since PON distances do not introduce significant fiber nonlinearity or chromatic dispersion, the DSP focuses on equalization and demodulation of the received signal. The baud rate is set to 28 Gbaud and the noise bandwidth is equal to the baud rate, and the noise density is  $2 * 10^{-17} \text{W/Hz}$ .

The equalizer used in the DSP implementation is an LMS Decision-Aided (LMS-DA) equalizer operating in complex mode. The equalizer has 80 taps, providing the necessary filter length to address channel impairments. Additionally, the equalizer uses 50 symbols for its carrier phase estimation (CPE) memory, ensuring accurate phase recovery and signal demodulation.

We have used a raised cosine (RC) pulse shaping filter at the transmitter (TX) and an identical matching filter at the receiver (RX). The roll-off factor, a crucial parameter in our simulations, influences the system's behavior. In Figure 4.4, we plotted the RC pulse shaping in both the time and frequency domains.

When we increase the roll-off factor, the time-domain pulse becomes less compact, resulting in a broader pulse width. This increased roll-off reduces the risk of inter-symbol interference (ISI) since the pulse tails decay more gradually, leading to less temporal overlap between adjacent symbols.

On the contrary, in the frequency domain, as the roll-off factor increases, the frequency response of the RC filter becomes more spread out, with a wider main lobe. This means that the transition between the passband and stopband becomes smoother but at the expense of increased bandwidth occupancy. A higher roll-off factor allows the filter to more effectively suppress out-of-band frequencies, which reduces adjacent channel interference, but it also requires a larger bandwidth, which can be a limiting factor in bandwidth-constrained systems.

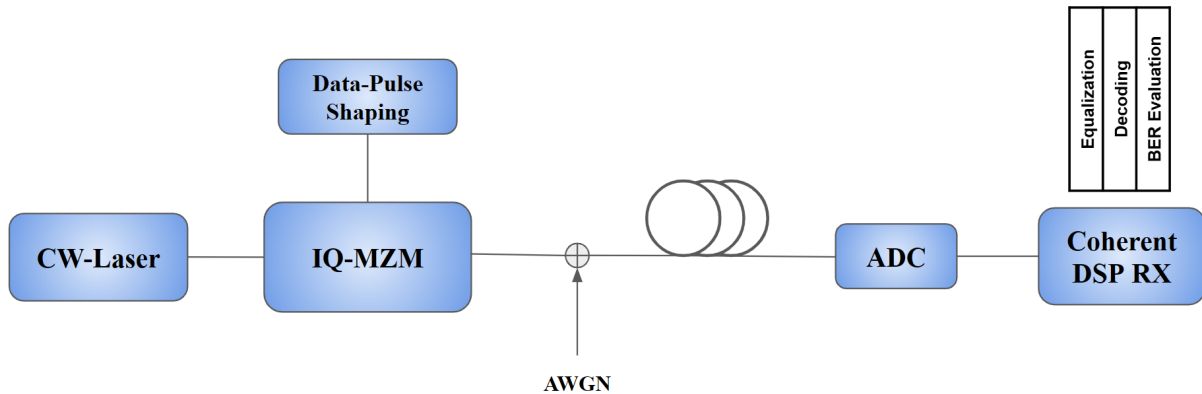


Figure 4.3: Simplified scheme of a coherent PON

#### 4.4.1 DSP Receiver Overview

The DSP receiver in this simulation setup is designed to handle various signal impairments encountered in coherent optical communication systems, including chromatic dispersion (CD), phase noise, and signal alignment. The key components and processing steps in the DSP receiver are outlined below:

- **Chromatic Dispersion (CD) Compensation:** If applicable, CD compensation is applied to counteract dispersion effects from long fiber transmission.
- **Matched Filtering:** A matched filter is applied to maximize the signal-to-noise ratio (SNR) by aligning the filter characteristics to the transmitted signal.
- **Adaptive Equalization:** An adaptive equalizer is employed to mitigate channel impairments such as residual CD and polarization mode dispersion (PMD).
- **Carrier Phase Estimation (CPE):** CPE is crucial in coherent optical systems for correcting phase noise from lasers, aligning the signal phase to reduce phase distortions.
- **Bit Error Rate (BER) Calculation:** Finally, the receiver calculates the BER to evaluate the system's performance.

Each of these steps involves parameters that define the receiver's behavior and impact the overall performance. The parameters used in the simulation are explained in detail below.

#### Explanation of DSP Parameters

##### 4.4.2 General Parameters

- **nsps\_comp** (Number of Samples Per Symbol for Compensation): Defines the over-sampling ratio. With `nsps_comp = 2`, the signal is processed at twice the symbol rate, which is common in coherent receivers for more accurate timing and phase adjustments.

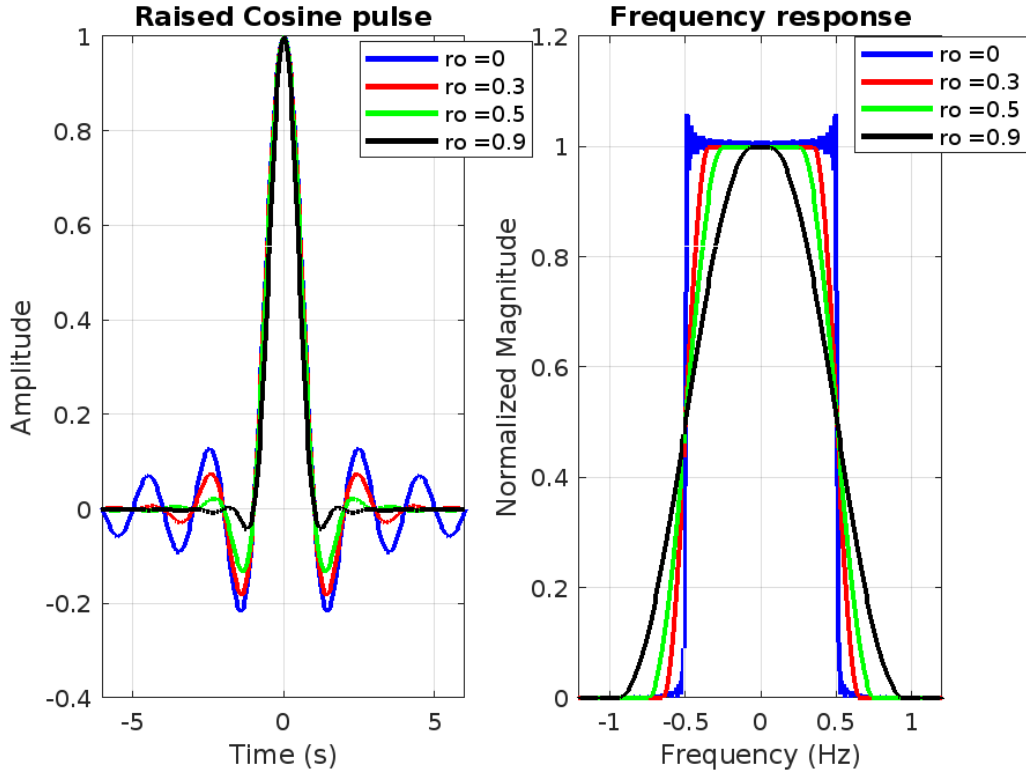


Figure 4.4: RC pulse shaping filter in the time and frequency domain for different values of roll-off factors.

- `ber_pp` (Pattern Periods for BER Calculation): Set to 4, this indicates the number of pattern periods over which the BER is calculated.

### Equalizer Parameters

The equalizer corrects channel distortions and mitigates residual impairments from dispersion or PMD. The key parameters are as follows:

- `eq_methods` (Equalizer Methods): Defined as `{'lms-da'; 'lms-da'}`, this specifies that a Least Mean Squares (LMS) Decision-Aided equalizer is used for both polarizations.
- `eq_mode` (Equalizer Mode): Set to `'complex'`, indicating that the equalizer is operating in complex mode, which is suitable for complex signals in coherent systems.
- `eq_mus` (Step Sizes): Defined as `[1e-3; 1e-4]`, these values are the step sizes for the LMS algorithm in the two polarizations, determining the convergence speed of the equalizer.
- `eq_Ntaps` (Number of Taps): Set to 80 taps, providing the equalizer with a sufficient number of taps to address channel distortions.
- `eq_Mlms` (Equalizer Memory): Specifies the equalizer's memory depth, set to 50.

- `eq_Ks` (Symbol Rate): Set to `[120e3; Inf]`, defining the cutoff rates for each polarization.

### Carrier Phase Estimation (CPE) Parameters

The CPE is responsible for correcting the phase noise of the signal and operates based on various strategies. The parameters governing its behavior are:

- `cpe_strategy`: Set to `'da'`, which indicates a Data-Aided CPE approach. Other common strategies include `'bps'` (Blind Phase Search) and `'vv'` (Viterbi & Viterbi).
- `cpe_conj`: A logical array set to `false` for both polarizations, indicating that conjugate operations are not applied in phase correction.
- `cpe_memory`: Set to 0, meaning that no additional memory is applied for the CPE, useful in low-phase-noise conditions.
- `cpe_blocksize`: Specifies the block size for CPE at 512, affecting the block processing of phase recovery.
- `cpe_sym` (Constellation Rotation Symmetry): Set to  $\pi/2$ , this parameter defines the rotational symmetry for QAM constellations, where a rotation of  $\pi/2$  is typical.

### Chromatic Dispersion (CD) and Center Frequency Parameters

- `CD`: Set to 0 in this simulation setup, indicating that no chromatic dispersion compensation is applied (for example, in a back-to-back scenario where dispersion is minimal).
- `f0` (Central Frequency): Specifies the absolute central frequency of the optical carrier in Hz, necessary for spectral alignment and filtering.

### Additional DSP Settings

- `Ntx` (Number of Transmit Waveforms): Indicates the number of transmit waveforms, used for separating different polarizations during signal alignment.
- `only_eq`: If set to `false`, this means the DSP does not only perform equalization but includes phase correction, filtering, and other processes as well.

#### 4.4.3 Step-by-Step Workflow in the Simulation

The DSP receiver in the simulation follows these steps with the specified parameters:

1. **Pre-filtering**: If required, a pre-filter (e.g., root-raised-cosine filter) is applied to the received signal.
2. **Chromatic Dispersion (CD) Compensation**: This optional step compensates for any accumulated CD in the transmission link.
3. **Downsampling**: After compensation, the received signal is downsampled to reduce the sample rate to twice the symbol rate (`nsps_comp = 2`).

4. **Matched Filtering:** A Raised Cosine (RC) filter is applied to match the receiver filter to the transmit filter.
5. **Adaptive Equalization:** An LMS Decision-Aided equalizer is employed with the specified taps and step size parameters to mitigate channel impairments.
6. **Carrier Phase Estimation (CPE):** A Data-Aided CPE strategy is used to correct phase noise, aligned to the QAM constellation with  $\pi/2$  symmetry.
7. **BER Calculation:** Finally, the receiver calculates the BER over the specified number of pattern periods (`ber_pp`).

## 4.5 Results

Here we present the simulation results for PM-16QAM and PM-QPSK with a symbol rate of 28 Gbaud. The ODN loss is fixed at 33 dB for PM-QPSK and 25 dB for PM-16QAM. Figure 4.5 shows the results for PM-16QAM. We have plotted BER versus Modulation Index for different roll-off factors. The optimal modulation index is around 1.5 for roll-off factors of [0.7, 0.8, 0.9]. This indicates that up to this point, we can achieve maximum transmitted power while maintaining a low BER.

The simulation results for the PM-QPSK modulation format are plotted in 4.6. In this case, due to the presence of only two points per quadrature, we were able to extend the modulation index further. The optimal modulation index was found to be approximately 1.6 when the roll-off factor was set to 0.6. For roll-off factors of 0.7 and higher, the optimal modulation index increased, ranging between 1.8 and 2.

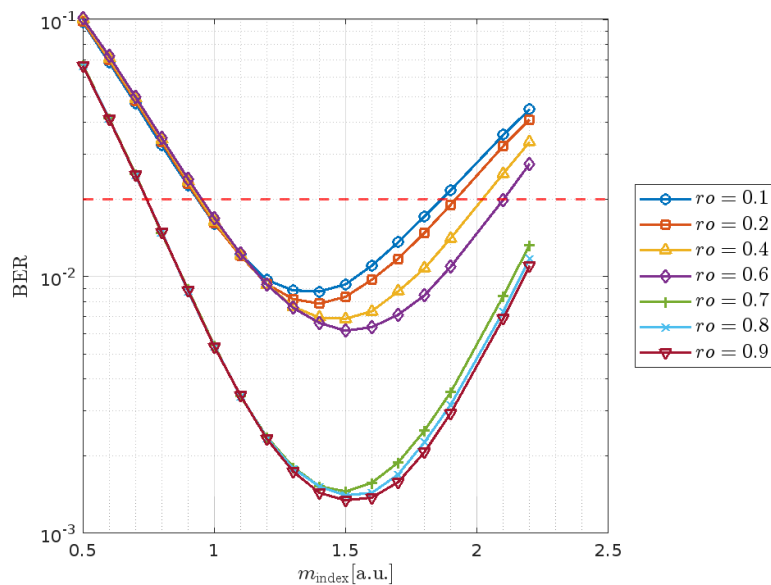


Figure 4.5: BER vs. Modulation Index for different Roll-Off Factors in PM-16QAM

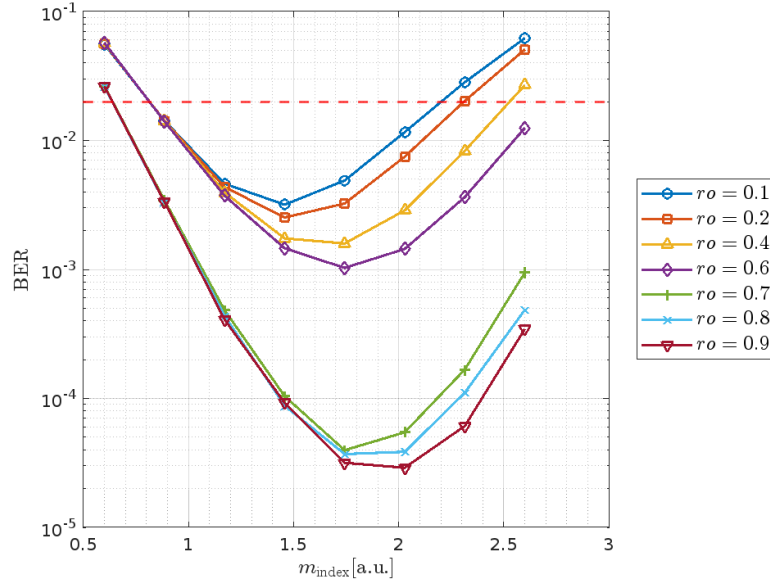


Figure 4.6: BER vs. Modulation Index for different Roll-Off Factors in PM-QPSK

In Figure 4.7, we have plotted the transmitted power, which is the signal's power at the output of the MZM, versus the modulation index for a roll-off factor of 0.4. By comparing the QPSK and 16QAM curves, we observe that the maximum transmitted power for 16QAM occurs at a modulation index greater than 2, while for the QPSK constellation, it occurs around a modulation index of 1.7. This difference arises because QPSK has only 2 constellation points per quadrature, whereas 16QAM has 4 constellation points per quadrature.

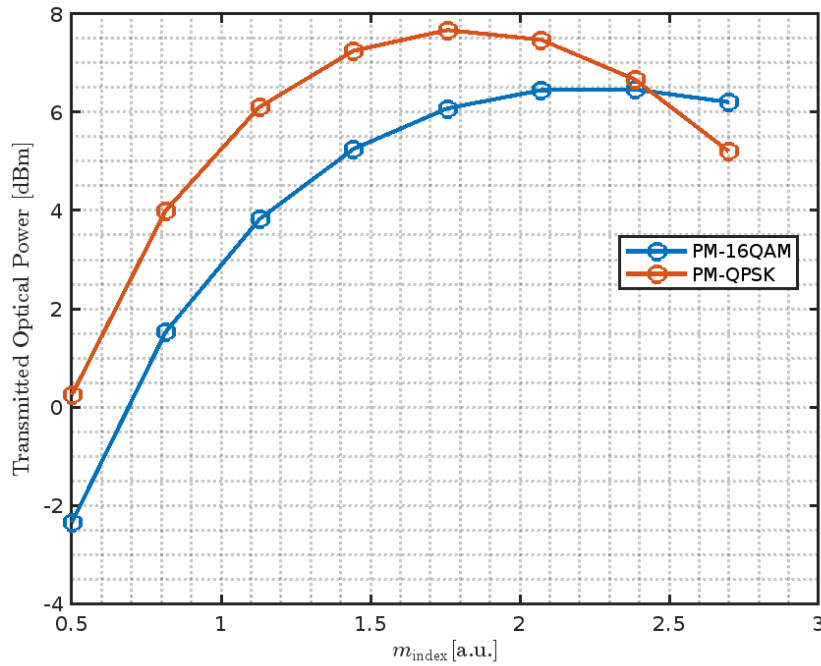


Figure 4.7: Transmitted optical power vs modulation index



## 4.6 Conclusion

In this chapter, we provided a systematic method for optimizing the modulation index in optical communication systems using MZM. By carefully balancing the modulation index and roll-off factor, we find an optimal point  $m_{\text{opt}}$  that maximizes transmitted power without causing excessive nonlinear distortion. This optimization is important for improving the performance of modern optical communication systems, especially in high-data-rate, long-distance applications where both power efficiency and signal integrity are crucial. In the following chapters, we will use ODN loss as a key evaluation parameter, as commonly referenced in the literature on PON systems.

# Chapter 5

## Introducing the parameter ODN loss

In this section, we introduce the concept of ODN (Optical Distribution Network) loss, a key parameter commonly used in evaluating the performance of Passive Optical Networks (PONs). ODN loss refers to the total optical signal attenuation that occurs as light travels through the network's fiber, splitters, and connectors, making it a critical metric for benchmarking PON technologies. We will also define the maximum ODN loss, which is typically specified for a target bit error rate (BER). Since PON systems use forward error correction (FEC), they can tolerate BER values, in the range  $10^{-2}, 10^{-3}$ , before correction, while still maintaining reliable performance.

Throughout this study, we will use maximum ODN loss as a core evaluation metric. To optimize system performance, we will focus on two key variables: the modulation index and the roll-off factor. By exploring the relationship between these parameters and the maximum ODN loss, we aim to identify their optimal values, ensuring that the system performs effectively within the given ODN loss constraints.

### 5.1 Optical Distribution Network (ODN)

The Passive Optical Networks (PON) structure, based on an optical Point-to-Multipoint (P2MP) architecture, is illustrated in Figure 5.1. A PON consists of an Optical Line Terminal (OLT) located at the Central Office (CO) of the operators, a set of Optical Network Units (ONU) close to end customers, and an Optical Distribution Network (ODN) connecting the CO and end customers. The P2MP connection is accomplished by exploiting passive splitters. Moreover, there are only passive devices, such as optical fibers, connectors, and optical splitters, in the PON outside the plant.

#### Definition of ODN Loss

$$\text{ODN}_{\text{loss}} = P_{\text{TX}} - P_{\text{RX}} \quad (5.1)$$

#### Definition of Maximum ODN Loss

$$\text{Max ODN Loss (dB)} = P_{\text{TX}} - \text{RROP} \quad (5.2)$$

where  $P_{\text{TX}}$  is the transmitted optical power at the output of the MZM, and RROP is the Required Receiver Optical Power [dBm], typically defined at a specific target BER.

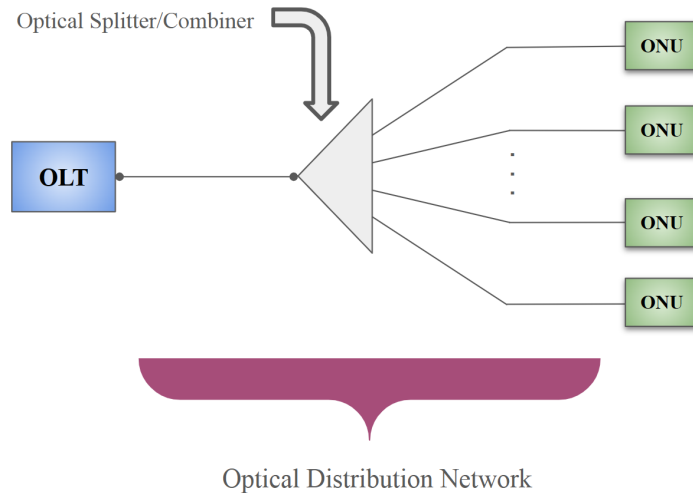


Figure 5.1: ODN loss in PON systems from transmitter at OLT to ONU.

## 5.2 Results

In Figure 5.2, we present the results of our simulation for a PM-QPSK constellation, where the BER is evaluated for a given range of ODN loss values. A threshold for the target BER, which can be corrected by FEC, is set at  $2 \times 10^{-2}$ . We present results for two different roll-off factors: 0.1 (left figure) and 0.5 (right figure).

For the roll-off factor of 0.1, we observe that even at a modulation index of 2.4, the maximum ODN loss that achieves the target BER of  $2 \times 10^{-2}$  is around 30 dB. However, for a stricter target BER of  $10^{-3}$ , the system is unable to reach the maximum ODN loss. In contrast, when the roll-off factor is increased to 0.5, the target BER of  $2 \times 10^{-2}$  is achievable at a higher modulation index of 2.4, with the maximum ODN loss reaching around 34 dB—an improvement of approximately 4 dB. This demonstrates that increasing the roll-off factor can enhance the maximum ODN loss, albeit at the cost of increased bandwidth usage.

In Figure 5.3, we present the BER results for a given ODN loss vector across multiple modulation indexes. It is evident from these results that starting  $m_i = 1.2$ , the behavior of the BER curve undergoes a significant change. As the modulation index increases, the nonlinearity of the sinusoidal characteristic of the MZM begins to show its influence, impacting system performance.

As shown in Figure 5.4, For PM-QPSK modulation we conducted simulations using a range of ODN loss values, roll-off factors, and modulation indexes. For each combination of roll-off and modulation index, we determined the maximum ODN loss that can be achieved while maintaining a specific target BER. Based on these simulation results, we generated a contour plot illustrating the relationship between modulation index, roll-off factor, and maximum ODN loss.

In Figure 5.4 (left plot), we present results for a target BER of  $10^{-3}$ . The optimal maximum ODN loss is observed at roll-off factors greater than 0.7, with modulation indices in the range of 1.65 to 2. A secondary maximum ODN loss occurs over a wider modulation index range, from approximately 1.2 up to 2.2, at roll-off values above 0.6. The ability

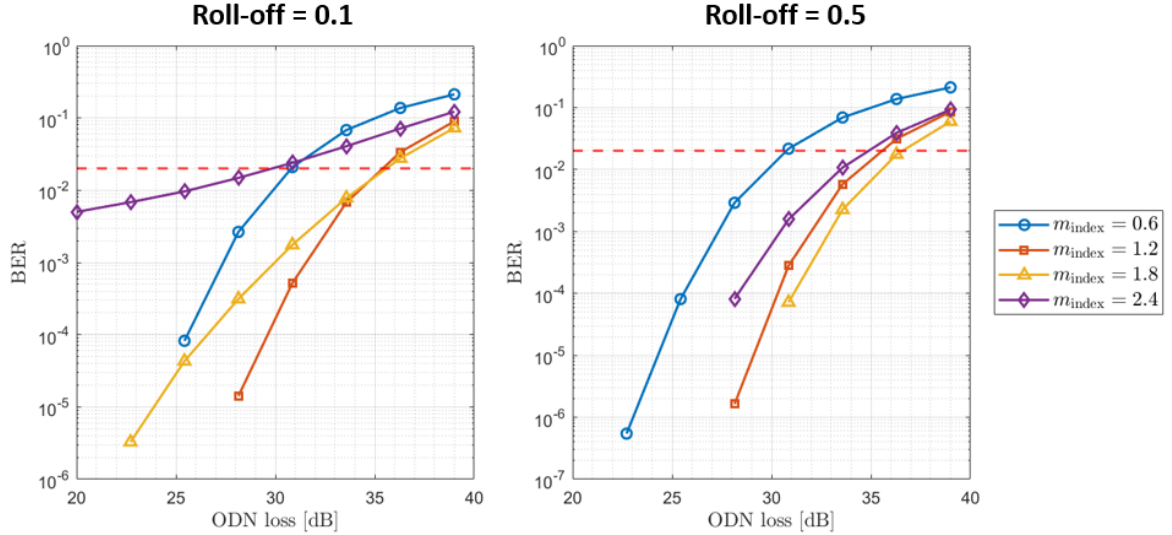


Figure 5.2: BER versus ODN loss [dB] for different modulation indexes and PM-QPSK signal. The dotted line is for target BER =  $2 \times 10^{-2}$  for finding the maximum ODN loss. The left figure is for roll-off=0.1 and the right figure is for roll-off=0.5

to exceed a modulation index of 2 without substantial performance degradation is due to the QPSK constellation's simplicity, which has only two points per quadrant, reducing the impact of MZM nonlinearity at higher modulation indices.

In the middle plot of Figure 5.4, which corresponds to a target BER of  $10^{-2}$ , we observe an interesting trend: the secondary maximum ODN loss occurs across a broad range of modulation indices, from 0.1 to 0.9. This indicates that, at this target BER, QPSK can operate effectively with lower roll-off factors, allowing for more efficient bandwidth usage while minimizing spectral occupancy. In the right plot, we present the results for a target BER of  $2 \times 10^{-2}$ . In this case, the optimal maximum ODN loss is achieved at modulation indices around 1.4 and above 2.2, with roll-off factors greater than 0.65.

We have repeated the same simulation for PM-16QAM modulation, as shown in Figure 5.5. A key observation is that, for PM-QPSK, we can use a higher modulation index, up to approximately 2.4, without significant degradation in performance. However, in the case of PM-16QAM, system performance begins to degrade when the modulation index exceeds 1.8. This is because PM-QPSK only has two points per arm of the MZM, whereas PM-16QAM has four. If we attempt to use higher-order modulation schemes like 64QAM, which involves eight points per quadrant of the MZM, the optimum modulation index becomes even lower. As a result, we are limited in increasing the transmit power to achieve higher maximum ODN loss when using higher-order modulation formats.

In the left plot of Figure 5.5, we present results for a PM-16QAM signal with a target BER of  $10^{-3}$ . Here, the optimal maximum ODN loss is 24 dB, which occurs for roll-off values greater than 0.7 and modulation indices between 1.3 and 1.6. A secondary maximum ODN loss is observed for roll-off values above 0.55 and modulation indices between 1.0 and 1.9. It's noteworthy that, for modulation indices between 1.5 and 2.0, no maximum ODN loss is achieved, indicating that the system could not meet the target BER in this range.

In the middle plot, which corresponds to a target BER of  $10^{-2}$ , the optimum maximum

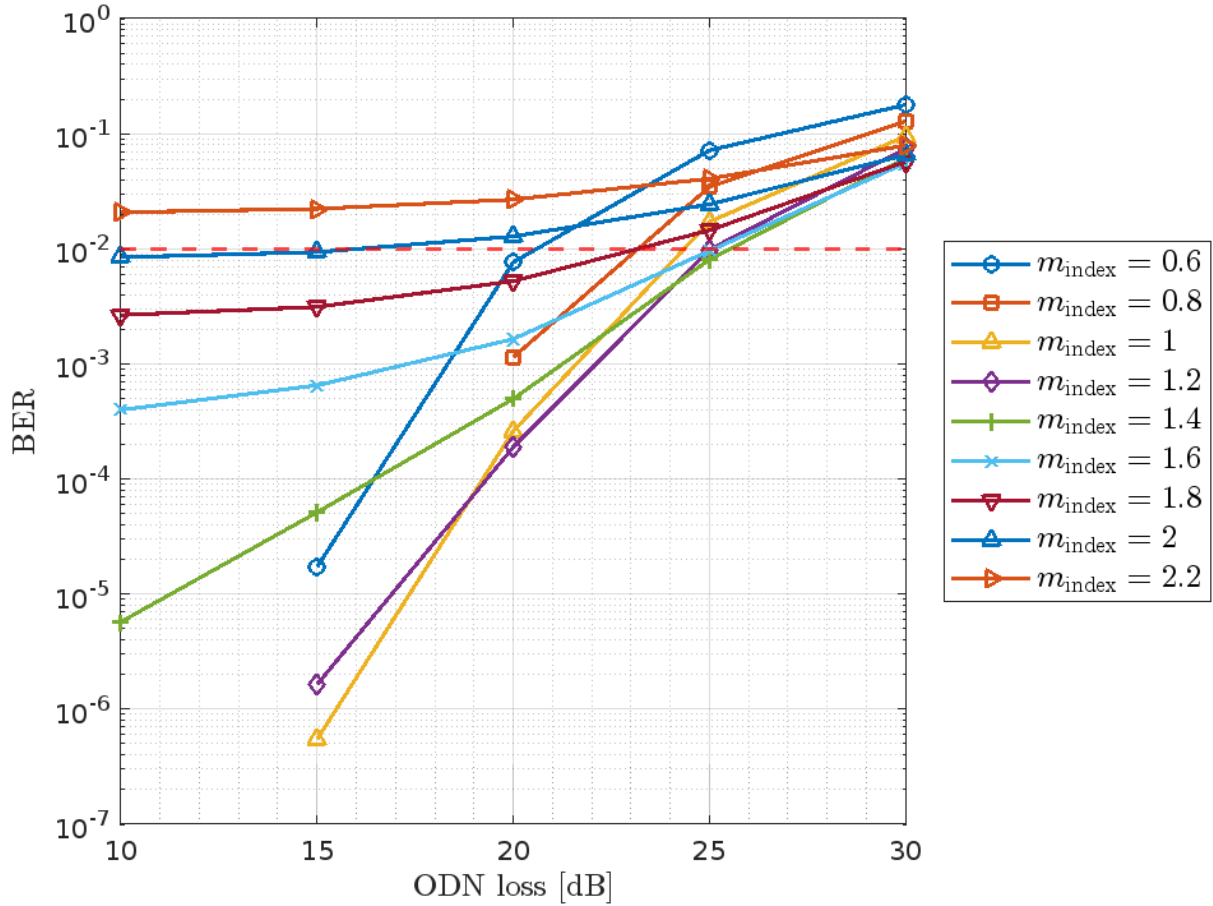


Figure 5.3: BER versus ODN loss [dB] for different modulation indexes and PM-16QAM signal. The dotted line is for target BER =  $10^{-2}$  for finding the maximum ODN loss

ODN loss occurs over a broader range of modulation indices compared to the previous plot, although the range of roll-off values remains consistent. Additionally, we observe a third maximum ODN loss of 25 dB, which can be achieved across all roll-off values.

Finally, in the right plot, we display results for a target BER of  $2 \times 10^{-2}$ . Here, the optimal maximum ODN loss reaches 29 dB, but it is limited to modulation indices between 1.4 and 1.6 at a roll-off factor of 0.9. The third maximum ODN loss, with a value of 26 dB, can be achieved across all roll-off values and modulation indices ranging from 0.9 to 2.0.

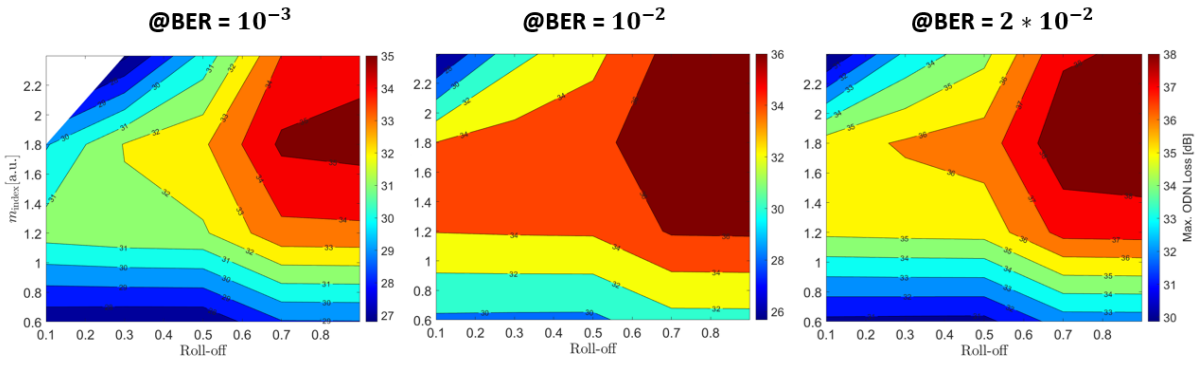


Figure 5.4: Contour plot of modulation index versus roll-off factor, showing the maximum ODN loss [dB] for various target BERs using a PM-QPSK signal.

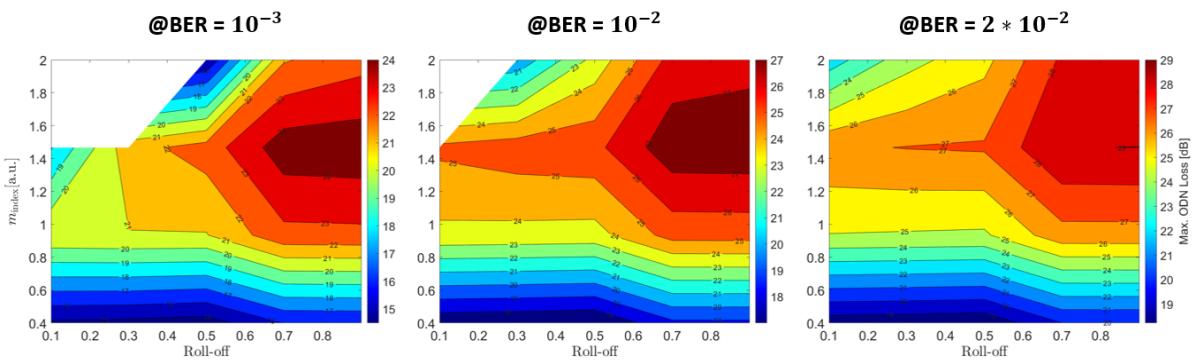


Figure 5.5: Contour plot of modulation index versus roll-off factor, showing the maximum ODN loss [dB] for various target BERs using a PM-16QAM signal.

### 5.3 Conclusion

In this chapter, we introduced the concept of Optical Distribution Network (ODN) loss, an essential metric for evaluating the performance of Passive Optical Networks (PONs). Through simulations, we examined the impact of two primary parameters—modulation index and roll-off factor—on the maximum achievable ODN loss, while maintaining target Bit Error Rates (BER) in PON systems. We demonstrated that increasing the roll-off factor can enhance the maximum tolerable ODN loss, although this comes with a trade-off in bandwidth efficiency.

Our results for PM-QPSK modulation show that, with an optimized modulation index and roll-off factor, the system can support a relatively high maximum ODN loss. These findings indicate that PM-QPSK modulation benefits from increased tolerance to ODN loss due to its lower susceptibility to nonlinearity effects, allowing higher modulation indices without significant performance degradation. In contrast, PM-16QAM modulation, with its more complex constellation, shows sensitivity to modulation index increases, limiting its achievable ODN loss at high BER targets. For PM-16QAM, the optimum modulation index for achieving high maximum ODN loss is lower, especially as we aim to maintain acceptable BER values.

Overall, our analysis highlights the interplay between modulation index, roll-off factor, and maximum ODN loss in determining the optimal configuration for PON systems. For PON designs focused on minimizing BER, using PM-QPSK modulation with higher roll-off factors and moderate modulation indices offers a robust solution with increased tolerance to ODN loss. On the other hand, achieving comparable performance with PM-16QAM requires a careful balance, as it is more sensitive to increases in the modulation index.

This study provides a framework for selecting modulation parameters in PON systems to optimize ODN loss tolerance, contributing to more efficient and reliable PON deployment strategies. In the next chapter, we will consider Extinction Ratio and modulation index at TX to see how they can effect on the ODN loss.

# Chapter 6

## Impact of Extinction Ratio on ODN loss

In this chapter, we investigate the impact of the extinction ratio (ER) on optical distribution network (ODN) loss and CPON performance. Specifically, we examine whether adding a bias voltage can address the nonlinearity terms in the MZM transfer function.

### What is Extinction Ratio?

In optical communications, the extinction ratio (ER) of an MZM refers to the ratio of the optical power output in the "on" state (when the modulator allows maximum light transmission) to the optical power output in the "off" state (when the modulator blocks or minimizes light transmission). It is a critical parameter that measures how effectively the modulator can distinguish between the "on" and "off" states, which correspond to the binary data (1s and 0s) in digital optical signals.

The *extinction ratio* can be expressed in terms of optical power as:

$$ER = \frac{P_{\text{on}}}{P_{\text{off}}}$$

where:

- $P_{\text{on}}$  is the power transmitted in the "on" state,
- $P_{\text{off}}$  is the power transmitted in the "off" state.

A high extinction ratio indicates a clearer distinction between the "on" and "off" states, which improves signal clarity and reduces bit errors. However, a low extinction ratio implies that the "off" state is not fully suppressed, leading to potential signal degradation.

In practical terms:

- **Higher extinction ratios** are desirable in optical communication systems, especially for long-distance or high-data-rate applications, as they contribute to better signal quality.
- **Lower extinction ratios** can lead to more noise and signal errors due to insufficient contrast between light and dark states.

The extinction ratio is usually measured in decibels (dB), where a higher dB value indicates a more effective modulator.



## 6.1 Mathematical model for ER

In this chapter, we investigate the impact of the extinction ratio (ER) on ODN loss and CPON performance. Specifically, we examine whether adding a bias voltage can address the nonlinearity terms in the MZM transfer function. To do this, we first analyze how the nonlinear terms affect the constellation diagram. We rewrite the equation by defining  $\phi_q = \frac{\pi v_q}{2V_\pi}$  and  $\phi_p = \frac{\pi v_p}{2V_\pi}$ , as shown in equation 6.1. In equation 6.1, we separate the real and imaginary parts of the transfer function and plot them in Fig. 6.1.

$$E_{\text{out}}(t) = E_{\text{in}}(t) \frac{1}{2} \left\{ \sin\left(\frac{\pi v_p}{2V_\pi}\right) - \frac{j}{\sqrt{ER}} \cos\left(\frac{\pi v_p}{2V_\pi}\right) + j \left[ \sin\left(\frac{\pi v_q}{2V_\pi}\right) - \frac{j}{\sqrt{ER}} \cos\left(\frac{\pi v_q}{2V_\pi}\right) \right] \right\} \quad (6.1)$$

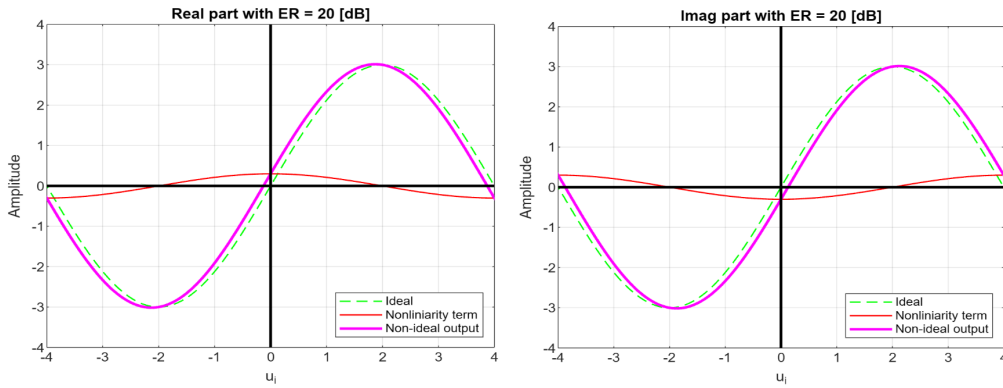


Figure 6.1: MZM transfer function with nonlinearity terms for ER = 20 dB. The left plot shows the real part, and the right plot shows the imaginary part.

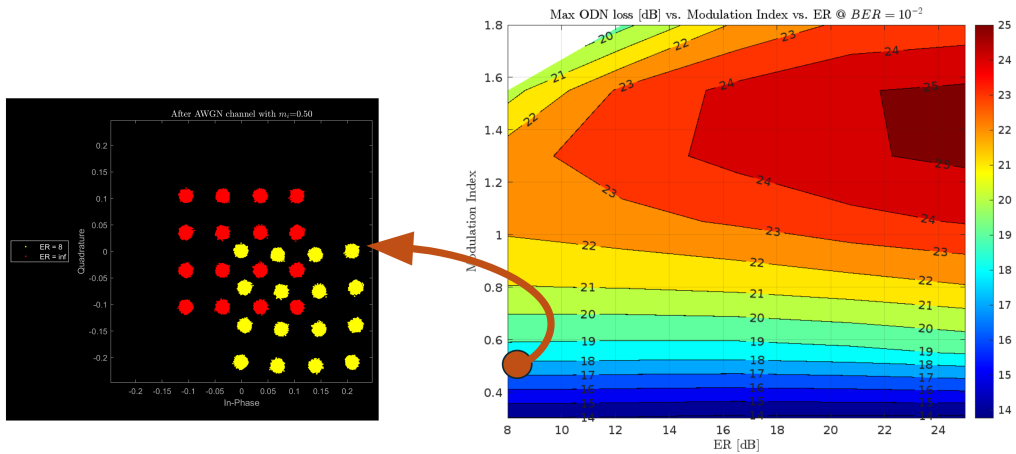


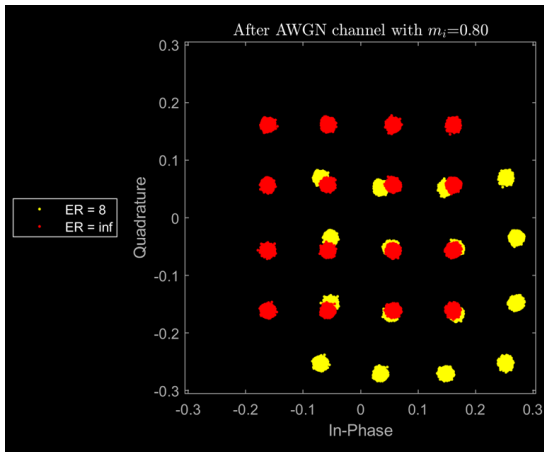
Figure 6.2: The constellation points of the signal for low ER and low modulation index(left); Maximum ODN loss vs Modulation Index vs Extinction Ratio(ER) for Target BER  $10^{-2}$  (right).

## 6.2 Results

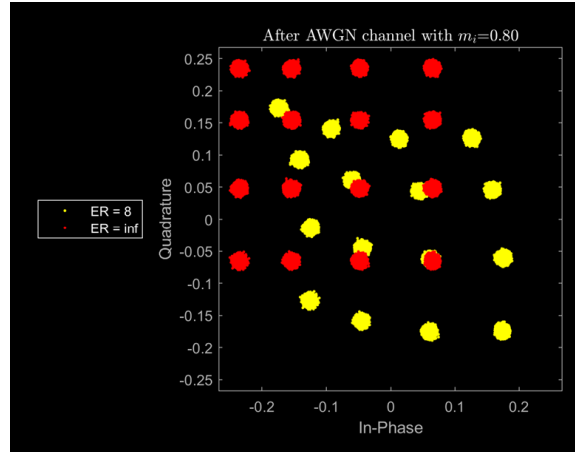
In this section, we evaluate the impact of our proposed mathematical model on the maximum ODN loss for transmission. The simulation setup remains consistent with previous chapters; however, in this case, the MZM is modeled as non-ideal. While the previous chapter assumed an ideal MZM, here we present results based on a non-ideal MZM to examine the effects of a low ER and its nonlinearities on the maximum ODN loss. In Figure 6.2 (left), we show an example constellation for a low modulation index and low extinction ratio. On the right, we present a contour plot of maximum ODN loss as a function of modulation index and ER. In Figure 6.3, Part (a), we examine the MZM with a bias voltage, while in Part (b), we consider the MZM without bias voltage. As shown, the bias voltage helps reduce the constellation's offset; however, the nonlinearity resulting from the sinusoidal nature of the MZM remains unaffected. Typically, the coherent DSP receiver can easily compensate for the constellation offset. Therefore, adding a bias voltage does not mitigate the nonlinearity effect.

We consider four scenarios in our evaluation:

- **Low ER and low modulation index:** As shown in Figure 6.5 part (a), in this scenario, we observe a constant shift for all points in the constellation. Importantly, the shift vector for all points is identical. This behavior is consistent with operating in the linear region (low modulation index), where both the real and imaginary components of the constellation points exhibit equal changes. The coherent DSP receiver can easily handle and compensate for this uniform shift, as confirmed by the results in Figure 6.5 part (a).
- **Low ER and high modulation index:** In Figure 6.5 part (b), we enter the nonlinear region due to the higher modulation index, which corresponds to increased transmitted power but with a low ER. In this case, we observe different effects of nonlinearity across the constellation points. For the two points near the center of the quadrature, the error vector magnitude is larger, while for the two points on the outer edges, the error vector magnitude is smaller. This effect is shown in Figure 6.4. This behavior is explained by the cosine nonlinearity term of the ER model, as depicted in Figure 6.1. Near the center, the cosine term is relatively constant, but as we move further from the center, the term changes significantly for constellation points further away from the center.
- **High ER and low modulation index:** This scenario, shown in Figure 6.5 part (c), is quite similar to the low ER and low modulation index scenario in part (a). At low modulation indexes, increasing the ER does not provide any noticeable improvement in ODN loss when compared to the low ER case. This is because the effect of ER in this situation is simply a constant shift in the constellation. Even with a higher ER, the shift remains uniform across all constellation points. The coherent DSP receiver can easily detect and compensate for this constant shift, regardless of its magnitude, allowing it to accurately reconstruct the signal.
- **High ER and high modulation index:** This represents the ideal scenario, where a higher ER ensures better separation between signal levels, and a high modulation index (near the optimum) indicates that the MZM is operating at a point that maximizes transmission power while minimizing overshoot.



(a) Without bias voltage



(b) With bias voltage

Figure 6.3: Comparison of images with and without bias voltage.

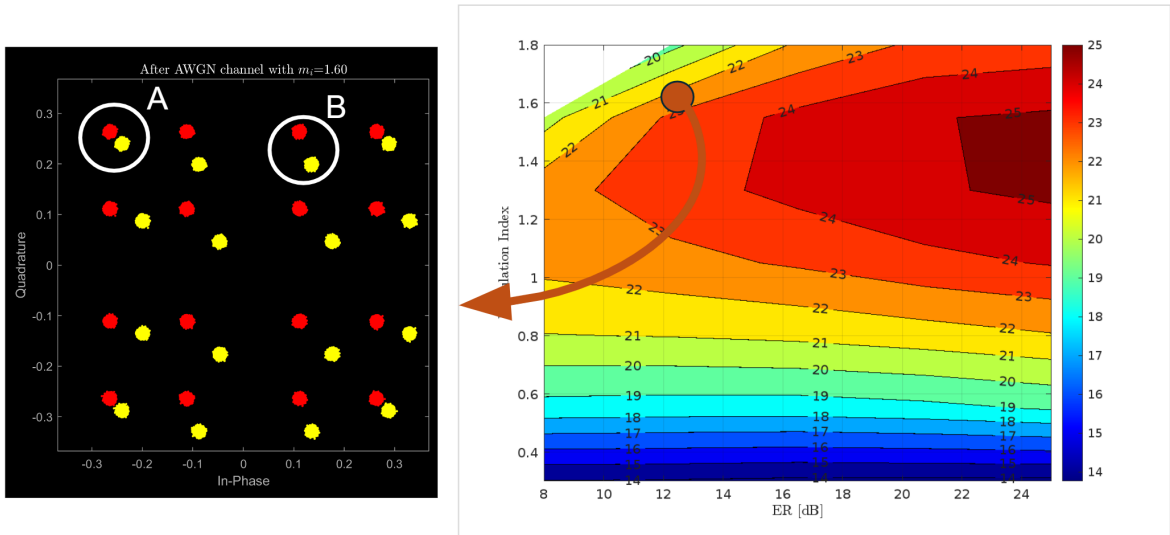


Figure 6.4: The constellation points of the signal for low ER and high modulation index(left); Maximum ODN loss vs Modulation Index vs ER for Target BER  $10^{-2}$  (right).

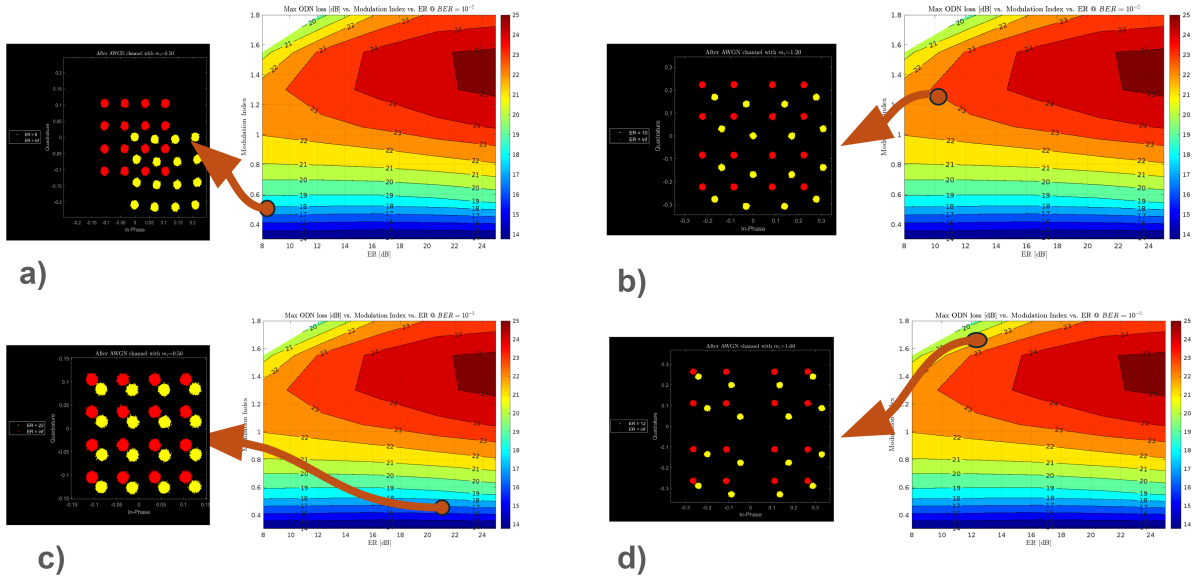


Figure 6.5: Maximum ODN loss vs Modulation Index vs ER for Target BER  $10^{-2}$ . Figure a shows the 16QAM constellation for low ER and low  $m_i$ , Figure b shows the 16QAM constellation for low ER and high  $m_i$ , Figure c shows the 16QAM constellation for high ER and low  $m_i$  and Figure d shows the 16QAM constellation for low ER and high  $m_i$

### 6.3 Conclusion

In this chapter, we explored the impact of the ER on ODNloss in CPONs and analyzed how modulator nonlinearity, particularly in a non-ideal MZM, affects system performance. By introducing a bias voltage, we investigated whether the nonlinearity inherent to the MZM's transfer function could be mitigated, specifically focusing on ER's effect on constellation stability and the maximum ODN loss achievable within acceptable BER limits.

Our results indicate that a higher ER leads to better signal clarity by improving the distinction between the "on" and "off" states of the MZM, especially when combined with a high modulation index. This configuration provides superior separation between constellation points, which enhances system resilience to ODN loss while maintaining the target BER. However, for lower ER values, nonlinear effects are more noticeable, particularly at higher modulation indices. This manifests as varying error vector magnitudes across the constellation, with points near the origin of the quadrature showing greater error vectors due to cosine nonlinearity.

Overall, our findings underscore that increasing the extinction ratio while optimizing the modulation index enhances CPON performance by minimizing nonlinear distortions and maximizing ODN loss tolerance. This chapter contributes to understanding the trade-offs associated with ER in CPON systems and serves as a guide for choosing modulation parameters that balance performance and reliability under realistic, non-ideal operating conditions.

# Chapter 7

## Advanced Topics in Coherent Transmission

This chapter discusses advanced topics in CPON. First, we study the filtering effect on the transmitter side, by considering an optical filter after MZM, and in the second part, we review techniques such as pre-emphasis to compensate for the bandwidth limitation at the transmitter.

### 7.1 Filtering Effect

In high-speed PON systems, the transceivers' electrical components (e.g., amplifiers and modulators) have inherent bandwidth constraints. These components, designed for lower bit rates, are often reused for higher data rates to reduce costs. However, this results in electrical bandwidth limitations, where the bandwidth of the components at the transmitter (TX) side becomes insufficient for handling the higher bit rates without performance degradation.

In this simulation setup similar to what we had in the previous chapters we have a signal with  $R_s = 16$  Gbaud and with PM-16QAM modulation format. We considered a Super Gaussian filter directly after MZM. We considered the AWG noise source after the filter. The reason for this is that we wanted to focus exclusively on the bandwidth limitation of SG filtering. After AWGN block we have fiber's loss and at RX we have ADC and a coherent DSP receiver. In this simulation setup, the AWG noise is added after the filter, representing a worst-case scenario. This approach is taken because the impact of unfiltered noise is more severe compared to the situation where both the noise and the signal are equally filtered [18].

The simulation setup shown in Figure 7.1 represents a Coherent Passive Optical Network (CPON) system with a Super-Gaussian (SG) filter applied at the transmitter (TX) side. The setup can be described as follows:

- **CW-Laser:** A Continuous Wave (CW) laser source generates a stable optical carrier signal, serving as the starting point of the transmission. This provides the coherent optical signal necessary for the coherent transmission setup.
- **Data-Pulse Shaping:** The data signal undergoes pulse shaping to adjust its spectrum, reducing Inter-Symbol Interference (ISI) and aligning with the system's bandwidth requirements. This pulse-shaped data is subsequently modulated.

- **DP-IQ-MZM:** This block represents a Dual-Polarization In-Phase and Quadrature Mach-Zehnder Modulator (DP-IQ-MZM). The modulator takes the pulse-shaped data and modulates it onto the optical carrier signal, creating an optical signal with In-Phase (I) and Quadrature (Q) components, enabling complex modulation schemes like QAM (Quadrature Amplitude Modulation) for coherent optical systems.
- **SG Filter:** A Super-Gaussian (SG) optical filter is applied after modulation to simulate the optical filtering effect at the transmitter (TX) side. This filter imposes a bandwidth limitation on the transmitted signal by attenuating higher frequency components, which helps in shaping the spectrum of the transmitted signal to match the channel requirements.
- **AWGN:** Additive White Gaussian Noise (AWGN) is introduced to simulate noise during transmission. This noise degrades signal quality and increases the Bit Error Rate (BER), providing a realistic assessment of the system's performance.
- **Optical Fiber Link:** The filtered signal with added AWGN is transmitted through an optical fiber link, represented by loops in Figure 7.1. The fiber link introduces attenuation.
- **ADC (Analog-to-Digital Converter):** The received optical signal is converted to an electrical signal by a photodetector and subsequently digitized by an ADC. The ADC samples the received signal at high speed, enabling further digital signal processing. Here we do not have considered a model for photodetector and we assumed it is ideal.
- **Coherent DSP (Digital Signal Processing):** The digitized signal undergoes digital processing, which includes:
  - **Equalization:** This compensates for signal impairments such as dispersion and filtering effects introduced by the SG filter, aiming to correct distortions and improve signal quality.
  - **Decoding:** The equalized signal is demodulated and decoded to recover the original transmitted data bits.
  - **BER Evaluation:** Finally, the system's performance is evaluated by calculating the Bit Error Rate (BER), which quantifies the error rate in the received signal compared to the original transmitted signal.

### Super Gaussian Function

The filter transfer function is modeled with a Super Gaussian profile with variable order, 3dB-bandwidth (BW). Here is the transfer function of the SG filter in the frequency domain:

$$D_{\text{DAC,REAL}}(f) = \exp\left(-0.5 \left(\frac{f}{f_0}\right)^{2n}\right)$$

where:

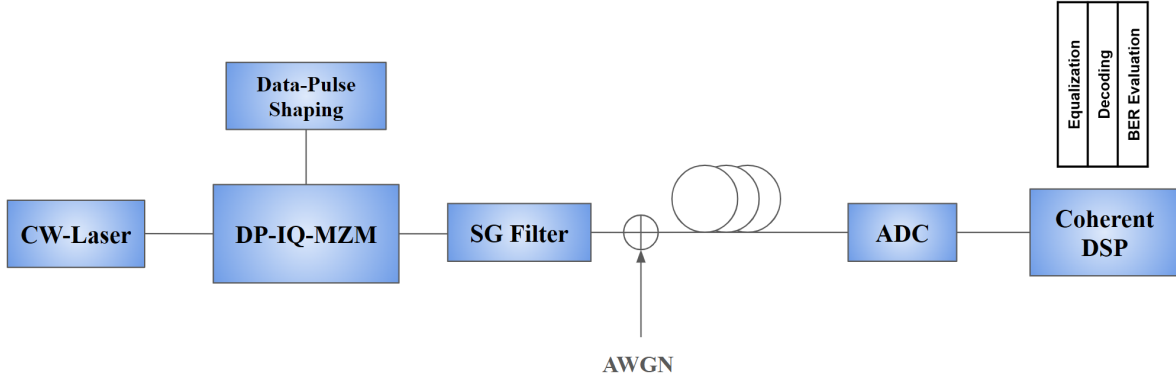


Figure 7.1: Simulation setup for CPON with SG filtering effect at TX.

- $B$  is the 3 dB bandwidth.
- $n$  is the order of the Super Gaussian filter.
- $a_{\text{pass}}$  is the linear attenuation for 3 dB attenuation.
- $f_0 = \frac{B}{(-2 \log(a_{\text{pass}}))^{1/(2n)}}$  is the central frequency.

In Figure 7.2, we have plotted the frequency response of the SG filter for various orders  $n$ . The figure demonstrates that as the order  $n$  increases, the filter's roll-off becomes steeper, resulting in more abrupt attenuation at the cutoff frequency. This means that higher-order SG filters have a more defined transition between the passband and the stopband. In other words, increasing the filter's order sharpens the frequency response, making the filter more selective. It allows the filter to more effectively distinguish between frequencies that are just inside the passband and those that are just outside it, thereby improving its ability to suppress unwanted frequencies. This characteristic is particularly advantageous in applications requiring precise filtering where minimal overlap between passband and stopband is critical.

In Figure 7.3, we present the frequency response of the SG filter for three different 3dB bandwidths: 0.3, 0.5, and 1.2 times the baudrate  $R_s$ . As shown, the bandwidth significantly influences the filter's performance, particularly in terms of selectivity and attenuation characteristics.

- For the smallest bandwidth,  $0.3 \times R_s$ , the filter exhibits a narrow passband with a steep roll-off, effectively limiting the range of frequencies that pass through. This configuration is ideal for applications where strict control over the passband is required, and unwanted frequencies need to be strongly suppressed.
- As the bandwidth increases to  $0.5 \times R_s$ , the passband widens, allowing a broader range of frequencies to pass. The roll-off becomes slightly less steep, indicating a trade-off between passband width and frequency selectivity. This configuration balances the need for filtering with a broader frequency range.
- For the largest bandwidth,  $1.2 \times R_s$ , the filter's passband is significantly wider, with a much gentler roll-off. While this allows for a larger range of frequencies to pass through, the filter becomes less effective at distinguishing between frequencies

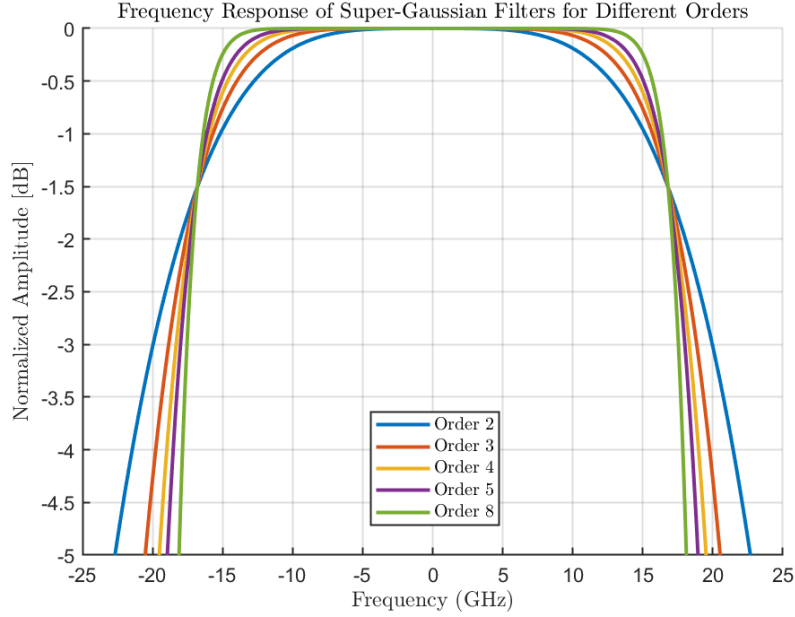


Figure 7.2: Frequency response of SG filter for different orders

near the cutoff point. As a result, the ability to suppress frequencies outside the passband diminishes, which may not be suitable for applications requiring high selectivity.

In summary, 7.3 demonstrates how adjusting the 3dB bandwidth affects the SG filter’s frequency response. A smaller bandwidth provides greater selectivity with a sharper roll-off, while a larger bandwidth increases the passband at the cost of reduced filtering precision.

Figure 7.4: Filtering effect on the Power Spectral Density (PSD) of the PM-16QAM signal for different 3 dB bandwidths of the SG filter. The left plot shows a stricter filter with a 3 dB bandwidth of  $B_{3\text{dB}} = 0.3 \times R_s$ , which significantly attenuates higher frequencies outside the passband. In contrast, the right plot shows a more relaxed filter with a 3 dB bandwidth of  $B_{3\text{dB}} = 0.7 \times R_s$ , allowing more high-frequency components to pass through. we will see in the next section evaluate its impact on Optical Distribution Network (ODN) loss at the receiver.

Counter plots of maximum ODN loss in dB at different target BERs is shown in Figures [ 7.5 7.6 7.7 ] as a function of the roll-off factor and modulation index. Here we have used the SG filter for 3 different 3dB bandwidths.

In Figure 7.5, we examine three scenarios for optical bandwidth filtering. It is important to note that, by convention in the literature, the optical bandwidth of a filter is typically considered twice the filter’s specified bandwidth.

In the Figure 7.5 left plot, with a 3 dB bandwidth of  $2 \times 1.2R_s$ , we observe that the maximum ODN loss occurs at a roll-off factor greater than 0.7 and a modulation index between 1.4 and 1.8. When the roll-off factor is reduced to 0.67, the optimal maximum ODN loss can be achieved over a broader range of modulation indices, approximately between 1.2 and 2. Finally, at a minimum roll-off factor of 0.4, the third peak in maximum ODN loss reaches 27 dB, occurring again across a higher range of modulation indices.

In the middle plot of Figure 7.5, we consider a 3 dB bandwidth of  $2 \times 0.7R_s$ . Compared



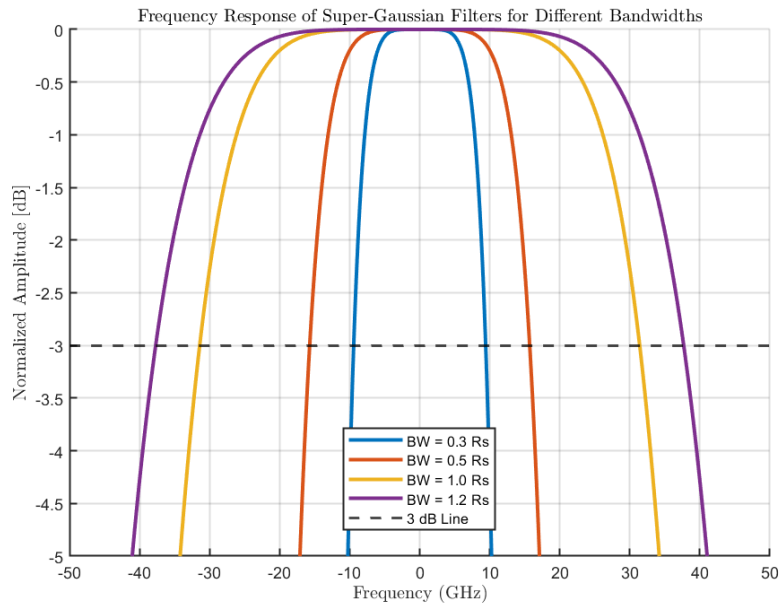


Figure 7.3: Frequency response of SG filter for different 3dB bandwidths

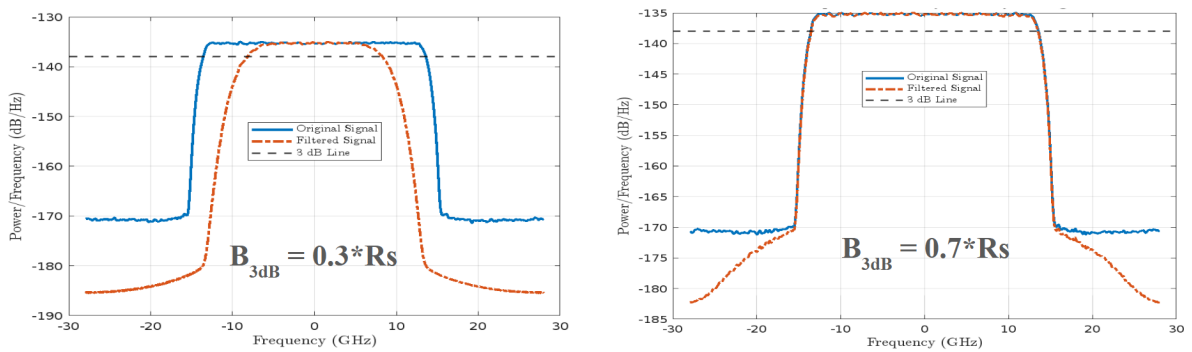


Figure 7.4: Filtering effect on the PSD of the PM-16QAM signal for different 3dB bandwidth of SG filter.

to the previous scenario, we observe that the optimal maximum ODN loss occurs at a lower range of the modulation index. However, the second optimal maximum ODN loss remains similar in terms of both roll-off factor and modulation index range. The third optimal maximum ODN loss, while occurring at the same modulation index as before, now requires a roll-off factor greater than 0.6, whereas in the previous scenario, it was achievable with a roll-off factor greater than 0.4.

In the right plot of Figure 7.5, we examine a scenario with a severe bandwidth limitation, where the 3 dB bandwidth is  $2 \times 0.4R_s$ . In this case, the optimal maximum ODN loss is approximately 1 dB lower than in the previous two scenarios. The highest ODN loss is achieved with a roll-off factor above 0.7 and a modulation index range between approximately 1.25 and 1.94. Notably, in the roll-off range of 0.6 to 0.73, the maximum ODN loss demonstrates a high sensitivity to changes in the roll-off factor. Additionally, secondary and subsequent optimal ODN loss points occur over a broader modulation index range compared to the primary optimal value, highlighting a trade-off between bandwidth limitations and modulation efficiency.

In Figure 7.6, we present results for a target BER of  $10^{-2}$ . In the left plot, we consider a relatively large 3 dB bandwidth for the filter, set to  $2 \times 1.2R_s$ . Under this configuration, the optimal maximum ODN loss of 27 dB occurs with a roll-off factor above 0.68 and a modulation index range of 1.22 to 1.85. A second local maximum for ODN loss is observed for a higher modulation index range and a lower roll-off factor. Specifically, for roll-off values above 0.6 and modulation indices between 1.05 and 2, the second highest ODN loss can be achieved. Interestingly, the third optimal ODN loss remains achievable across a broad range of roll-off factors from 0.1 to 0.9, indicating a degree of robustness.

In the middle plot of Figure 7.6, we reduce the 3 dB bandwidth to  $2 \times 0.7R_s$ . The results indicate minimal penalty in terms of ODN loss compared to the left plot, suggesting that performance is maintained under moderate bandwidth constraints.

In the Figure 7.6, right plot, we examine a more restrictive 3 dB bandwidth of  $2 \times 0.4R_s$ . Here, we observe a 1 dB penalty in the first optimal ODN loss compared to the wider bandwidth cases. The corresponding range for the modulation index is between 1.1 and 2, with the optimal ODN loss achievable at roll-off factors above 0.7. These findings underscore the trade-offs between filter bandwidth limitations and ODN loss performance, as stricter bandwidth constraints lead to higher sensitivity in modulation and roll-off parameters.

## Max ODN Loss @ $BER = 2 \cdot 10^{-2}$

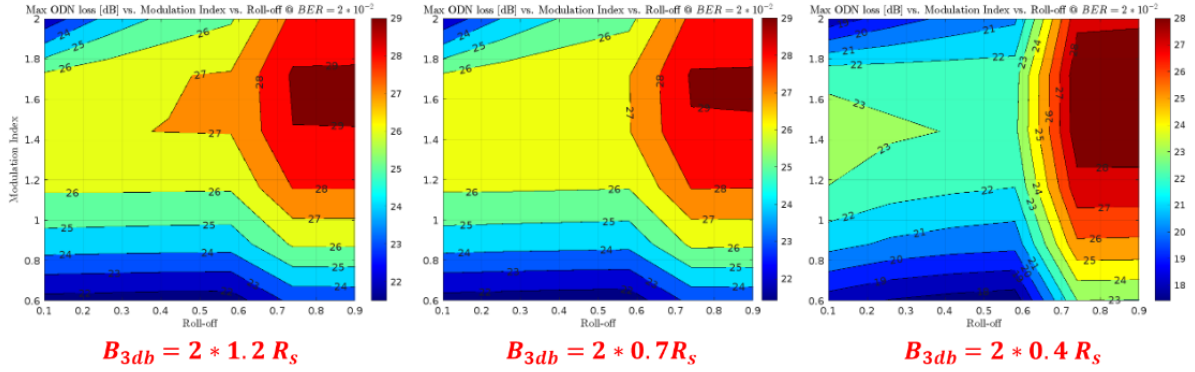


Figure 7.5: Filtering effect on the PSD of the PM-16QAM signal for different 3dB bandwidth of SG filter @  $BER = 2 * 10^{-2}$ .

## Max ODN Loss @ $BER = 10^{-2}$

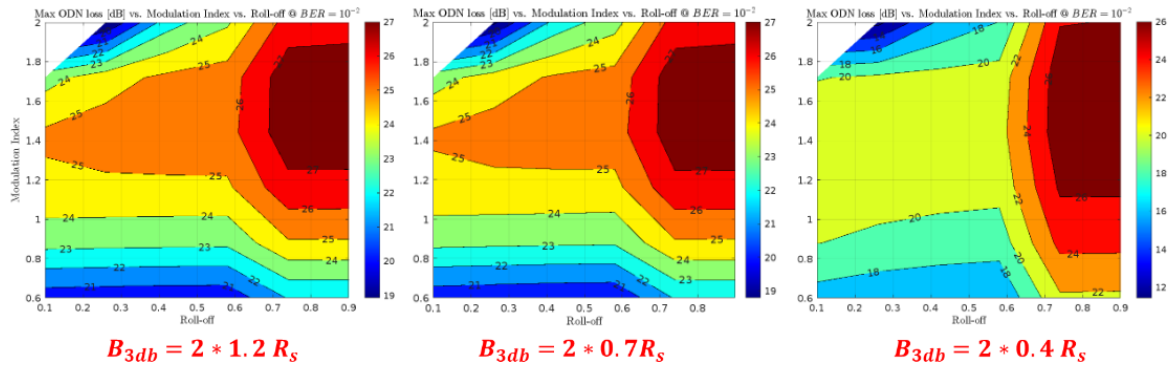


Figure 7.6: Filtering effect on the PSD of the PM-16QAM signal for different 3dB bandwidth of SG filter @  $BER = 10^{-2}$ .

## Max ODN Loss @ $BER = 10^{-3}$

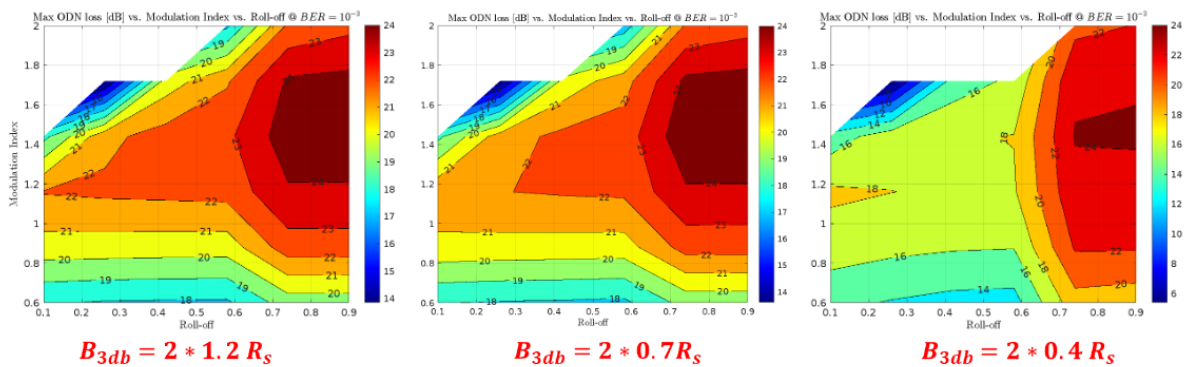


Figure 7.7: Filtering effect on the PSD of the PM-16QAM signal for different 3dB bandwidth of SG filter @  $BER = 10^{-3}$ .

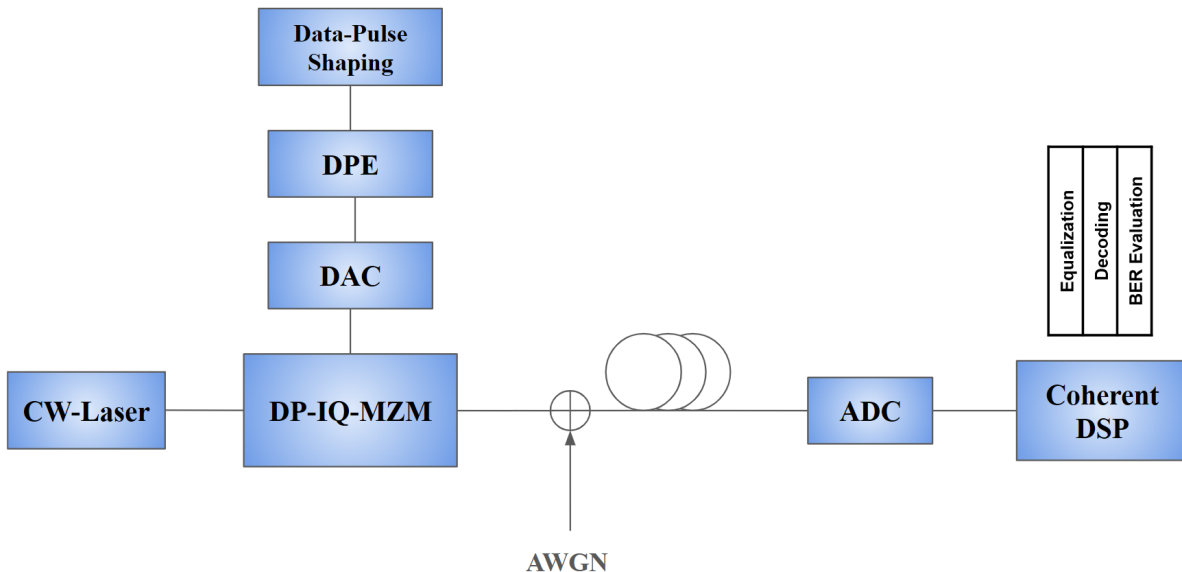


Figure 7.8: Simulation setup of applying DPE for compensating bandwidth limitations of DAC at TX.

## 7.2 Digital Pre-Emphasis (DPE)

### 7.2.1 Simulation Setup

In this section, we study the techniques which are used for pre-distortion of the signal at TX. In high-frequency electronic systems, the bandwidth limitations of electronic devices, such as Digital-to-Analog Converters (DACs), can degrade the signal quality. These limitations often manifest as a frequency-dependent attenuation, where higher frequencies experience more significant loss compared to lower frequencies. To counteract this effect and maintain signal fidelity, a technique called pre-emphasis is employed. Figure 7.8 illustrates the simulation setup incorporating Digital Pre-Emphasis (DPE) in the system. As shown, the DPE block is placed before the DAC to pre-distort the signal prior to DAC processing. This configuration allows the DPE filter to pre-compensate for anticipated signal distortions, improving overall system performance.

### Digital Pre-Emphasis (DPE)

Digital Pre-Emphasis [19] involves modifying the signal in the digital domain before it is converted to an analog signal by the DAC. The goal is to apply a frequency-dependent gain that compensates for the expected losses in the analog components, effectively flattening the overall system response. In the equation below, the original signal after the Pulse Shaping Filter is  $S(f)$ ,  $P(f)$  is the DPE filter and the  $DAC_{REAL}$  is a low pass filter which in the continue of this chapter we see how we implement it.

$$D(f) = P(f) \times DAC_{REAL} \times S(f)$$

The pre-emphasis filter  $P(f)$  is designed based on the transfer functions of the real DAC  $D_{DAC,REAL}(f)$  and the desired DAC response  $D_{DAC,DESIRED}(f)$ . The formula for the

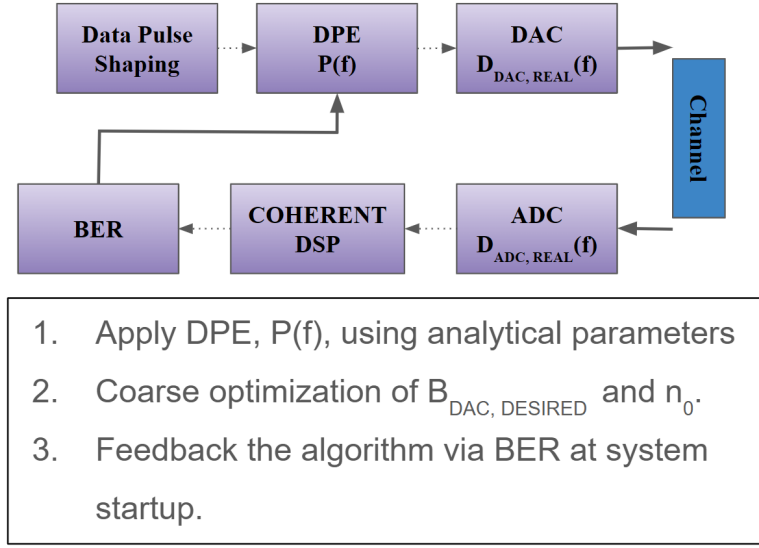


Figure 7.9: The proposed DPE scheme, based on the work in [19], selects the parameters of  $P(f)$  using BER feedback from the RX.

pre-emphasis filter is:

$$P(f) = \frac{D_{\text{DAC, DESIRED}}(f)}{D_{\text{DAC, REAL}}(f) + n_0}$$

where:

- $f$  is the frequency.
- $D_{\text{DAC, REAL}}(f)$  is the transfer function of the real DAC.
- $D_{\text{DAC, DESIRED}}(f)$  is the transfer function of the desired DAC response.
- $n_0$  is a noise adjustment term that ensures stability and prevents division by zero.

As illustrated in Figure 7.9, the filter's 3dB bandwidth is determined using BER feedback from the receiver (RX). Note that this optimization is performed only at the start of transmission and remains fixed thereafter.

## Real DAC Transfer Function

The real DAC transfer function  $D_{\text{DAC, REAL}}(f)$  can be modeled using different functions, such as a third-order Bessel function or a Super Gaussian function.

### Third-Order Bessel Function

$$D_{\text{DAC, REAL}}(f) = \frac{1}{\sqrt{1 + \left(\frac{f}{f_{c, \text{real}}}\right)^6}}$$

where  $f_{c, \text{real}}$  is the cutoff frequency of the real DAC.

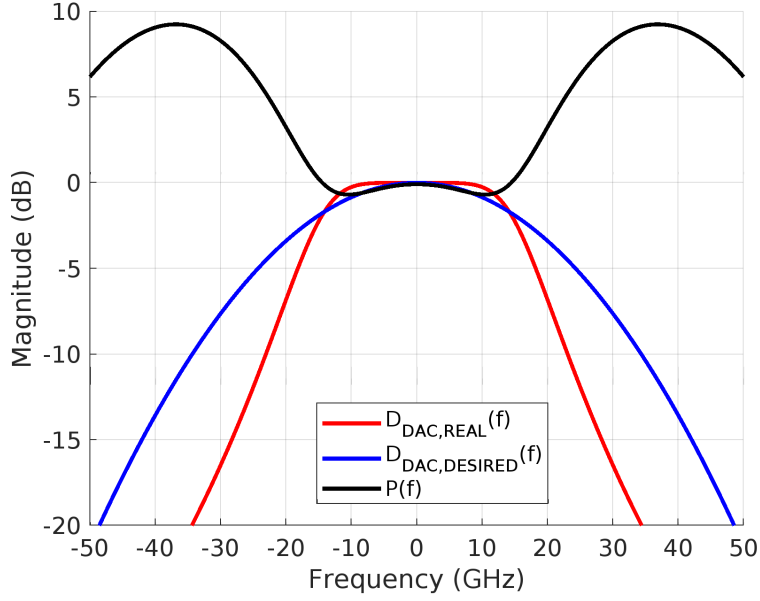


Figure 7.10: Transfer Functions of real and desired DAC and Pre-Emphasis Filter

### Super Gaussian Function

$$D_{\text{DAC,REAL}}(f) = \exp\left(-0.5 \left(\frac{f}{f_0}\right)^{2n}\right)$$

where:

- $B$  is the 3 dB bandwidth.
- $n$  is the order of the Super Gaussian filter.
- $a_{\text{pass}}$  is the linear attenuation for 3 dB attenuation.
- $f_0 = \frac{B}{(-2 \log(a_{\text{pass}}))^{1/(2n)}}$  is the central frequency.

### Desired DAC Transfer Function

The desired DAC transfer function  $D_{\text{DAC,DESIRED}}(f)$  is often modeled as a Gaussian function:

$$D_{\text{DAC,DESIRED}}(f) = \exp\left(-\left(\frac{f}{f_{c,\text{desired}}}\right)^2\right)$$

where  $f_{c,\text{desired}}$  is the cutoff frequency of the desired DAC.

Figure 7.10 shows the transfer functions of the real DAC  $D_{\text{DAC,REAL}}(f)$ , desired DAC  $D_{\text{DAC,DESIRED}}(f)$ , and the pre-emphasis filter  $P(f)$ . The real DAC exhibits bandwidth limitations, causing significant high-frequency attenuation. The desired DAC has a flatter response, aiming to preserve higher frequencies. The pre-emphasis filter compensates for these limitations by amplifying high frequencies, effectively flattening the system response and preserving signal fidelity across the frequency spectrum. This approach helps to counteract DAC-induced losses, enhancing overall transmission quality. In Figure 7.11, we

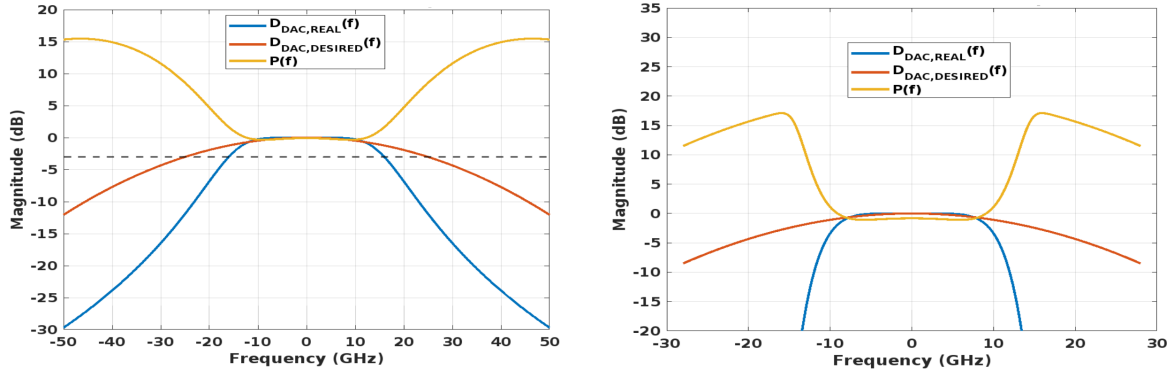


Figure 7.11: Transfer functions of the DAC, Pre-Emphasis Filter, and the desired DAC transfer function. The left plot shows the DAC transfer function with a real third-order Bessel function, and the right plot shows the DAC transfer function with a Super Gaussian (SG) filter.

see the difference between the third-order Bessel and Super Gaussian (SG) filters in their attenuation behavior. The Bessel filter (left plot) attenuates the signal more gradually, maintaining a smoother roll-off, while the SG filter (right plot) exhibits a much sharper attenuation, particularly in the transition band. This distinction is especially noticeable in how quickly each filter suppresses higher frequencies.

In the Figure 7.12, we present a joint optimization process for determining the parameters of the DPE filter. The contour plots represent the BER, showing that with a real DAC 3dB bandwidth of 11.2 GHz, a minimum of 15 GHz is required for  $D_{DAC,DESIRED}$  in order to design the  $P(f)$  to compensate the DAC bandwidth limitations accordingly. The parameter  $n_0$  is not so much relevant, we just have to consider that choose a reasonable value for it, because if we choose a very low value ( $10^{-6}$ ) for higher frequencies the filter's transfer function goes to infinite.

### 7.3 Results

Here, we have analyzed two different scenarios for bandwidth limitations. In the first scenario, we assumed a 3 dB bandwidth of  $B_{3dB} = 0.5$ , representing a moderate bandwidth limitation. In the second scenario, we imposed a stricter limitation with  $B_{3dB} = 0.35$ . For both cases, we plotted the maximum ODN loss against the roll-off and modulation index under two conditions: first, by considering only the bandwidth limitations of the DAC, and second, by employing digital pre-emphasis (DPE) techniques at the transmitter side for three different target BERs.

Figure 7.13 illustrates that the use of DPE enables a wider range of modulation indices to achieve maximum ODN loss. In the scenario with moderate bandwidth limitations, we observe no significant improvement in the maximum ODN loss. However, with the stricter bandwidth limitation and a target BER of  $10^{-2}$  which is shown in Figure 7.14(b) and (e), we observe an approximate 1 dB improvement in the maximum achievable ODN loss when DPE is applied.

In Figure 7.14, with severe bandwidth limitations, the effectiveness of DPE is clearly demonstrated. For a target BER of  $10^{-3}$ , as shown in Figure 7.14 (a), when DPE is

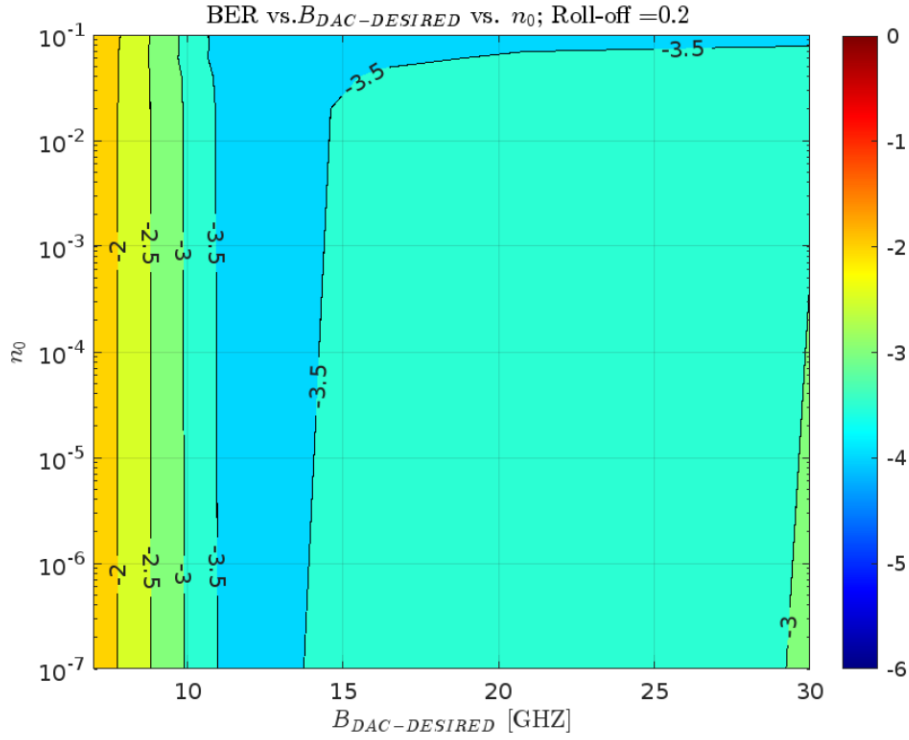


Figure 7.12: Optimization of pre-emphasis filter response through joint tuning of DAC bandwidth and noise adjustment coefficient. Applied to PM-16QAM (28 Gbaud) with real DAC parameters of 16 GHz bandwidth with real DAC 11.2 GHz.

disabled, the system cannot achieve the target BER across a wide range of roll-off factors and modulation indices. However, once DPE is applied, it effectively compensates for the bandwidth limitations, enabling the system to achieve the target BER of  $10^{-3}$ .



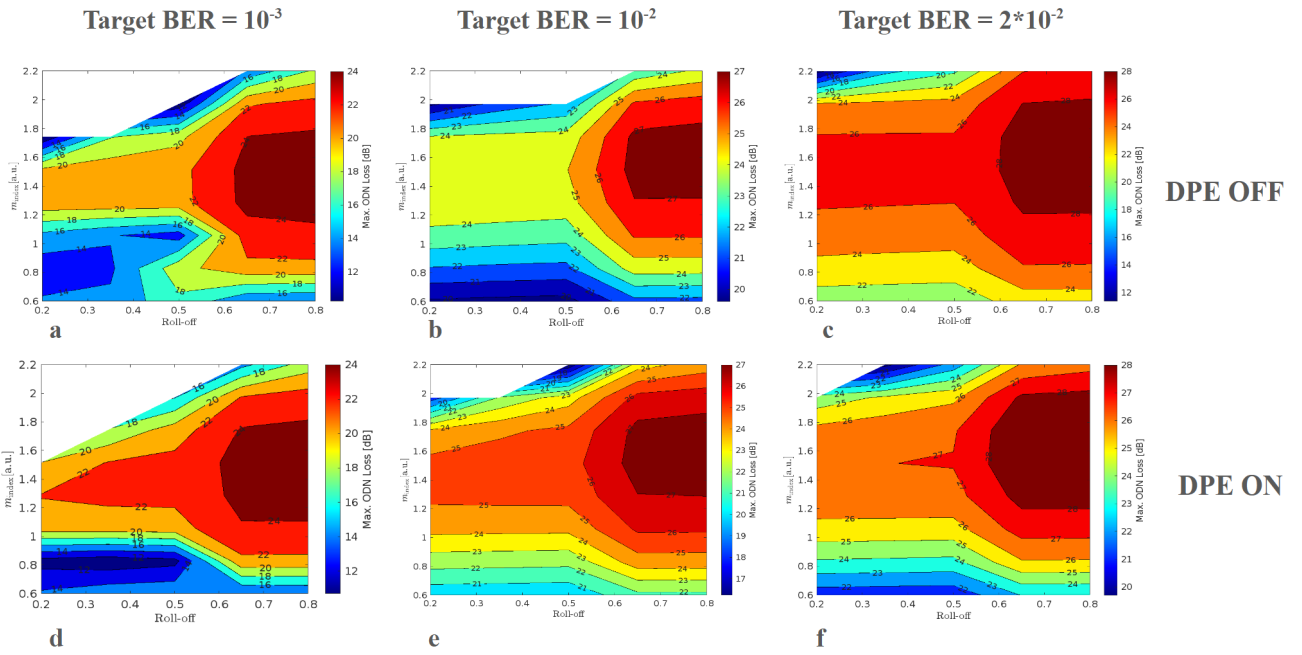


Figure 7.13: Maximum ODN loss as a function of roll-off and modulation index with DPE and without DPE for different target BER with  $BW = 0.5 * R_s$ .

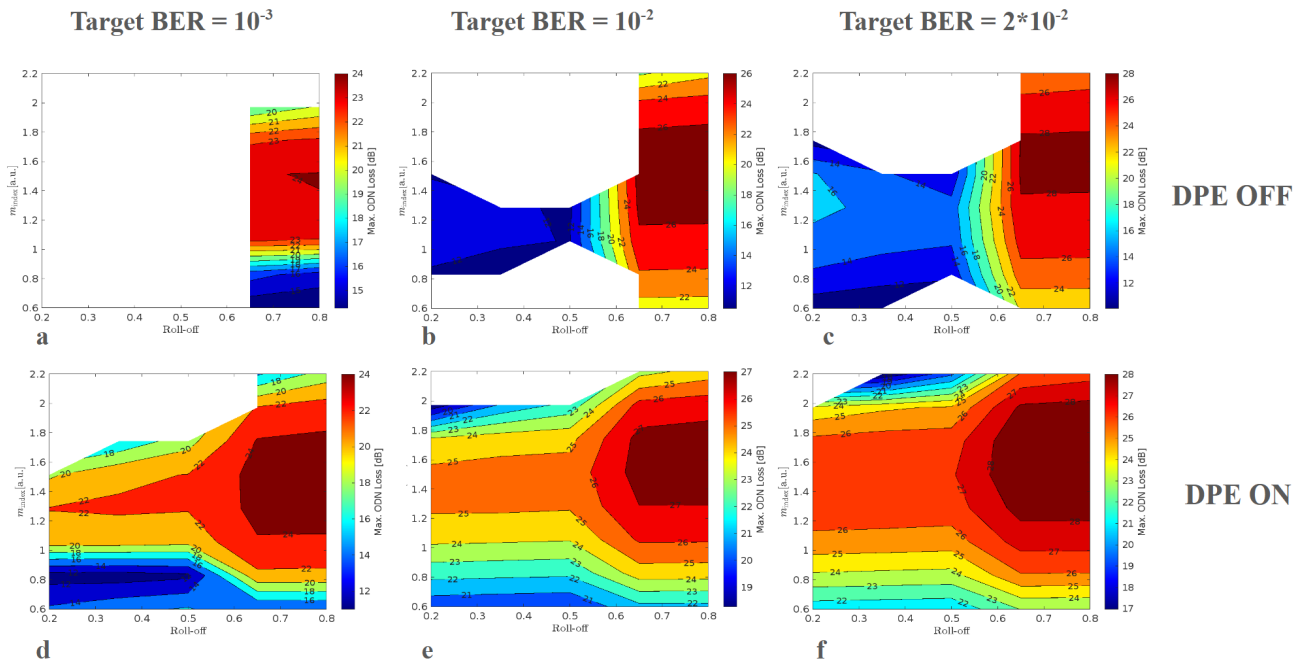


Figure 7.14: Maximum ODN loss as a function of roll-off and modulation index with DPE and without DPE for different target BER with  $BW = 0.35 * R_s$ .

## 7.4 Conclusion

This chapter explored advanced techniques for addressing bandwidth limitations in CPON with a focus on mitigating transmitter-side constraints through filtering and pre-emphasis. The first part examined the impact of bandwidth limitations on high-speed transceivers, especially when reusing electrical components originally designed for lower data rates. We studied the use of Super Gaussian (SG) filters at the transmitter to address bandwidth constraints, analyzing the filter's response with different 3 dB bandwidths to understand their influence on our main evaluation metric ODN loss.

The second part of the chapter focused on digital pre-emphasis (DPE) as a pre-distortion technique to mitigate DAC bandwidth limitations. DPE compensates for frequency-dependent attenuation, allowing the signal to maintain fidelity through a frequency-dependent gain. The simulation results indicate that implementing DPE at the transmitter improves system robustness by countering the effects of bandwidth limitations prior to DAC processing, which is particularly beneficial in high-frequency CPON systems. Joint optimization of DPE parameters using BER feedback from the receiver underscores the need for adaptive parameter tuning to achieve optimal performance.

In summary, the findings of this chapter highlight the filtering effect and pre-emphasis techniques in CPON systems. The optimization of SG filter parameters and the strategic use of DPE can substantially improve system performance by compensating for inherent bandwidth limitations in high-speed optical networks. In the next chapter we will introduce another method to predistort the signal before entering MZM in order to remove the nonlinearity caused by MZM.

# Chapter 8

## Compensation of Nonlinearities in MZM Using DPD

### 8.1 Introduction

The MZM is a key component in optical communication systems, and it is used to modulate optical signals with data carried by electrical signals. The main challenge of MZM comes from inherent nonlinearities due to its sinusoidal transfer function. As the modulation index increases, these nonlinearities become more pronounced, leading to signal distortions that degrade the system's performance.

In recent years, the use of digital pre-distortion (DPD) has emerged as an effective technique for mitigating the nonlinear distortions introduced by optical modulators in high-speed communication systems. Zhalehpour et al. proposed a DPD method based on a memory polynomial model to linearize the output of silicon photonic Mach-Zehnder modulators (SiP MZMs) used in short-range applications and data centers. The SiP MZMs experience both amplitude and phase nonlinearity, which can degrade system performance, particularly with higher-order modulation formats such as 64-QAM. Their work demonstrates how DPD can significantly reduce the bit error rate (BER) by compensating for these nonlinearities at the transmitter side, improving overall system efficiency [20].

Similarly, Bao et al. explored the application of DPD for mitigating nonlinear distortions in high-speed Optical Orthogonal Frequency Division Multiplexing (OOFDM) systems, particularly in Mach-Zehnder modulators (MZMs) and Electro-Absorption Modulated Lasers (EMLs). They implemented a polynomial-based DPD algorithm to linearize modulators in OOFDM transmitters with bit rates up to 30 Gb/s. This approach, which considers memory effects, was shown to enhance the performance of OOFDM signals in various optical network applications [21].

One of the most effective methods for compensating for the nonlinear behavior of the MZM is *Polynomial Digital Pre-Distortion (PDPD)*. This technique applies a compensating function to the input signal before it is modulated, ensuring that the combined response of the pre-distorted signal and the MZM produces a linear output. In this chapter, we explore the implementation of PDPD, its mathematical principles, and its practical application in compensating MZM nonlinearities.

## 8.2 The Nonlinear Transfer Function of MZM

The MZM operates based on interference between two optical waves. The transfer function for an ideal MZM without any impairments can be expressed as:

$$E_{\text{out}} \propto \sin\left(\frac{\pi v_p}{2V_\pi}\right)$$

Where:

- $E_{\text{out}}(t)$  is the optical output field.
- $v_p$  is the electrical signal.
- $V_\pi$  is the voltage required for a phase shift of  $\pi$ .

This transfer function introduces significant nonlinearities, especially when large modulation index is considered. These nonlinearities appear as distortion of the signal constellation, reducing the system's performance and increasing the BER.

## 8.3 Polynomial Digital Pre-Distortion (PDPD)

The main idea behind PDPD is to pre-distort the input signal in such a way that the nonlinear transfer function of the MZM effectively linearizes the output. The pre-distortion function compensates for the MZM's nonlinearity, making the output signal appear as if the MZM were linear.

The pre-distortion function is represented as a polynomial that adjusts both the real and imaginary parts of the input signal. Mathematically, the process involves fitting a polynomial to the output of the MZM for a given input signal and then applying the inverse of this polynomial to pre-distort future input signals.

## Polynomial Fitting for Predistortion

In order to compensate for the nonlinearities introduced by the Mach-Zehnder Modulator (MZM), polynomial fitting techniques can be employed. Specifically, we use the `polyfit` and `polyval` functions in MATLAB to model the nonlinear relationship between the modulated signal and the ideal 16-QAM constellation. The fitted polynomial is used to apply pre-distortion to the input signal, ensuring that the output resembles the original signal after passing through the MZM.

### 8.3.1 Polynomial Fitting Using `polyfit`

The `polyfit` function in MATLAB fits a polynomial of a specified degree to the given data in a least-squares sense. For a set of data points  $\{x_i, y_i\}$ , the goal is to find a polynomial  $P(x)$  of degree  $n$  such that the sum of the squared residuals between the actual values  $y_i$  and the polynomial's predicted values  $P(x_i)$  is minimized. The polynomial can be expressed as:

$$P(x) = a_n x^n + a_{n-1} x^{n-1} + \dots + a_1 x + a_0 \quad (8.1)$$

where  $a_n, a_{n-1}, \dots, a_0$  are the polynomial coefficients determined by the `polyfit` function.

The syntax for fitting a polynomial of degree  $n$  to the data points is given by:

```
p = polyfit(x, y, n);
```

Here,  $\mathbf{x}$  represents the input data,  $\mathbf{y}$  represents the target data, and  $\mathbf{n}$  is the degree of the polynomial.

The `polyfit` function minimizes the least-squares error:

$$\min \sum_{i=1}^N (y_i - P(x_i))^2 \quad (8.2)$$

where  $P(x)$  is the fitted polynomial and  $\{(x_i, y_i)\}$  are the data points.

### 8.3.2 Polynomial Evaluation Using `polyval`

Once the polynomial coefficients are determined using `polyfit`, we use the `polyval` function to evaluate the polynomial at any new input values. This allows us to predict the pre-distorted values based on the fitted model. The syntax for evaluating the polynomial is:

```
y_fit = polyval(p, x_new);
```

Here,  $\mathbf{p}$  contains the coefficients obtained from `polyfit`, and  $\mathbf{x\_new}$  represents the new input data for which we want to predict the corresponding output values.

The polynomial evaluation at a new data point  $x_{\text{new}}$  is computed as follows:

$$P(x_{\text{new}}) = a_n x_{\text{new}}^n + a_{n-1} x_{\text{new}}^{n-1} + \dots + a_1 x_{\text{new}} + a_0 \quad (8.3)$$

### 8.3.3 Application to Digital Predistortion

In the context of our work, we apply polynomial fitting and evaluation separately to the real and imaginary components of the modulated signal. The aim is to pre-distort the input signal in such a way that after passing through the MZM, the output signal closely resembles the ideal 16-QAM constellation.

Let  $\text{Re}(s)$  and  $\text{Im}(s)$  represent the real and imaginary components of the modulated signal, and let  $\text{Re}(s_{\text{ideal}})$  and  $\text{Im}(s_{\text{ideal}})$  denote the real and imaginary parts of the ideal signal. We fit a 5th-degree polynomial to both the real and imaginary components of the signal using `polyfit`:

```
real_poly = polyfit(inputData(:,1), targetData(:,1), 5);
imag_poly = polyfit(inputData(:,2), targetData(:,2), 5);
```

The fitted polynomials can be expressed as:

$$P_{\text{real}}(x) = a_5 x^5 + a_4 x^4 + a_3 x^3 + a_2 x^2 + a_1 x + a_0 \quad (8.4)$$

$$P_{\text{imag}}(x) = b_5 x^5 + b_4 x^4 + b_3 x^3 + b_2 x^2 + b_1 x + b_0 \quad (8.5)$$

where  $a_5, a_4, \dots, a_0$  and  $b_5, b_4, \dots, b_0$  are the polynomial coefficients for the real and imaginary components, respectively.

Once the polynomials are fitted, we evaluate them using `polyval` to obtain the pre-distorted real and imaginary parts of the signal:

```
preDistorted_real = polyval(real_poly, real(modulatedData));
preDistorted_imag = polyval(imag_poly, imag(modulatedData));
```

Thus, the pre-distorted signal is given by:

$$s_{\text{dpd}}(t) = P_{\text{real}}(\text{Re}(s(t))) + jP_{\text{imag}}(\text{Im}(s(t))) \quad (8.6)$$

where  $j$  is the imaginary unit. The pre-distorted signal  $s_{\text{dpd}}(t)$  is then applied to the MZM, and the nonlinearity of the modulator is compensated, resulting in an output signal that more closely resembles the ideal 16-QAM constellation.

### 8.3.4 Applying PDPD

The key steps for applying PDPD are as follows:

1. **Normalize the Input Signal:** The input signal *sig* is first normalized to ensure that both the input and output are on comparable scales.
2. **Nonlinear MZM Output:** The normalized input signal is passed through the MZM's nonlinear transfer function, simulating the modulator's output.
3. **Polynomial Fitting:** Polynomial models of a specified degree (typically between 2 and 6) are fitted to the real and imaginary parts of the MZM output using `polyfit`. The input data corresponds to the MZM's nonlinear output, while the target data is the original linear signal.
4. **Pre-Distortion:** The fitted polynomial coefficients are then used to compute the pre-distorted signal using `polyval`. This pre-distorted signal compensates for the MZM's nonlinearity.
5. **Signal Transmission:** The pre-distorted signal is transmitted through the MZM. After modulation, the output of the MZM closely approximates a linear response, mitigating the nonlinear distortions.

The algorithm is executed for a range of modulation indices and polynomial degrees to identify the optimal parameters that minimize BER while maintaining linearity at the output.

## 8.4 Simulation Setup

We have shown the simulation setup in Figure 8.1. The parameters of transmission and DSP receiver is the same as in previous chapters but we have removed filters and digital pre-emphasis in order to focus exclusively on the distortion of the signal before MZM.

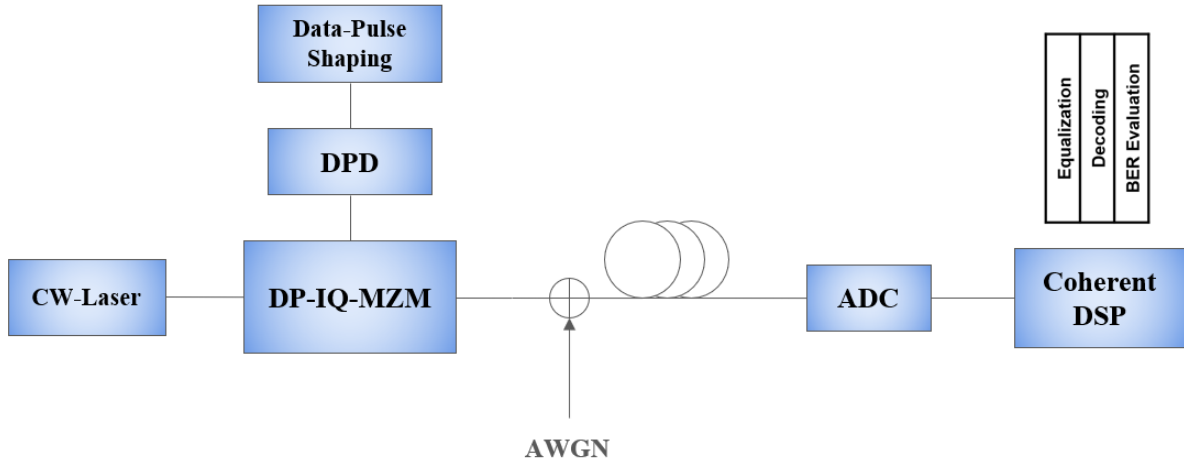


Figure 8.1: Simulation setup of applying DPD for compensating bandwidth limitations of DAC at TX.

## 8.5 Results and Performance Evaluation

In this section, we first introduce the definition of Error Vector Magnitude (EVM) and analyze the MZM output in both cases— with and without DPD. EVM serves as a key performance metric, indicating the effectiveness of predistortion in compensating for the nonlinear distortion introduced by the sinusoidal transfer function of the MZM. Following the EVM analysis, we compare the transmitted power for both scenarios (with and without DPD) to evaluate how predistortion impacts power efficiency. Lastly, we assess the BER performance of the system for different polynomial degrees used in the predistortion process, providing a comprehensive evaluation of the method’s effectiveness.

### 8.5.1 Error Vector Magnitude (EVM)

Error Vector Magnitude (EVM) is a measure used to quantify the performance of a communication system, particularly the accuracy of a received signal compared to the ideal transmitted signal. It is commonly used in optical communications and modulation schemes such as Quadrature Amplitude Modulation (QAM). EVM is defined as the ratio of the root-mean-square (RMS) error vector to the RMS magnitude of the ideal reference vector, expressed as a percentage:

$$\text{EVM}(\%) = \frac{\sqrt{\frac{1}{N} \sum_{i=1}^N |s_i - \hat{s}_i|^2}}{\sqrt{\frac{1}{N} \sum_{i=1}^N |s_i|^2}} \times 100$$

where:

- $s_i$  is the ideal reference symbol (expected constellation point),
- $\hat{s}_i$  is the received symbol (actual received constellation point),
- $N$  is the total number of symbols (constellation points).

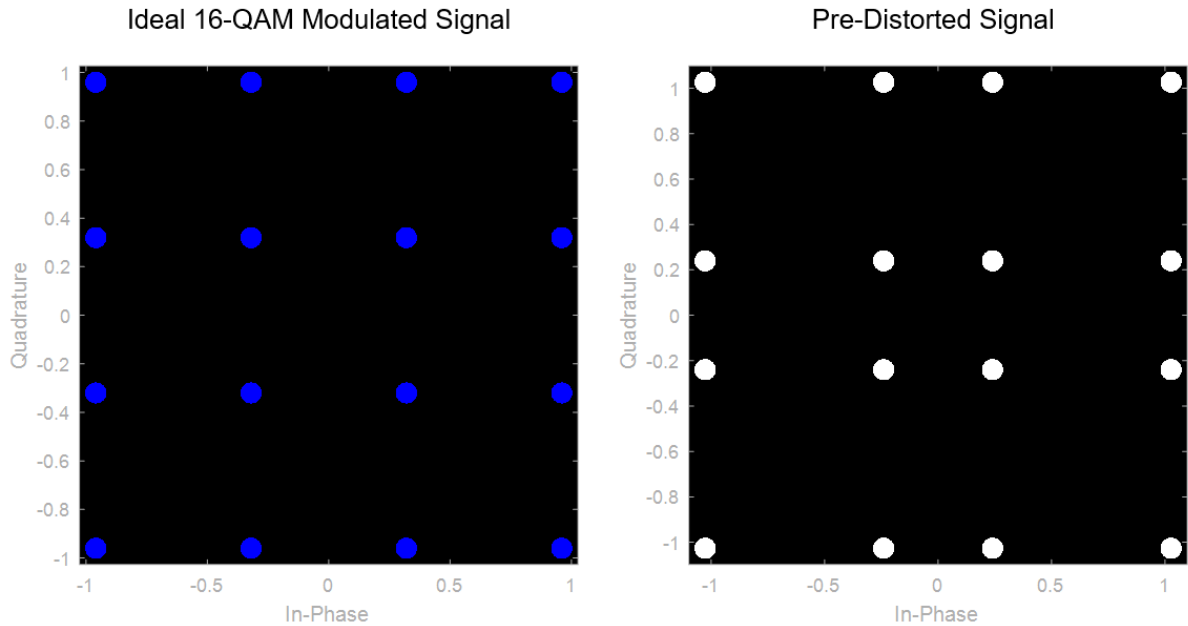


Figure 8.2: 16-QAM constellation diagram with and without pre-distortion applied before entering the MZM

The error vector  $e_i$  is the difference between the transmitted symbol and the received symbol:

$$e_i = s_i - \hat{s}_i$$

### Discussion on the results

For the first step we look at the EVM to see the performance of the proposed method. EVM measures how far the received constellation points are from their ideal positions. A lower EVM value indicates that the received signal is closer to the ideal transmitted signal, implying better signal quality.

Figures 8.2 and 8.3 show the constellation scatter plots of the 16-QAM signal before and after the MZM, with and without Digital Pre-Distortion (DPD). As observed, DPD slightly penalizes the four inner points of the constellation before entering the MZM. However, the nonlinearity of the MZM is effectively compensated by the DPD, resulting in a more symmetric constellation at the output. The neighboring points are more equidistant compared to the scenario without DPD, indicating improved signal quality.

In Figure 8.4, we present the modulation index versus EVM for the signal after the MZM, both with and without DPD. As shown, incorporating the DPD block before the MZM significantly reduces the EVM compared to the system without the DPD block, indicating that the job of DSP receiver would be simpler.

We have also plotted the transmitted power versus the modulation index. As shown in the Figure 8.5, in the linear region, the DPD does not affect the constellation shape. However, beyond  $m = 1$ , where nonlinearity begins to become noticeable, a penalty is observed for the signal with DPD. As the nonlinearity increases, the penalty in transmitted power becomes more extreme.

We found that the degree of the DPD polynomial is a critical factor in determining



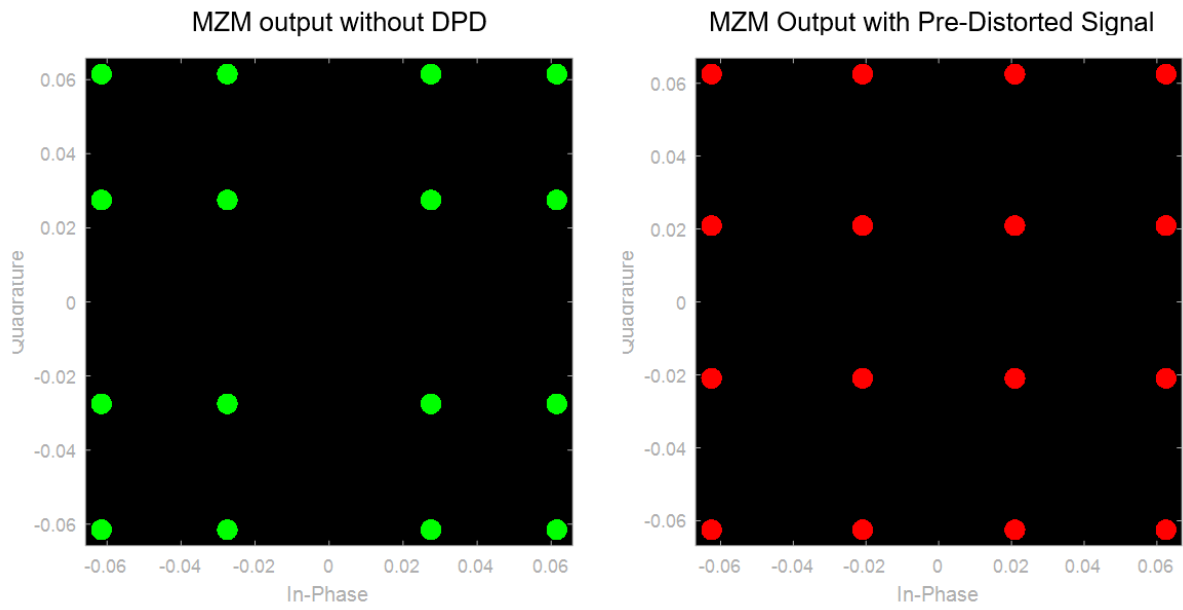


Figure 8.3: 16-QAM constellation diagram with and without pre-distortion applied after entering the MZM

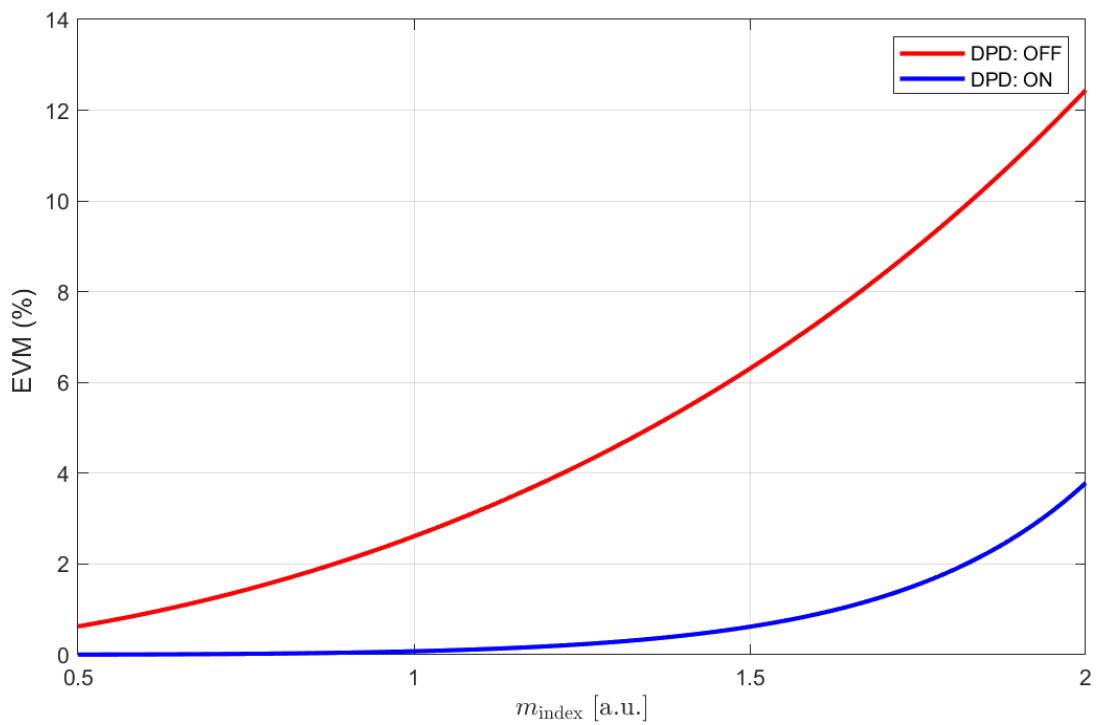


Figure 8.4: EVM vs Modulation Index for 16-QAM

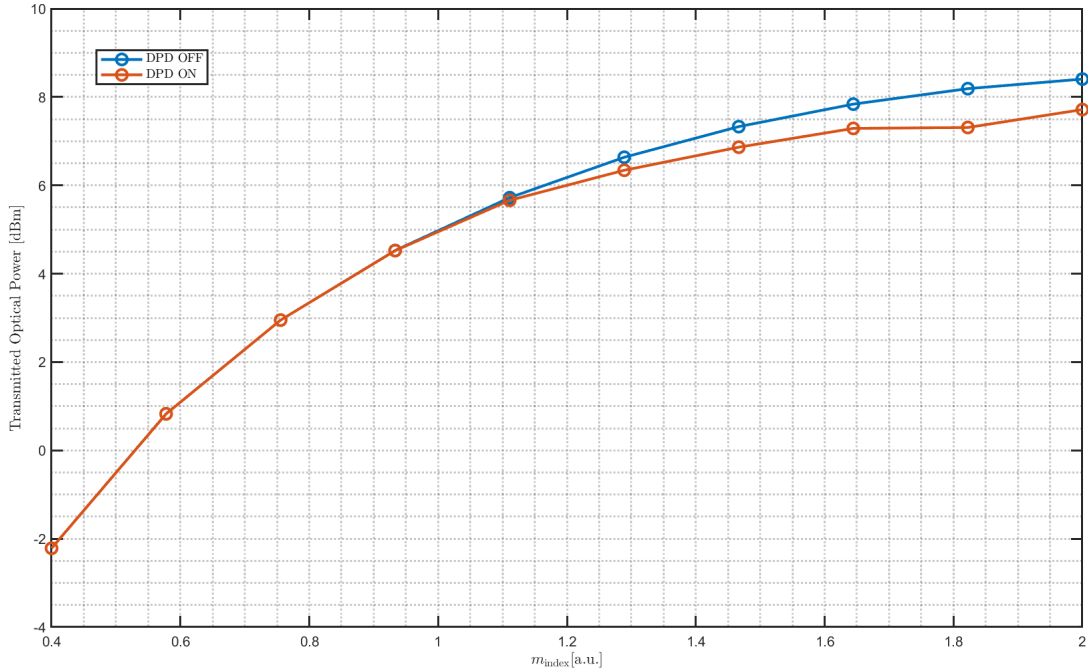


Figure 8.5: Transmitted Power(the power of the signal at the output of MZM).

system performance, in terms of BER. Figure 8.6 shows the modulation index versus BER for various polynomial degrees of DPD, as well as the case without DPD. The results indicate that the effectiveness of DPD varies with different modulation indexes. For instance, a sixth-degree DPD performs poorly in the range  $1.2 < m_i < 1.9$ , but shows good performance at  $m_i = 2$ . Additionally, for the linear region ( $0.4 < m_i < 1.2$ ), lower-degree DPD models work well, but as the modulation index increases, their performance degrades. Therefore, the optimal degree of DPD should be selected based on the MZM design and other system parameters. To provide further insight, Figure 8.7 presents a contour plot similar to Figure 8.6, providing a clearer illustration of how the polynomial degree impacts DPD performance across different modulation indexes.

### 8.5.2 Maximum ODN Loss

In this section, we focus on the key performance metric of maximum ODN loss for different target BERs, which are within the correction capability of current FEC codes. We evaluate a PM-16QAM signal while accounting for bandwidth limitations imposed by the DAC, modeled as a super-Gaussian filter with a  $B_{3dB}$  bandwidth of  $0.6 \times$  the baud rate, where the baud rate is set to 28 Gbaud.

The simulation was conducted in two scenarios: first, without DPD, and then with the DPD technique, to see whether DPD can improve the maximum ODN loss for various target BERs. It is important to note that the performance of Polynomial DPD is highly sensitive to the modulation index. Based on the findings from the previous section, we selected a third-degree Polynomial DPD, as it is an odd function and symmetrical to the coordinate center, making it well-suited to the sinusoidal transfer function of the MZM. Figure 8.8 presents the results without DPD, and Figure 8.9 shows the results with DPD.

Based on the results in Figure 8.6, we expect Polynomial DPD to improve performance for modulation indexes between 0.8 and 1.5. However, beyond a modulation index of 1.5,

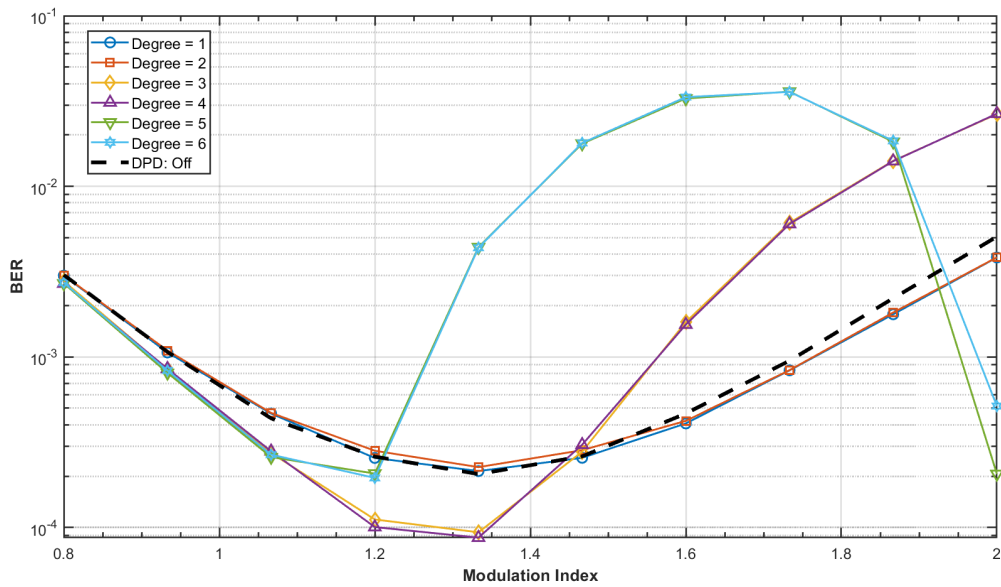


Figure 8.6: BER v.s. modulation index with different degrees of PDPDs and without DPD.

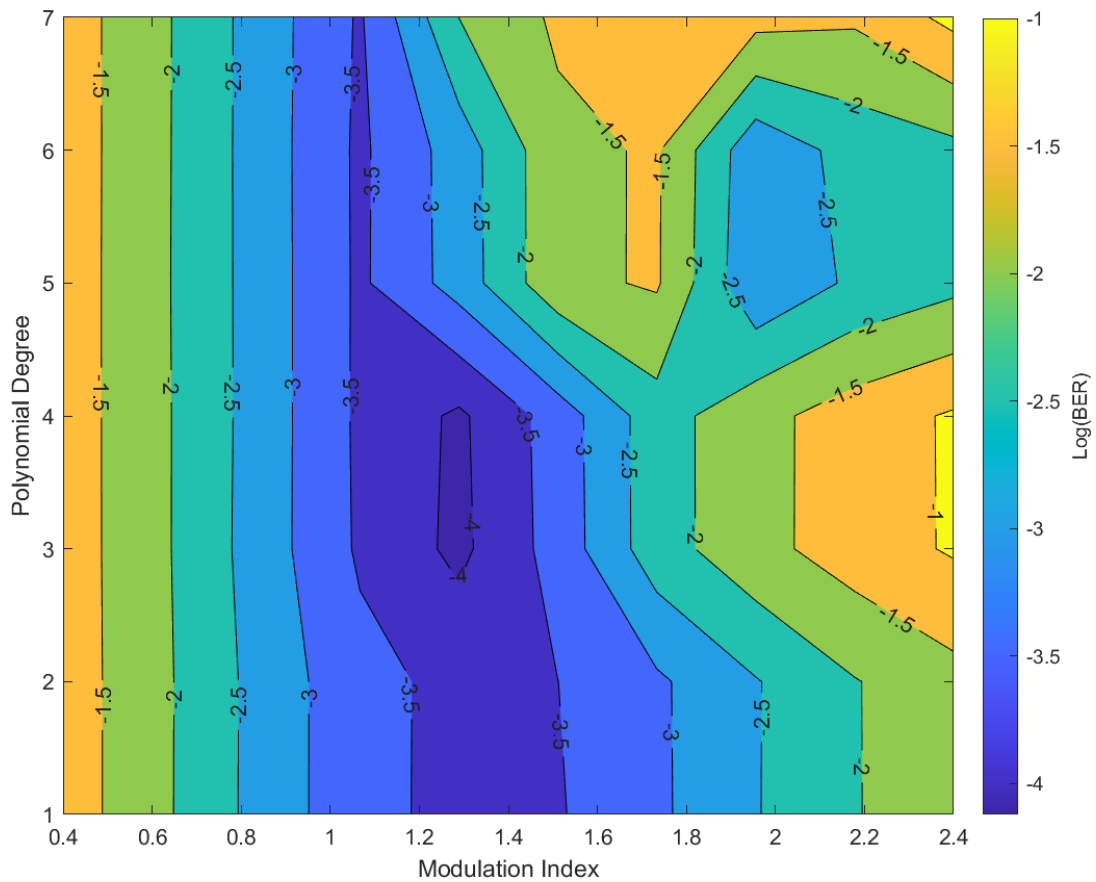


Figure 8.7: BER v.s. modulation index with different degrees of PDPDs.

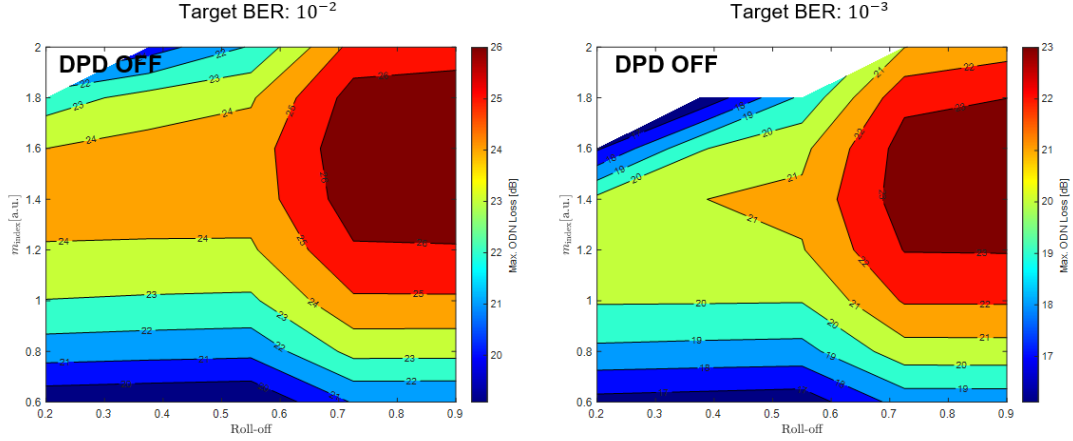


Figure 8.8: Maximum ODN vs. roll-off factor and modulation index under bandwidth limitations, with 3 dB bandwidth equal to  $0.6 \times$  symbol rate ( $R_s$ ), without DPD.

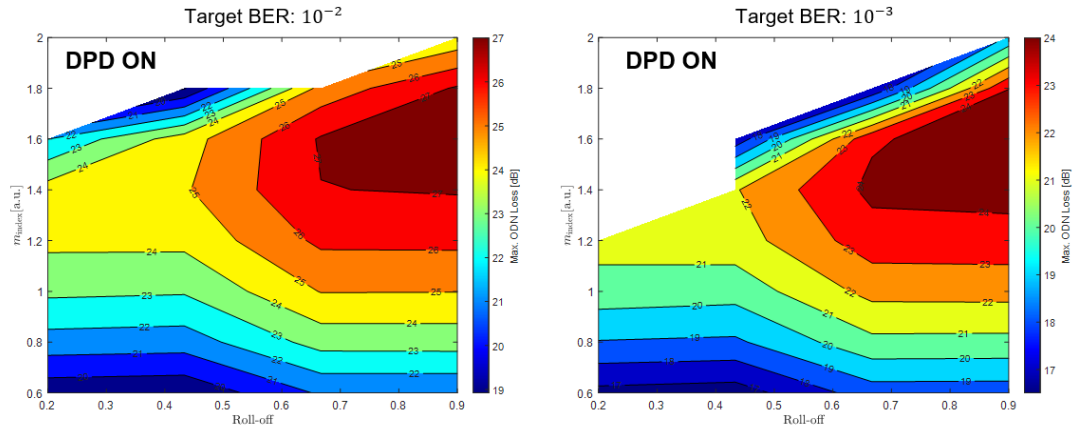


Figure 8.9: Maximum ODN vs. roll-off factor and modulation index under bandwidth limitations, with 3 dB bandwidth equal to  $0.6 \times$  symbol rate ( $R_s$ ), with DPD.

the performance begins to degrade. This is also evident in Figure 8.9, where, for low roll-off factors and high modulation indexes (greater than 1.5), the system fails to achieve the target ODN loss for a BER of  $10^{-3}$ .

## 8.6 Neural Network for MZM Nonlinearity Compensation

Neural networks (NNs) are a class of machine learning models inspired by the structure and function of biological neural networks in the human brain. Fundamentally, an NN consists of interconnected layers of nodes, or neurons, where each layer applies mathematical transformations to the input data. Typically, an NN is organized into an input layer, one or more hidden layers, and an output layer as it is shown in the Figure 8.10. Each neuron in a layer receives inputs from the neurons in the previous layer, applies a weighted sum followed by a non-linear activation function, and passes the result to the next layer. Through training, NNs learn the optimal weights and biases that best

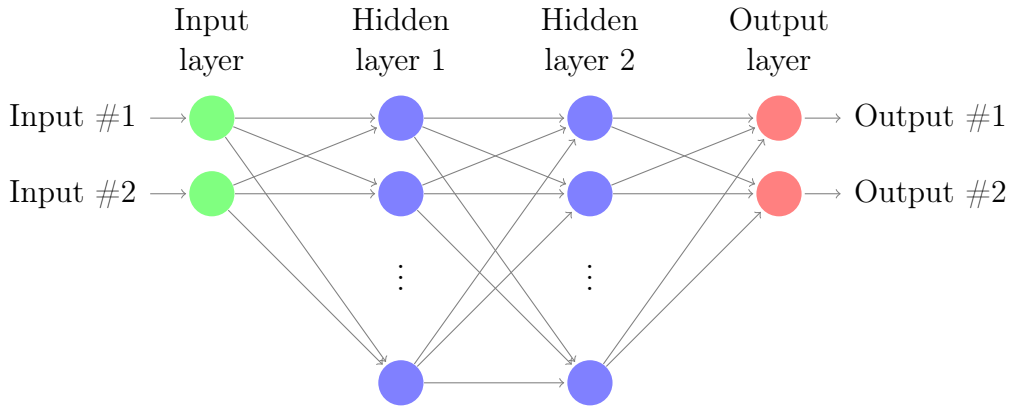


Figure 8.10: Diagram of a generic neural network architecture .

approximate the relationship between inputs and outputs in the given dataset.

Neural networks have gained significant attention as digital predistortion (DPD) techniques to mitigate nonlinearities in Mach-Zehnder modulators (MZMs) in high-speed optical communication systems. In [22], Imtiaz et al. propose an NN-based DPD approach designed to reduce quantization and bandwidth-limited impairments introduced by digital-to-analog converters (DACs) in high-bandwidth systems. Their work compares NN-DPD with traditional methods, such as Volterra series, look-up tables (LUT), and linear DPD, showing that NN-DPD, particularly when trained with direct learning, achieves superior signal-to-noise ratio (SNR) gains. They demonstrate that an indirect learning architecture with a recurrent NN offers a favorable trade-off between performance and complexity, which is advantageous in high-symbol-rate optical systems.

Schaedler et al. [23] focus on a low-complexity DPD using an extreme learning machine (ELM) to compensate for MZM nonlinearities in 400ZR systems over a 40 km unamplified link. Their results indicate that the ELM-based DPD achieves comparable performance to the more complex Volterra-based methods. Similarly, Bajaj et al. [24] explore an NN-based DPD trained via both direct and indirect learning architectures, specifically for a 128 GBaud coherent optical transmission. Their findings highlight the superior performance of NN-DPD in reducing transmitter-induced nonlinearities, especially at higher symbol rates and with complex modulation formats like 64-QAM and 256-QAM, achieving substantial SNR gains and setting a new record transmission rate of 1.61 Tb/s over 80 km of single-mode fiber.

In this section, we employ a neural network to learn the nonlinearity of the MZM. The network is trained to output a pre-distorted signal that, after passing through the MZM, results in an output signal as close as possible to the ideal signal. This adaptive model is structured as follows:

### 8.6.1 Neural Network Architecture

A fully connected neural network is used, consisting of an input layer, two hidden layers with ReLU activation functions, and an output layer. The network takes the distorted signal (from the MZM output) and learns to map it to the target ideal signal (16-QAM). The architecture is detailed below:

- **Input Layer:** Accepts the real and imaginary components of the distorted signal

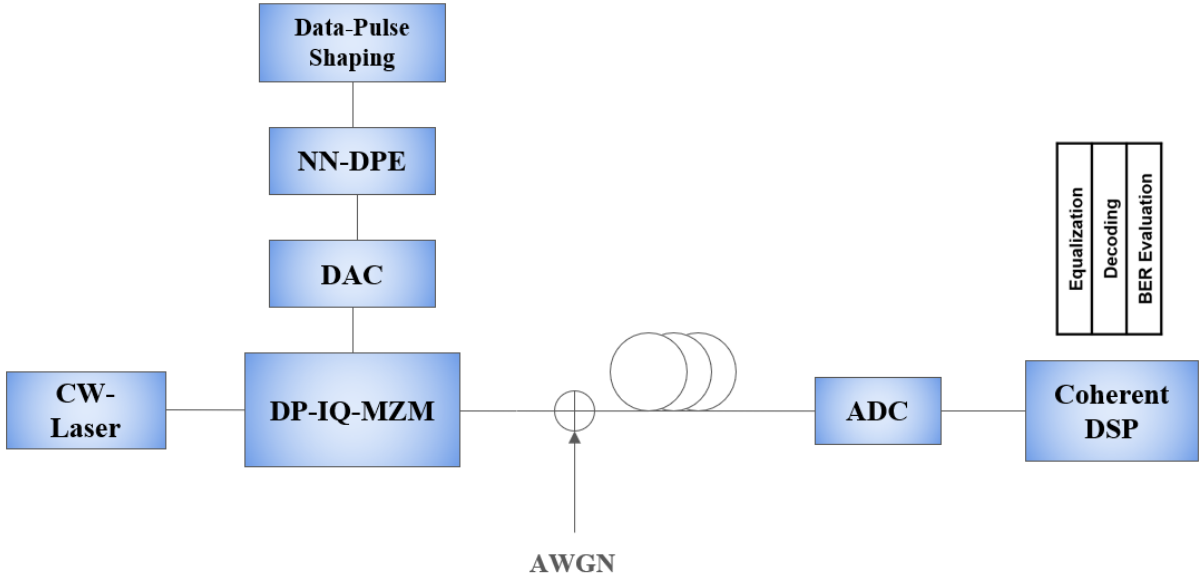


Figure 8.11: Simulation setup with NN-DPD block before DP-IQ-MZM.

from the MZM.

- **Hidden Layers:** Two hidden layers, each containing 64 neurons with ReLU activation functions. These layers are designed to capture the complex nonlinear transformations necessary for effective predistortion.
- **Output Layer:** Outputs the real and imaginary components of the predistorted signal, which will then serve as the input to the MZM.

### 8.6.2 Cost Function

To train the network, we minimize the mean squared error (MSE) between the neural network's predistorted output and the ideal signal. This cost function allows the network to iteratively adjust its weights, reducing the error caused by MZM nonlinearity. The cost function  $L$  is defined as:

$$L = \frac{1}{N} \sum_{i=1}^N \|\hat{y}_i - y_i\|^2 \quad (8.7)$$

where  $\hat{y}_i$  is the predistorted output from the neural network,  $y_i$  is the ideal signal, and  $N$  is the number of training samples.

## 8.7 Steps for NN-Based Predistortion

In Figure 8.11 we have shown the simulation setup with the block for NN-DPD before MZM and in Figure 8.12, we present the block diagram of the neural network architecture designed for signal pre-distortion. This model includes an input layer that processes the real and imaginary components of the signal, followed by two fully connected hidden

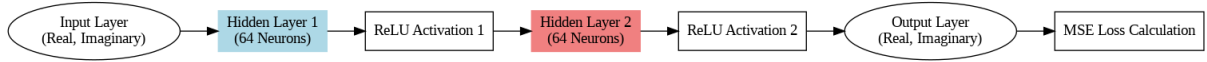


Figure 8.12: Neural network architecture for pre-distortion, showing input, hidden layers, ReLU activations, and MSE loss calculation.

layers with ReLU activations, and an output layer. The MSE loss function calculates the error, guiding the model’s optimization during training.

To implement neural network (NN)-based predistortion for an MZM system, the following steps are followed:

### 8.7.1 Data Preparation

To train the neural network model effectively, two datasets are required:

1. **Distorted Signal (Input Data):** This dataset consists of the MZM output signal, which has been distorted due to nonlinearities introduced by the modulator.
2. **Ideal Signal (Target Data):** This is the original, undistorted signal that we aim to achieve post-modulation.

Training data generation involves:

- Sampling a sequence of points from the distorted MZM output for the input dataset.
- Sampling the corresponding points from the undistorted modulated data for the target dataset.

Both the input and target data are complex signals. To facilitate neural network training, each signal is decomposed into its real and imaginary components, effectively doubling the feature space while allowing the network to handle complex data in a structured form.

### 8.7.2 Neural Network Architecture

The architecture of the neural network is designed to predict the real and imaginary components of the predistorted signal, and it comprises the following layers:

- **Feature Input Layer:** This initial layer has 2 nodes, one each for the real and imaginary parts of the input signal.
- **Hidden Layers:** Two fully connected layers with 64 neurons each, interleaved with ReLU activation layers. These hidden layers enable the network to learn complex, nonlinear relationships between the distorted input signal and the desired predistorted output.
- **Output Layer:** This layer has 2 nodes, corresponding to the real and imaginary components of the output signal.

- **Regression Layer:** The final layer uses Mean Squared Error (MSE) as the loss function, which is suitable for regression tasks. The network minimizes this loss function to reduce the error between the predicted and target signals.

This architecture enables the neural network to learn a mapping that effectively compensates for MZM-induced nonlinearities.

### 8.7.3 Training Process

The neural network is trained using the Adam optimizer, which adjusts the network’s weights to minimize the MSE between the predicted predistorted signal and the ideal target signal. The training is carried out over 50 epochs, using mini-batches of size 128. The initial learning rate is set to  $10^{-3}$  a small value to ensure gradual, stable updates to the network’s weights. For training, the dataset consists of the first 4000 symbols, empirically chosen to balance convergence and computational efficiency.

During training, the neural network iteratively refines its parameters to learn the optimal transformation that maps the distorted input to the ideal target signal. By the end of this process, the network is capable of generating a predistorted signal that, once processed by the MZM, closely approximates the ideal undistorted output.

### 8.7.4 Applying Predistortion

After training, the neural network is used to apply predistortion to any modulated signal before it undergoes modulation by the MZM. For a given modulated signal, we separate its real and imaginary components, feed them through the trained neural network, and obtain the corresponding predistorted values. These values are then combined back into a complex signal, which serves as the predistorted input to the MZM.

## Root Mean Square Error (RMSE) vs. Iterations

The **Root Mean Square Error (RMSE)** is a measure of the difference between the predistorted signal (output of the neural network or polynomial DPD) and the ideal target signal. In this context, RMSE provides a quantitative assessment of how effectively the DPD method minimizes the distortion caused by MZM nonlinearities.

Mathematically, RMSE is defined as:

$$\text{RMSE} = \sqrt{\frac{1}{n} \sum_{i=1}^n (y_{\text{pred},i} - y_{\text{ideal},i})^2}$$

where  $y_{\text{pred},i}$  represents the output from the DPD model for the  $i$ -th sample, and  $y_{\text{ideal},i}$  is the corresponding ideal (distortion-free) signal sample.

In the **RMSE vs. Iterations** plot, the RMSE is plotted as a function of training iterations, indicating the model’s ability to reduce distortion. A downward trend in RMSE suggests that the model is successfully minimizing the error between the predistorted and ideal signals, thus improving signal quality. Ideally, the RMSE should converge to the lowest possible value, indicating optimal compensation for MZM nonlinearity.



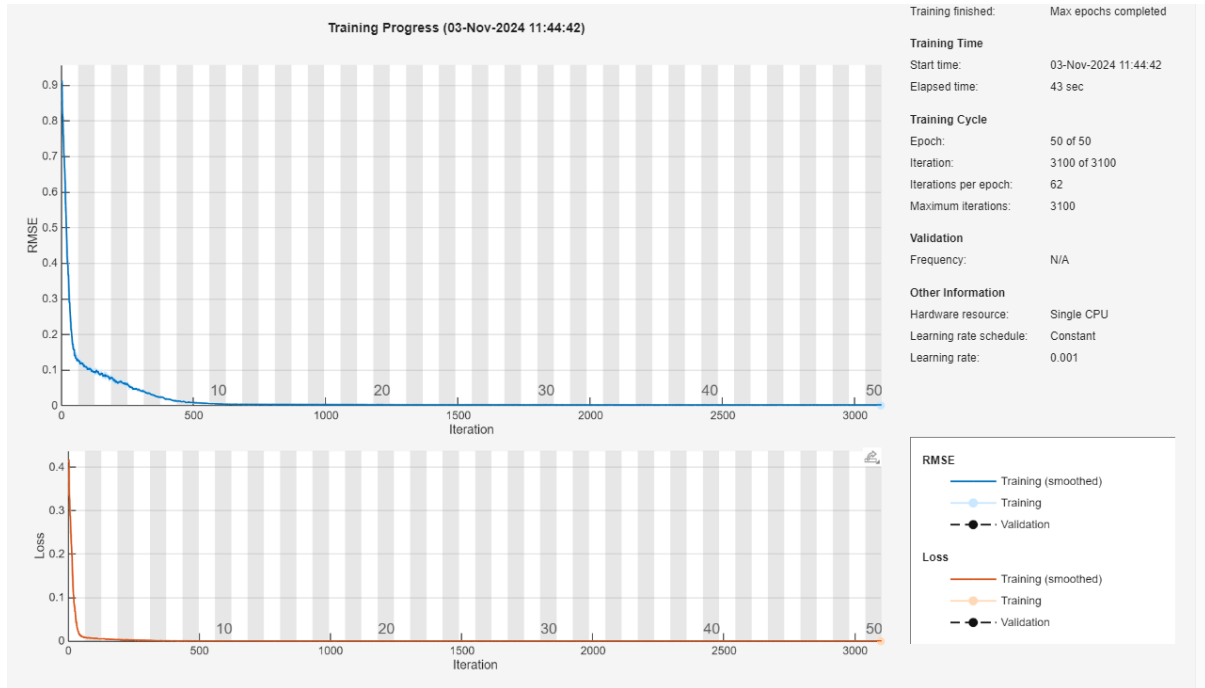


Figure 8.13: Training process for Neural Network pre distortion for DP-16QAM signal using Matlab.

## Loss vs. Iterations

The **Loss** function serves as the cost function that the neural network minimizes during training. This loss function quantifies the error between the predistorted and ideal signals, guiding the model to adjust its parameters to achieve better predistortion. Typically, the Mean Squared Error (MSE) is used as the loss function, defined as:

$$\text{Loss} = \frac{1}{n} \sum_{i=1}^n (y_{\text{pred},i} - y_{\text{ideal},i})^2$$

In the **Loss vs. Iterations** plot, the loss value is plotted against the number of training iterations. A decreasing loss indicates that the model is progressively learning to minimize the distortion, and convergence to a low loss value suggests effective training and optimal predistortion.

In Figure 8.13, we observe the **RMSE** and **Loss** plots against the number of iterations during the neural network training process.

- The top plot shows the **Root Mean Square Error (RMSE)**, which represents the error between the predicted output from the digital predistortion (DPD) model and the ideal signal. The RMSE quickly decreases within the first few hundred iterations and converges to a very low value, indicating that the neural network is effectively minimizing the signal distortion and learning an optimal mapping.
- The bottom plot displays the **Loss** (Mean Squared Error), which is used as the cost function guiding the neural network training. Similar to RMSE, the Loss also drops sharply in the initial iterations and stabilizes around a low value as the training progresses. This rapid convergence reflects the model's efficiency in minimizing the error and achieving a near-optimal pre-distortion performance.

Overall, the plots demonstrate fast convergence of both RMSE and Loss, indicating effective training of the neural network for signal predistortion with minimal distortion remaining by the end of the process. The low values achieved in both metrics suggest that the neural network model is well-suited for compensating nonlinearities in the MZM system.

### 8.7.5 Results and Performance Evaluation

To evaluate the performance of the NN-based DPD, we first consider the EVM versus modulation index 8.14. In the plot, the green curve represents the NN-DPD. As shown, the NN-DPD closely aligns with the Polynomial DPD in the linear region (modulation index between 1 and 1.6) and achieves lower EVM than the Polynomial DPD in the nonlinear region (modulation index greater than 1.6). This demonstrates that the NN-DPD significantly outperforms the case without DPD, especially under nonlinear conditions.

To evaluate the impact of neural network digital predistortion (NN-DPD) on the constellation of a DP-16QAM signal at the receiver, we present the constellation diagrams for a modulation index of 1.8 (representing the nonlinear operating region of the MZM) in Figure 8.15. The simulations assume an AWGN channel with no bandwidth limitations, and the constellations are normalized. Without NN-DPD, we observe significant distortion in the constellation, demonstrating the nonlinear effects introduced by the MZM at the transmitter. As expected, and consistent with EVM analysis, these nonlinear distortions are effectively mitigated when NN-DPD is applied.

Figure 8.16 shows the same setup, but with additional bandwidth limitations at the transmitter, simulated using a super-Gaussian filter with a 3 dB bandwidth of  $B = 0.5R_s$ . Under these conditions, we observe that the outer constellation points experience greater distortion compared to the inner points, highlighting the combined effect of bandwidth constraints and MZM nonlinearity.

In Figure 8.17, we present the BER vs. modulation index for two scenarios: with and without neural network-based digital pre-distortion (NN-DPD). The simulation is conducted using a DP-16QAM signal without any bandwidth constraints. As shown, across the entire nonlinear operating range of the MZM, the BER performance with NN-DPD is consistently superior to that without DPD. This improvement highlights the effectiveness of NN-DPD in mitigating the nonlinear distortions inherent in the MZM, resulting in a more robust signal transmission over all modulation index values.

To further evaluate the effectiveness of NN-DPD, we focus on our primary performance metric: the maximum Optical Distribution Network (ODN) loss for various target BER levels. In this analysis, we also consider the impact of electrical bandwidth limitations at the transmitter (TX), modeled by a super-Gaussian filter with a 3 dB bandwidth of  $B_{3\text{dB}} = 0.6 \times R_s$ , replicating the same simulation setup used in the previous section for Polynomial DPD.

In Figure 8.18, we present the maximum ODN loss results for target BERs of  $10^{-2}$  and  $10^{-3}$  with NN-DPD applied.

Figure 8.19 provides a comparison of system performance with and without NN-DPD for a target BER of  $10^{-2}$ , where the left side shows results with NN-DPD and the right side shows results without DPD. As observed, employing NN-DPD results in a 1 dB improvement in the achievable maximum ODN loss compared to the case without NN-DPD. Additionally, NN-DPD extends the system's capability to achieve the target BER

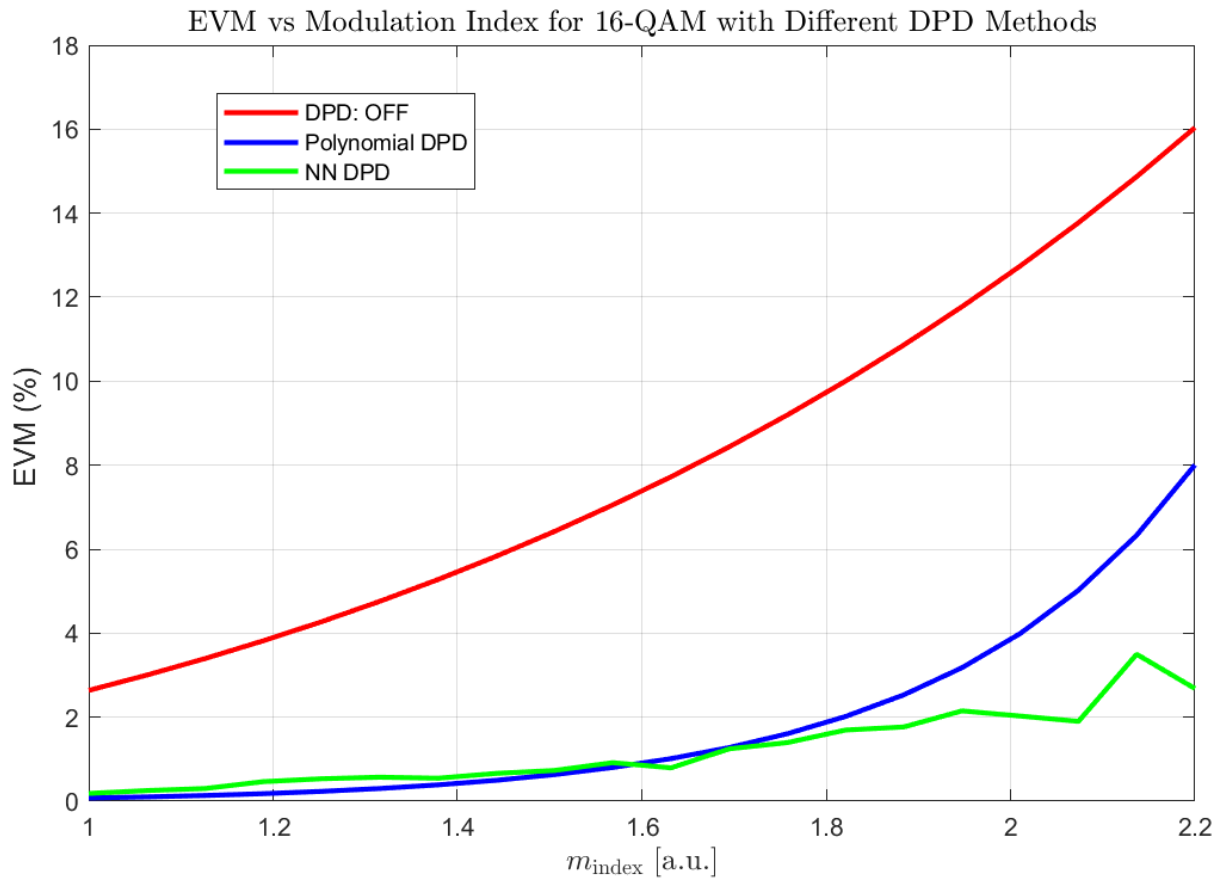


Figure 8.14: EVM vs. Modulation Index for Three Scenarios: No DPD, Polynomial DPD, and NN-DPD.

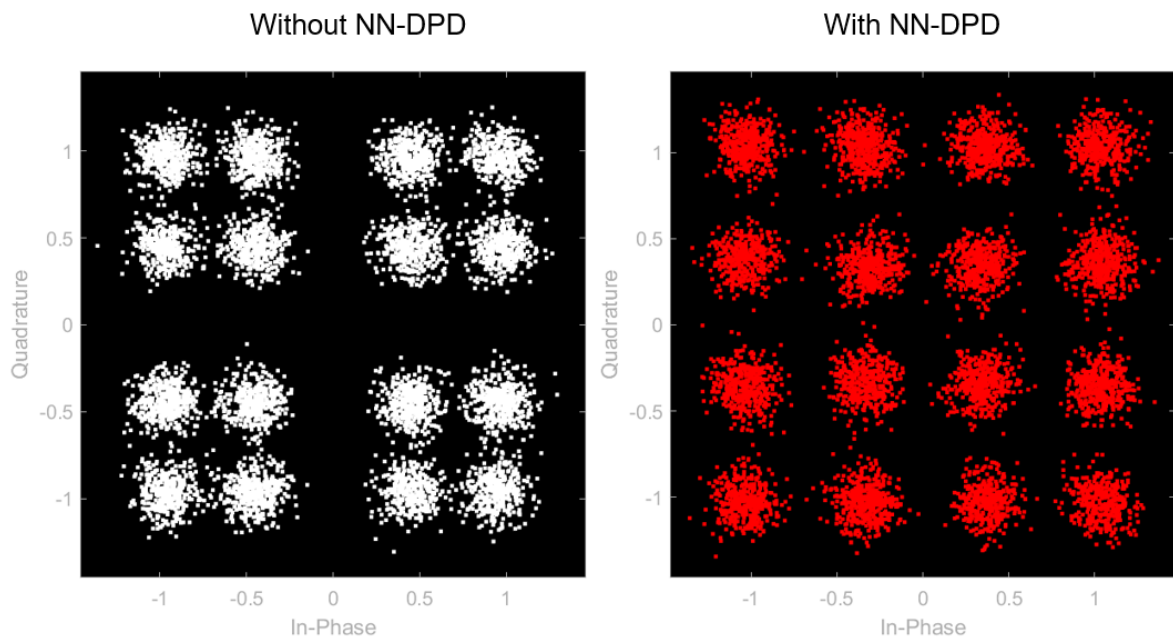


Figure 8.15: Predistorted signal output with and without NN-DPD for a signal with a modulation index of 1.8, observed at the receiver side after passing through an AWGN channel, without bandwidth limitations.

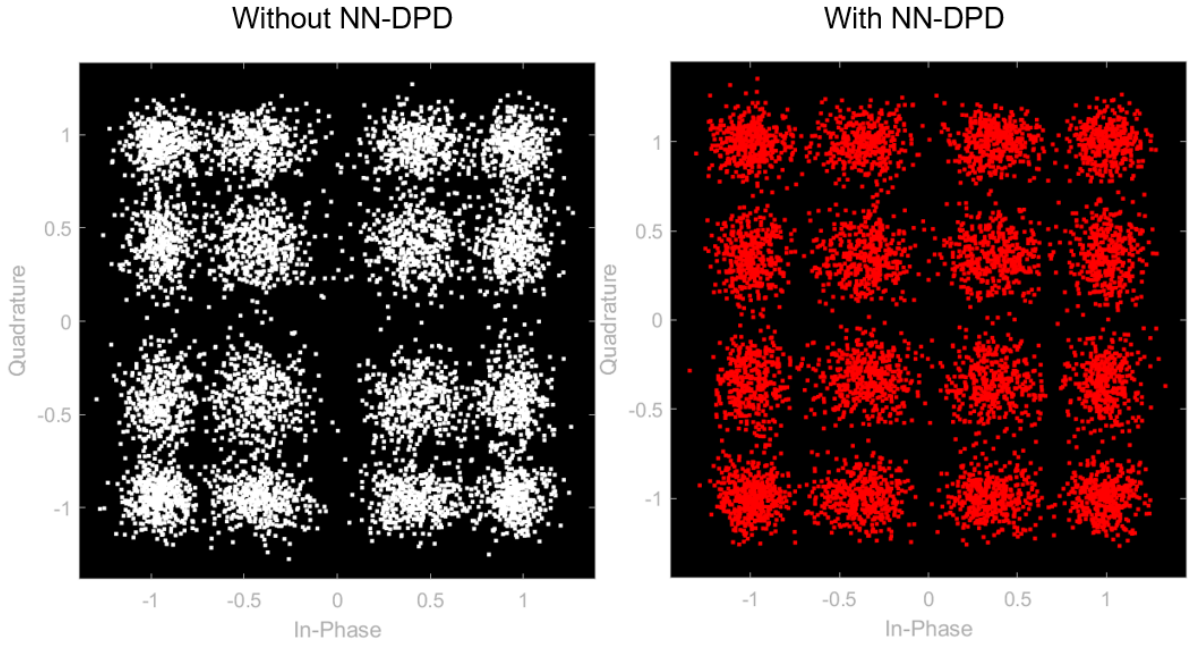


Figure 8.16: Predistorted signal output with and without NN-DPD for a signal with a modulation index of 1.8, observed at the receiver side after passing through an AWGN channel, with bandwidth limitations  $B = 0.5R_s$ .

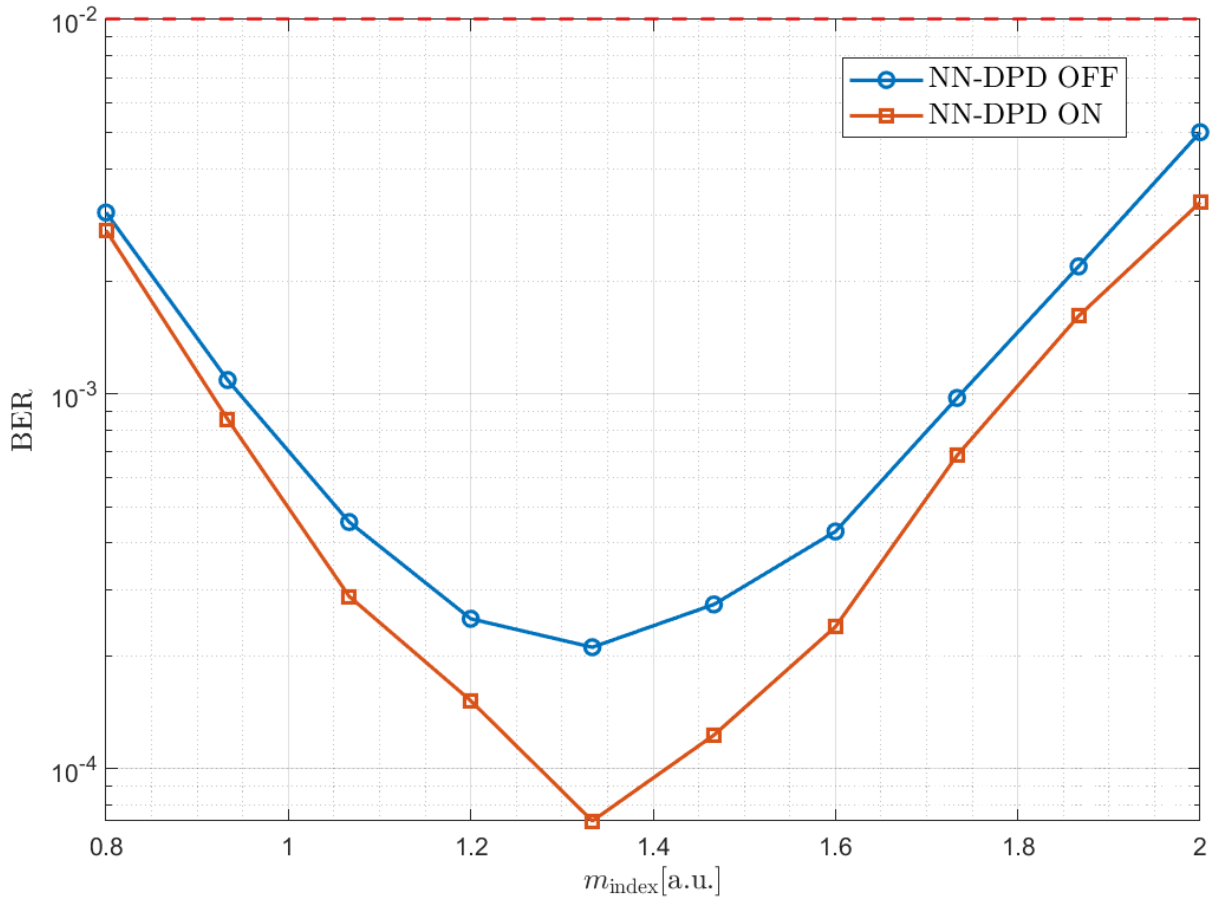


Figure 8.17: BER vs Modulation Index for DP-16QAM signal, comparison of NN-DPD and No DPD without bandwidth limitations

of  $10^{-2}$  within the region of lower roll-off factors (0.2 to 0.4). In this region, characterized by low roll-off and high modulation indices, the system without NN-DPD fails to reach the target BER, whereas NN-DPD enables the system to meet the performance requirements for these conditions.

Figure 8.20 repeats this comparison but with a target BER of  $10^{-3}$ , with NN-DPD results on the left and no-DPD results on the right. From these results, we observe a consistent 1 dB improvement in the maximum achievable ODN loss when utilizing NN-DPD. However, in regions with low roll-off values and high modulation indices, NN-DPD does not show improvement, as for both cases with NN-DPD or without it is not possible to achieve the target BER of  $10^{-3}$ . Additionally, for very high roll-off values (greater than 0.8) with high modulation indices, NN-DPD appears to result in slight degradation, as the system without NN-DPD is able to meet the target BER. Nevertheless, across most modulation index and roll-off factor ranges, NN-DPD provides a 1 dB improvement in maximum ODN loss.

To compare the performance of Polynomial DPD and NN-DPD, we include results for a target BER of  $10^{-2}$  in Figure 8.21, with Polynomial DPD shown on the left and NN-DPD on the right. Similarly, Figure 8.22 presents the results for a target BER of  $10^{-3}$ , with Polynomial DPD on the left and NN-DPD on the right.

The observations from Figure 8.14 regarding EVM are consistent with those for maximum ODN loss. In Figure 8.14, we noted that for modulation indices  $m_{\text{index}}$  greater than 1.6, NN-DPD achieves a lower EVM compared to Poly-DPD. Similarly, in Figure 8.21, we see that Poly-DPD fails to meet the target BER of  $10^{-2}$  for  $m_{\text{index}}$  values above 1.6 in regions of low roll-off. In contrast, NN-DPD successfully reaches the target BER across all tested modulation indices and roll-off values, demonstrating its robustness in compensating for nonlinearities at higher modulation indices. A similar observation is evident in Figure D, where Poly-DPD fails to achieve the target BER of  $10^{-3}$  for modulation indices greater than 1.2 with low roll-off values. In contrast, NN-DPD reaches the target BER for modulation indices up to 1.6 in the same low roll-off regions.

This set of figures provides a comprehensive assessment of NN-DPD's potential to improve ODN loss tolerance in comparison to Polynomial DPD, particularly under stringent BER requirements.

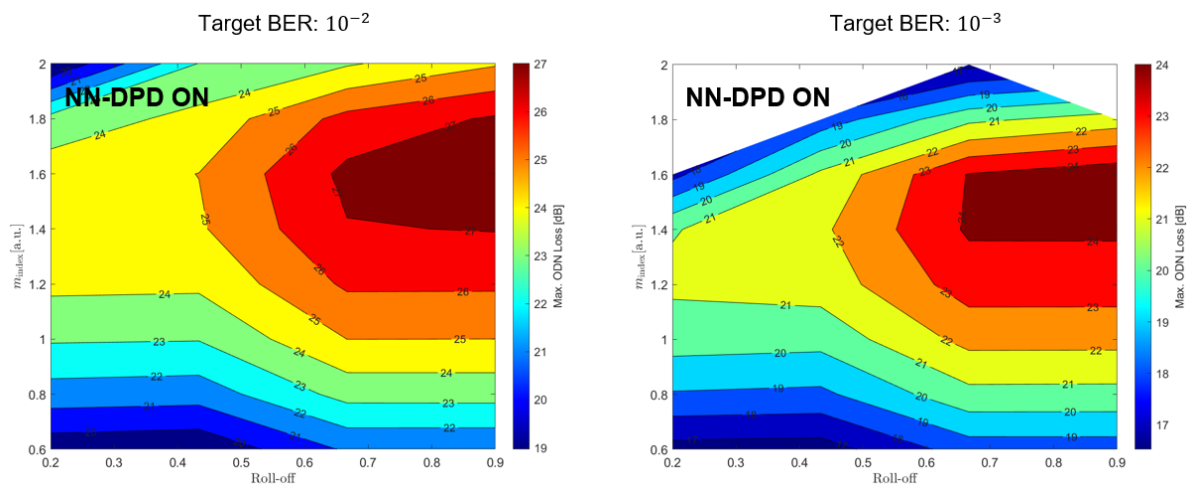


Figure 8.18: Maximum ODN vs. roll-off factor and modulation index under bandwidth limitations, with 3 dB bandwidth equal to  $0.6 \times$  symbol rate ( $R_s$ ), with NN-DPD for target BER= $10^{-2}$ (left) and BER= $10^{-3}$ (right) .

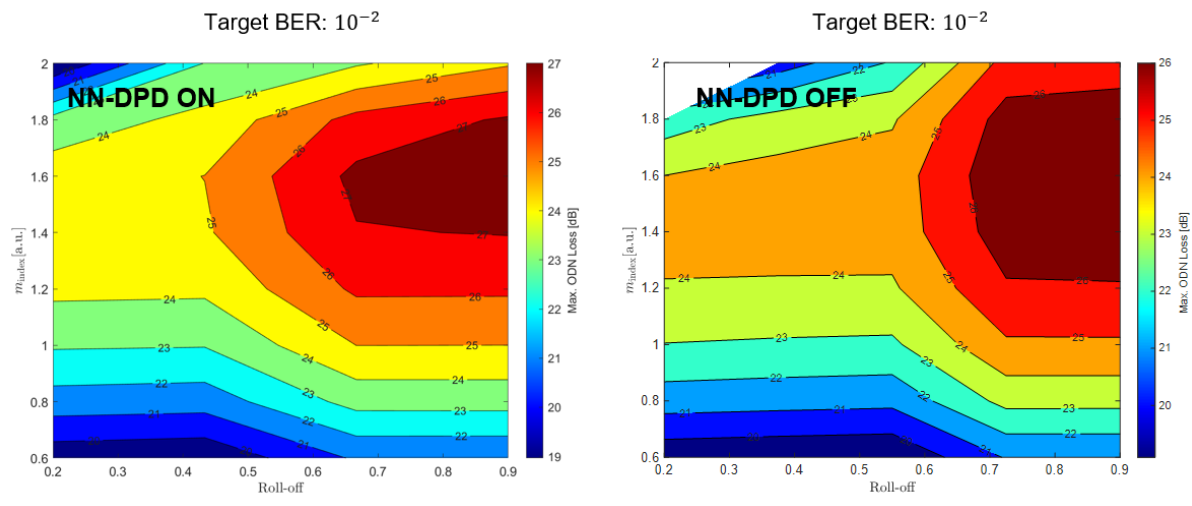


Figure 8.19: Maximum ODN vs. roll-off factor and modulation index under bandwidth limitations, with 3 dB bandwidth equal to  $0.6 \times$  symbol rate ( $R_s$ ), for target BER= $10^{-2}$  with NN-DPD(left) without NN-DPD(right).

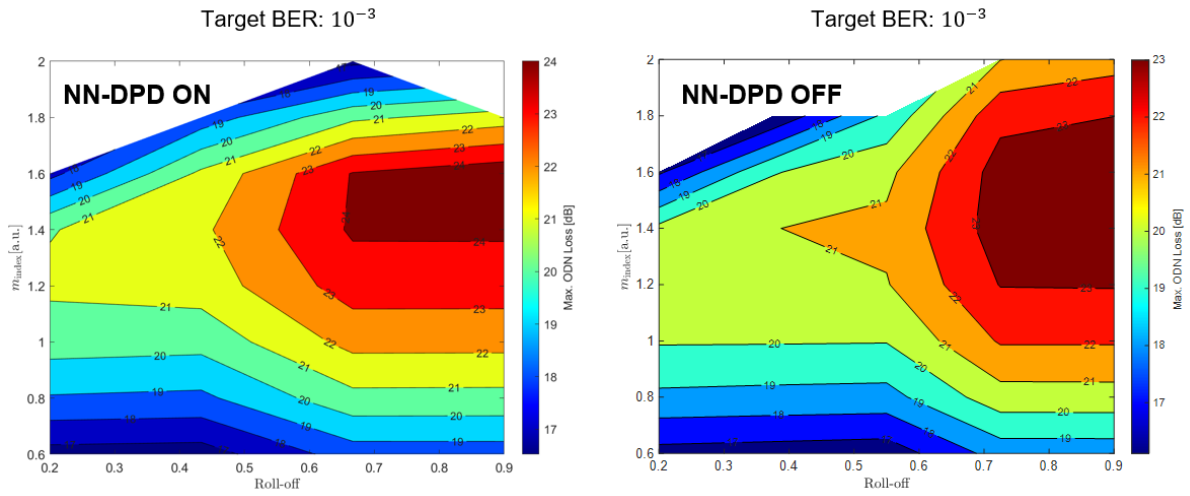


Figure 8.20: Maximum ODN vs. roll-off factor and modulation index under bandwidth limitations, with 3 dB bandwidth equal to  $0.6 \times$  symbol rate ( $R_s$ ), for target BER= $10^{-3}$  with NN-DPD(left) without NN-DPD(right).

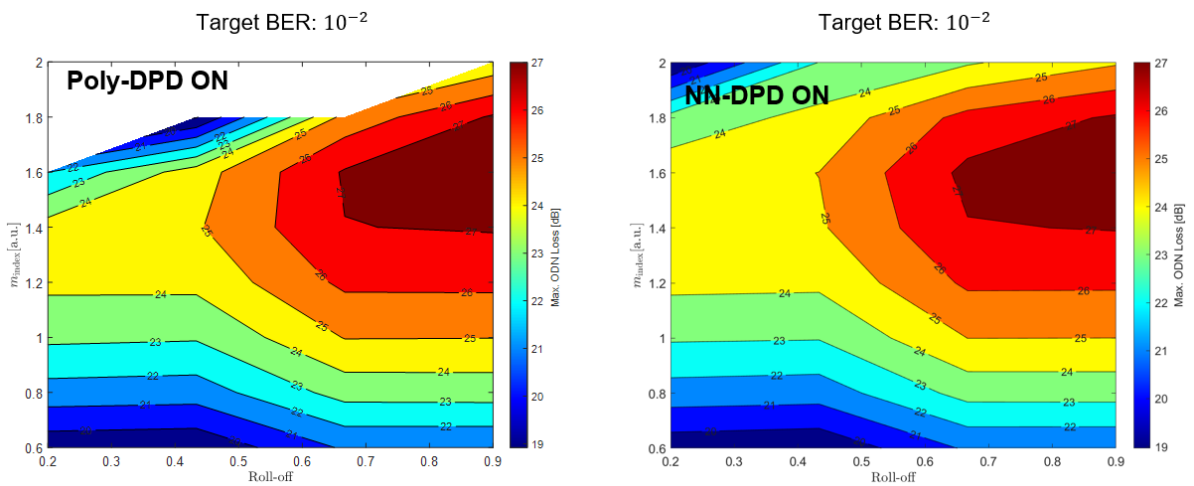


Figure 8.21: Maximum ODN vs. roll-off factor and modulation index under bandwidth limitations, with 3 dB bandwidth equal to  $0.6 \times$  symbol rate ( $R_s$ ), for target BER= $10^{-2}$  with Poly-DPD(left) NN-DPD(right).

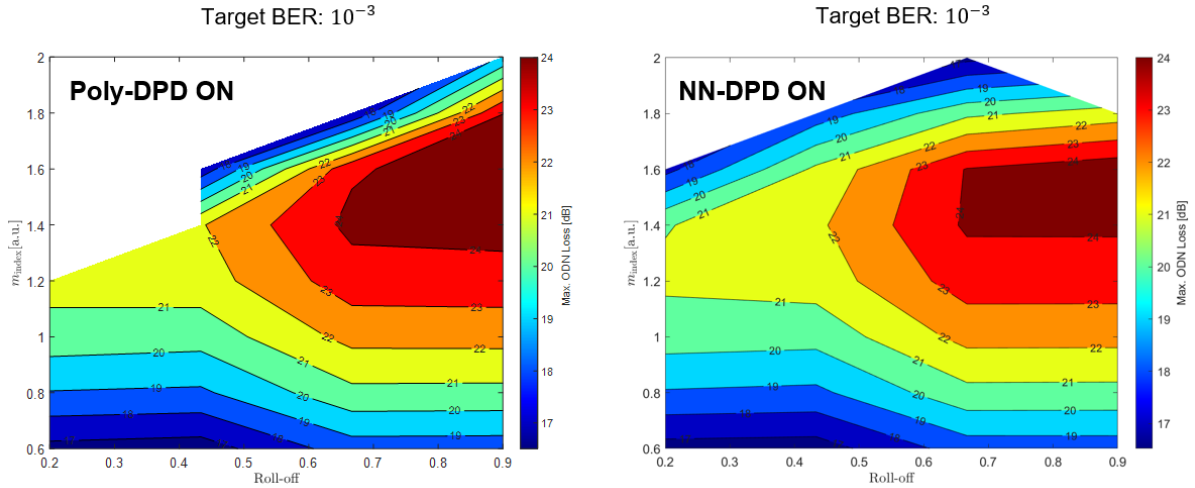


Figure 8.22: Maximum ODN vs. roll-off factor and modulation index under bandwidth limitations, with 3 dB bandwidth equal to  $0.6 \times$  symbol rate ( $R_s$ ), for target BER= $10^{-3}$  with Poly-DPD(left) and NN-DPD(right).

## 8.8 NN-DPD for Mitigating Nonlinearity Due to Low Extinction Ratio

In previous sections, we assumed an ideal MZM with an extinction ratio (ER) of 100, effectively neglecting nonlinear effects due to ER. In this section, however, we examine a more realistic scenario with a non-ideal MZM operating at a low ER. Our goal is to evaluate whether NN-DPD can learn and compensate for this type of nonlinearity at the transmitter by predistorting the signal prior to entering the MZM, thereby mitigating the impact of the reduced ER.

In [25], Napoli et al. proposed a DPD method using arcsin predistortion and gradient descent optimization to mitigate ER nonlinearity, while here we propose an NN-DPD approach to achieve similar compensation.

To begin, we use Error Vector Magnitude (EVM) as our evaluation metric. We calculate the EVM between the ideal constellation and the constellation after the MZM over a range of ER values, starting from a very low ER of around 5 and increasing up to 30. It is worth noting that most high-quality commercial MZMs typically have an ER between 20 and 30. In Figures 8.23, 8.24, we present the EVM vs. ER for three scenarios: with 3rd degree Polynomial DPD, NN-DPD, and without DPD, for a modulation index range of  $m_{index} = [1, 1.5, 1.7, 2]$ . As observed, NN-DPD outperforms Polynomial DPD at lower ER values, while at higher ER values, both methods show similar performance. In both cases, DPD significantly improves performance compared to the scenario without DPD.



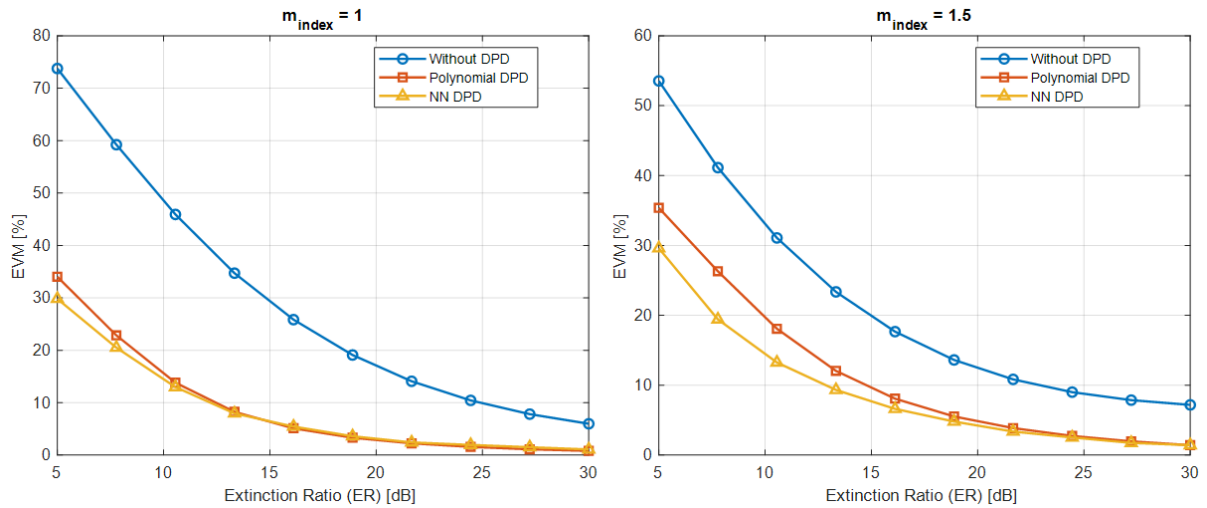


Figure 8.23: EVM vs. ER for systems with Polynomial DPD, NN-DPD, and without DPD for  $m_{index} = [1, 1.5]$ .

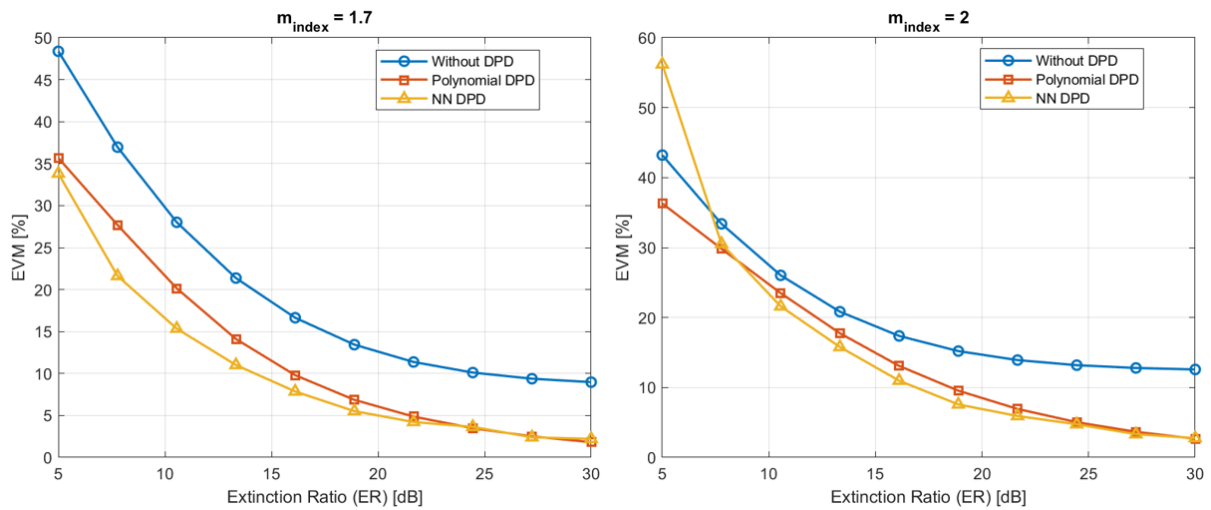


Figure 8.24: EVM vs. ER for systems with Polynomial DPD, NN-DPD, and without DPD for  $m_{index} = [1.7, 2]$ .

Metric	Polynomial-DPD	NN-DPD
Computational Complexity	Low (fixed number of multiplications)	High (multiple layers of operations)
Memory Requirements	Low (few coefficients)	High (many weights and biases)
Latency	Low	Higher (depends on network size)

Table 8.1: Comparison of Complexity, Memory Requirements, Latency for Polynomial-DPD and NN-DPD in Digital Predistortion of MZM.

## 8.9 Complexity Comparison

In terms of complexity, Polynomial-DPD and NN-DPD differ significantly in terms of computational complexity and resource requirements, which can impact their feasibility and efficiency for deployment on Digital Signal Processing (DSP) hardware. In Table 8.1 we compare the computational complexity, memory usage, and latency of both methods.

### 8.9.1 Polynomial-DPD

- **Computational Complexity:** Polynomial-DPD is computationally less intensive compared to neural networks. Once the polynomial coefficients are computed (e.g., using `polyfit` in MATLAB), applying the polynomial pre-distortion to each input sample involves a fixed number of multiplications and additions, determined by the polynomial degree. This makes it relatively simple to implement on DSP hardware, as polynomial evaluations are straightforward and can be efficiently parallelized.
- **Memory Requirements:** Polynomial-DPD requires storage for a small set of coefficients (one for each polynomial term), making it memory-efficient.
- **Latency:** The latency for Polynomial-DPD is low, as the polynomial operations are quick to execute on DSPs, especially when the degree of the polynomial is small.

### 8.9.2 Neural Network DPD (NN-DPD)

- **Computational Complexity:** NN-DPD is inherently more complex, involving a sequence of matrix multiplications, activation functions, and potentially more parameters across several layers. For a fully connected network with two hidden layers of 64 neurons, there are thousands of weights and biases that must be stored and processed for each inference. This complexity translates to significantly higher computational demands on DSP hardware, especially when considering the forward pass through multiple layers and non-linear activations.
- **Memory Requirements:** NN-DPD requires substantial memory to store the network's weights and biases, as well as intermediate values for each layer. This is particularly impactful when the network has a large number of layers or neurons, as these parameters must be stored and accessed during each inference step.
- **Latency:** Neural networks generally have higher latency compared to polynomial operations, as they require multiple layers of computation for each input sample. However, this latency can be mitigated if implemented on hardware accelerators designed for neural network operations (e.g., using GPUs or FPGAs), though DSPs alone may struggle with the speed requirements of real-time processing.

## 8.10 Conclusion

In this work, we explored the application of Polynomial Digital Pre-Distortion(DPD) to mitigate the nonlinearities introduced by the Mach-Zehnder Modulator (MZM). Our findings demonstrate that the Polynomial DPD technique effectively compensates for the MZM's nonlinear transfer function, resulting in significant performance improvements, particularly in terms of ODN loss and Error Vector Magnitude (EVM). By pre-distorting the input signal, PDPD linearizes the MZM output, leading to enhanced signal quality and reducing the complexity of the digital signal processing at the receiver.

The performance of Polynomial DPD was shown to be highly sensitive to the modulation index, with optimal results achieved for modulation indexes between 0.8 and 1.5. While the effectiveness of DPD diminishes beyond this range, the technique still provides considerable improvements in the linear region. Additionally, we demonstrated that selecting the appropriate polynomial degree is critical, with a third-degree polynomial offering a good balance between performance and simplicity. We have also considered a Neural Network based DPD and we observed that it improve the system performance in terms of EVM, BER, and maximum ODN loss. We have also noted that Polynomial-DPD cannot be effective in high modulation index values near 2, but NN-DPD can also improve the system's performance in that region.

In conclusion, NN-DPD and Polynomial-DPD offers a solution for addressing MZM nonlinearities in optical communication systems, improving key metrics such as ODN loss, EVM, and BER. These techniques enable better system performance and greater efficiency, making it viable for use in advanced coherent PONs and other high-speed optical networks. Future work may explore further optimization of the polynomial degree or using low-complexity Neural Networks.

# Chapter 9

## Conclusions and open research lines

### 9.1 Conclusion

In this thesis, we began by reviewing the current status and standards of passive optical networks (PONs), with a focus on the evolving interest in coherent solutions for access networks. Coherent PON systems face several challenges, one of the major issues being the inability to use EDFAs or other optical amplifications due to the high number of ONUs, which would result in prohibitive costs. To address this, we explored optimizing parameters such as the optical modulation index and roll-off factor.

Initially, we developed a detailed model of the Mach-Zehnder Modulator (MZM) to understand its operational characteristics and investigated the limits of increasing the modulation index while maintaining system performance. While a higher modulation index increases transmitted optical power, it also introduces distortions due to the nonlinear behavior of the MZM's transfer function. We identified the optimum modulation index for PM-QPSK and PM-16QAM modulations, which could serve as a potential guideline for future implementations of next-generation coherent PON systems.

Additionally, while low roll-off factors are commonly used in long-haul transceivers to optimize bandwidth usage, we suggest that for access networks, increasing the roll-off factor might enhance the performance of unamplified coherent systems. This could be another avenue for improving system performance in coherent PON deployments.

In the next chapter, we studied the impact of bandwidth limitations on system performance and proposed the use of digital pre-emphasis (DPE) as a compensatory technique. DPE acts as a filter to counter the low-pass filtering effects of the DAC, amplifying higher frequencies while smoothing the lower frequencies. This technique proved to be effective in mitigating bandwidth constraints, offering a practical solution to improve system performance in coherent PONs.

In the final chapter, we reviewed techniques for mitigating the nonlinearity of the MZM by predistorting the signal before it enters the modulator. Specifically, we examined two methods: Polynomial Digital Predistortion (Polynomial-DPD) and Neural Network Digital Predistortion (NN-DPD). Our simulations demonstrated that both approaches can effectively improve the achievable Optical Distribution Network (ODN) loss.

## 9.2 Future Work

While this thesis has addressed several key aspects of coherent PONs, numerous challenges and opportunities for further research remain. One significant area of focus is the optimization of coherent transceivers for cost-effective deployment in access networks. Unlike long-haul systems, PONs are highly cost-sensitive, particularly on the optical network unit (ONU) side, where the use of expensive components, such as EDFAs, is not feasible. Researchers and vendors need to explore innovative methods to enhance the performance of unamplified coherent systems, such as refining modulation techniques and optimizing transceiver designs. The balance between complexity, cost, and performance continues to be a central theme in coherent PON research.

One key challenge is the development of low-cost coherent receivers and transmitters that can operate efficiently without EDFAs while maintaining high optical power budgets. Simplified coherent architectures, including reduced-complexity modulation schemes and low-power DSP solutions, need further exploration. The integration of components, particularly through photonic integrated circuits (PICs), could also be a potential area of innovation. Such integration would enable compact, low-power, and high-performance transceivers suitable for cost-sensitive access networks. In particular, ongoing work on coherent DSP technology [4] could further reduce the complexity and cost of coherent PON deployments, making them more feasible for operators.

While this thesis explored the potential of modulation index optimization and the use of roll-off factors in pulse-shaping filters, further investigation is required into the robustness of these parameters under varying channel conditions and network architectures. Issues such as chromatic dispersion and polarization mode dispersion (PMD) in access environments remain critical challenges. There is a need for adaptive DSP algorithms capable of handling these impairments in burst-mode traffic and low-complexity equalization, which are essential for point-to-multipoint (P2MP) architectures. Advanced FEC schemes, such as soft-decision FEC, should also be explored to improve performance at higher data rates and under harsher transmission conditions.

To further enhance the performance of the proposed Neural Network Digital Pre-Distortion (NN-DPD) system, future research will focus on compensating for both bandwidth limitations and MZM nonlinearities. A novel approach will involve modifying the neural network architecture to incorporate memory effects by using three consecutive symbols as input and predicting one symbol as output. This extension will enable the NN-DPD to account for temporal dependencies, improving its ability to mitigate distortion more effectively.

Additionally, future investigations will explore the application of probabilistic modulation formats specifically designed for CPON. This will aim to improve spectral efficiency and adaptability in dynamic network conditions. Efforts will also be directed toward optimizing the NN-DPD model for real-time implementation, ensuring its feasibility in high-speed optical communication systems while maintaining low latency and computational efficiency.

Bandwidth limitations at both the transmitter and receiver sides also present significant challenges. While digital pre-emphasis (DPE) techniques have shown promise in mitigating bandwidth limitations, more research into adaptive filtering and machine learning-based dynamic bandwidth allocation could transform system efficiency. Such innovations could enable greater spectral efficiency and system scalability, particularly as

networks evolve to support 100 Gbps and beyond.

Another crucial challenge is the coexistence with legacy systems. Operators seek to deploy next-generation coherent PONs over existing optical distribution networks (ODNs), and ensuring seamless coexistence while maximizing the benefits of coherent technology will require careful consideration of wavelength planning, signal processing, and coexistence elements. Recent work in this area, such as the introduction of colorless phase-retrieval full-field recovery techniques and frequency-comb lasers, suggests promising directions for future PON research. Additionally, organizations like CableLabs are working on coherent PON specifications that enable the coexistence of new coherent systems with legacy IM/DD networks, which would allow for smooth transitions without significant infrastructure changes.

In summary, while coherent PONs offer significant potential for future access networks, considerable work remains in optimizing transceiver designs, handling system impairments, addressing bandwidth constraints, and ensuring coexistence with legacy systems. With continued research in these areas, coherent PONs could become a key enabler of future high-speed, cost-effective access networks.

# Bibliography

- [1] Govind Agrawal. *Fiber-Optic Communication Systems: Fourth Edition*. Jan. 2012. ISBN: 9780470505113. DOI: 10.1002/9780470918524.
- [2] Jun Shan Wey. “The Outlook for PON Standardization: A Tutorial”. In: *Journal of Lightwave Technology* 38.1 (2020), pp. 31–42. DOI: 10.1109/JLT.2019.2950889.
- [3] René Bonk et al. “50G-PON: The First ITU-T Higher-Speed PON System”. In: *IEEE Communications Magazine* 60.3 (2022), pp. 48–54. DOI: 10.1109/MCOM.001.2100441.
- [4] Erik Agrell et al. “Roadmap on optical communications”. In: *Journal of Optics* 26 (July 2024), p. 093001. DOI: 10.1088/2040-8986/ad261f.
- [5] CableLabs. *CPON Architecture Specification*. Accessed: 2024-08-06. 2024. URL: <https://www.cablelabs.com/specifications/CPON-SP-ARCH>.
- [6] Amitabha Banerjee et al. “Wavelength-division-multiplexed passive optical network (WDM-PON) technologies for broadband access: a review [Invited]”. In: *J. Opt. Netw.* 4.11 (Nov. 2005), pp. 737–758. DOI: 10.1364/JON.4.000737. URL: <https://opg.optica.org/jon/abstract.cfm?URI=jon-4-11-737>.
- [7] Klaus Grobe and Jorg-Peter Elbers. “PON in adolescence: from TDMA to WDM-PON”. In: *IEEE Communications Magazine* 46.1 (2008), pp. 26–34. DOI: 10.1109/MCOM.2008.4427227.
- [8] Jose A. Altabas, Samael Sarmiento, and Jose A. Lazaro. “Passive Optical Networks: Introduction”. In: *Wiley Encyclopedia of Electrical and Electronics Engineering*. John Wiley & Sons, Ltd, 2018, pp. 1–20. ISBN: 9780471346081. DOI: <https://doi.org/10.1002/047134608X.W8373>. eprint: <https://onlinelibrary.wiley.com/doi/pdf/10.1002/047134608X.W8373>. URL: <https://onlinelibrary.wiley.com/doi/abs/10.1002/047134608X.W8373>.
- [9] Pablo Torres-Ferrera et al. “Overview of high-speed TDM-PON beyond 50<replacement>Gbps per wavelength using digital signal processing [Invited Tutorial]”. In: *Journal of Optical Communications and Networking* 14.12 (2022), pp. 982–996. DOI: 10.1364/JOCN.468920.
- [10] Istvan Bence Kovacs et al. “200 Gb/s/<replacement> Bidirectional Coherent PON Solutions Demonstrated Over Field Installed Fiber”. In: *IEEE Photonics Technology Letters* 36.17 (2024), pp. 1089–1092. DOI: 10.1109/LPT.2024.3434640.
- [11] Md Saifuddin Faruk et al. “Coherent Passive Optical Networks: Why, When, and How”. In: *IEEE Communications Magazine* 59.12 (2021), pp. 112–117. DOI: 10.1109/MCOM.010.2100503.

- [12] Istvan Bence Kovacs et al. “Simplified coherent optical network units for very-high-speed passive optical networks”. In: *J. Opt. Commun. Netw.* 16.7 (July 2024), pp. C1–C10. DOI: 10.1364/JOCN.514867. URL: <https://opg.optica.org/jocn/abstract.cfm?URI=jocn-16-7-C1>.
- [13] Antonio Teixeira et al. “DSP Enabled Optical Detection Techniques for PON”. In: *J. Lightwave Technol.* 38.3 (Feb. 2020), pp. 684–695. URL: <https://opg.optica.org/jlt/abstract.cfm?URI=jlt-38-3-684>.
- [14] Kazuro Kikuchi. “Fundamentals of Coherent Optical Fiber Communications”. In: *J. Lightwave Technol.* 34.1 (Jan. 2016), pp. 157–179. URL: <https://opg.optica.org/jlt/abstract.cfm?URI=jlt-34-1-157>.
- [15] Tomáš Huszaník, Ján Turán, and Lubos Ovsenik. “Utilization of 10 Gbps DWDM System with Duobinary Modulation into Passive Optical Network”. In: *Journal of Communications Software and Systems* 14 (Dec. 2018). DOI: 10.24138/jcomss.v14i4.644.
- [16] Giuseppe Rizzelli Martella et al. “Scaling Laws for Unamplified Coherent Transmission in Next-Generation Short-Reach and Access Networks”. In: *Journal of Lightwave Technology* 39.18 (2021), pp. 5805–5814. DOI: 10.1109/JLT.2021.3092523.
- [17] Md. Saifuddin Faruk and Seb J. Savory. “Digital Signal Processing for Coherent Transceivers Employing Multilevel Formats”. In: *Journal of Lightwave Technology* 35.5 (2017), pp. 1125–1141. DOI: 10.1109/JLT.2017.2662319.
- [18] Ivan Fernandez de Jauregui Ruiz et al. “An accurate model for system performance analysis of optical fibre networks with in-line filtering”. In: *45th European Conference on Optical Communication (ECOC 2019)*. 2019, pp. 1–4. DOI: 10.1049/cp.2019.1112.
- [19] Danish Rafique et al. “Digital Preemphasis in Optical Communication Systems: On the DAC Requirements for Terabit Transmission Applications”. In: *Journal of Lightwave Technology* 32.19 (2014), pp. 3247–3256. DOI: 10.1109/JLT.2014.2343957.
- [20] Sasan Zhalehpour, Jiachuan Lin, and Leslie Rusch. “SiP IQ modulator Linearization by memory polynomial pre-distortion model”. In: Oct. 2017, pp. 317–318. DOI: 10.1109/IPCon.2017.8116123.
- [21] Yuan Bao et al. “Nonlinearity mitigation for high-speed optical OFDM transmitters using digital pre-distortion”. In: *Optics Express* 21 (Mar. 2013), pp. 7354–61. DOI: 10.1364/OE.21.007354.
- [22] Hamza Imtiaz et al. “Performance vs. complexity in NN pre-distortion for a nonlinear channel”. In: *Opt. Express* 31.23 (Nov. 2023), pp. 38513–38528. DOI: 10.1364/OE.500467. URL: <https://opg.optica.org/oe/abstract.cfm?URI=oe-31-23-38513>.
- [23] Maximilian Schaedler et al. “AI-Based Digital Predistortion for IQ Mach-Zehnder Modulators”. In: *2019 Asia Communications and Photonics Conference (ACP)*. 2019, pp. 1–3.



- [24] Vinod Bajaj et al. “Deep Neural Network-Based Digital Pre-Distortion for High Baudrate Optical Coherent Transmission”. In: *Journal of Lightwave Technology* 40.3 (2022), pp. 597–606. DOI: 10.1109/JLT.2021.3122161.
- [25] Antonio Napoli et al. “Digital Predistortion Techniques for Finite Extinction Ratio IQ Mach–Zehnder Modulators”. In: *Journal of Lightwave Technology* 35.19 (2017), pp. 4289–4296. DOI: 10.1109/JLT.2017.2729603.